MICROWAVE INTERFERENCE CANCELLATION SYSTEM

Jessada Konpang

Submitted in accordance with the requirements for the degree of
Doctor of Philosophy

The University of Leeds
School of Electronic & Electrical Engineering
February 2018

Declaration

The candidate confirms that the work submitted is his own, except where work which has formed part of jointly-authored publications has been included. The contribution of the candidate and the other authors to this work has been explicitly indicated below. The candidate confirms that appropriate credit has been given within the thesis where reference has been made to the work of others.

The details of chapter 3 to 5 of the thesis are based on the following published paper:

[1] Jessada Konpang, Muhammad Y Sandhu, Nutapong Somjit and Ian C Hunter, "Novel synthesizing technique for interference rejection in future integrated base station," presented at Thailand-Japan MicroWave (TJMW2016) Conference, June 2016.

[2] Jessada Konpang, Muhammad Y Sandhu, Nutapong Somjit and Ian C Hunter, "Four-port microstrip diplexer for RF interference rejection," presented at Electrical Engineering/Electronics, Computer, Telecommunications and Information Technology (ECTI-CON) Conference, June 2016.

[3] Jessada Konpang, Muhammad Y Sandhu, Nutapong Somjit and Ian C Hunter, "Novel RF interference rejection technique using a four-port diplexer," presented at European Microwave Conference (EuMC 2016), October 2016.

[4] Jessada Konpang, Muhammad Y Sandhu, Nutapong Somjit and Ian C Hunter, "A four-port diplexer for high Tx/Rx isolation for integrated transceivers," published at IET Microwaves, Antennas & Propagation, January 2018.

Prof. Ian C Hunter, Dr Nutapong Somjit and Dr Muhammad Y Sandhu supervised the work, proof read the drafts and made suggestions and corrections to the draft paper. The student (Jessada Konpang) performed the experimental work and prepared the initial draft along with the graphical and tabular presentation, calculation and summarization of the paper.

Jessada Konpang

Acknowledgements

I would like to express my utmost gratitude to my supervisors, Professor Dr. Ian Hunter and Dr. Nutapong Somjit for their valuable suggestions, guidance and support in my academic research. I would like to thank Radio Design Ltd for supporting technical technique. I also appreciated some individual support from my colleagues and friends.

I would also like to thank the Ministry of Science and Technology, Thailand, for giving me the opportunity to pursue my studies at the University of Leeds.

I am deeply indebted and grateful to my parents for their love and encouragement.

Abstract

A microwave interference cancellation system is presented in this thesis. The technique achieves high Tx/Rx isolation with relatively low degree filters. A four-port diplexer consists of two back-to-back three-port diplexers combined with a 180° phase shift in one branch. High signal isolation between Tx and Rx module is achievable by only using second-order filter topology and the design technique is based on amplitude and phase cancellation between two diplexer branches of the four-port diplexer. Three and four-port networks are intensively analysed and synthesised for solving S-parameter equations.

The four-port diplexer exploits the microstrip open-loop structure. A four-port microstrip diplexer for RF interference rejection is presented in IMT-2000 applications whereas device miniaturisation and low infrastructure cost are required. The microstrip-open loop structure with coupled-feed and tapped-feed are designed for alternative techniques and cost reduction. A 180° phase shift in one branch can be achieved by delayed transmission line. The simulated microstrip four-port network is designed at the centre frequency of Tx/Rx at 1.95 GHz and 2.14 GHz, respectively.

An alternative technology to reduce overall signal losses and increase power handling with the same or better isolation compared to the four-port microstrip technology is four-port combline coaxial resonator structures. To achieve filter design with a 180° different phase shift, the positive (90° inverter) and negative (-90° inverter) coupled filters are required. The design frequencies of the four-port combline diplexer are 1.73 GHz and 2.13 GHz for Rx and Tx modules, respectively. Two different designs of four-port diplexer prototypes, based on filter designs with similar and dissimilar Q-factors, are fabricated and measured to verify the new design technique. Finally, microwave interference cancellation techniques can be used in wireless communication systems where small size, low losses and low complexity are required.

Contents

Acknowledgements ……………………………………………………………iii

Abstract …………………………………………………………………….. iv

List of Figures viii

List of Tables xv

Abbreviations xvi

Notations.. xvii

Chapter 1 Introduction 1

1.1 Motivation 1

1.2 Application of microwave filters.. 1

1.3 Objectives 2

1.4 Scope of the study 3

1.5 Organisation of the thesis 3

Chapter 2 Literature Review of the Microwave Resonator Filter and Diplexer.. 4

2.1 Introduction 4

2.2 General types of filter and definitions................................. 4

2.3 Microwave resonators.. 5

2.4 Implementation of microwave filters................................... 5

2.5 Lumped-element resonator... 6

2.6 Microstrip resonator filter and diplexer 7

2.7 High-temperature superconductivity (HTS) filter and diplexer 10

2.8 Coaxial resonator filter and diplexer 12

2.9 Waveguide resonator filter and diplexer 15

2.10 Dielectric resonator filter and diplexer............................... 16

2.11 Other types and shapes of dielectric resonators.................. 19

2.12 Summary 21

Chapter 3 Four-port Diplexer Analysis 22

3.1 Introduction 22

3.2 Four-port diplexer analysis and synthesis............................ 22

3.3 Lumped-element model of the four-port diplexer 27

3.3.1 Second-order lumped-element impedance inverter filters 28

3.3.2 Second-order inverter coupled diplexer............................... 32

3.3.3 Second-order inverter coupled four-port diplexer 35

3.4 Summary 41
Chapter 4 Modelling and Development of a Low-Q Four-port Diplexer 42
4.1 Introduction 42
4.2 Chebyshev filter design 42
4.3 Microstrip resonator filter design 48
4.4 Half-wavelength microstrip resonator and Q-factor 49
4.5 Second-order microstrip resonator with coupled-feed 51
4.5.1 External coupling 52
4.5.2 Inter-resonator coupling 54
4.5.3 Physical simulation microstrip filter with coupled-feed 56
4.5.4 Second-order microstrip resonator diplexer with coupled-feed 58
4.5.5 Second-order microstrip four-port diplexer with coupled-feed 62
4.6 Second-order microstrip resonator with tapped-feed 66
4.6.1 External coupling 66
4.6.2 Inter-resonator coupling 69
4.6.3 Physical simulation of the microstrip filter with tapped-feed . 71
4.6.4 Second-order microstrip resonator diplexer with tapped-feed 73
4.6.5 Second-order microstrip four-port diplexer with tapped-feed 76
4.7 Summary 79
Chapter 5 Modelling and Development of a High-Q Four-port Diplexer 80
5.1 Introduction 80
5.2 Lumped-element combline filter design 80
5.3 Combline resonator filter with input transformer 85
5.4 Second-order combline resonator filter with the same Q-factors ... 87
5.4.1 External coupling 90
5.4.2 Positive inter-resonator coupling 92
5.4.3 Negative inter-resonator coupling 94
5.4.4 Physical simulation of the combline resonator filter 95
5.4.5 Second-order combline three-port diplexer 98
5.4.6 Second-order four-port diplexer with similar Q-factors 101
5.4.7 Fabrication and Measurement results 105

5.5 Second order combline resonator filter with the different Q-factors 108
5.5.1 External coupling 109
5.5.2 Inter-resonator positive coupling 111
5.5.3 Inter-resonator negative coupling 112
5.5.4 Physical simulation of the combline resonator filter 113
5.5.5 Second-order four-port diplexer with dissimilar Q-factors ... 116
5.5.6 Fabrication and measurement results 120
5.6 Summary 122
Chapter 6 Conclusion and future work 124
6.1 Conclusion 124
6.2 Comparison of each different filter methodology 125
6.3 Future work 128
References 129

List of Figures

Figure 1-1: RF front end of a cellular base station [3] 2

Figure 2-1: Four general types of ideal filters [10] 4

Figure 2-2: A comparison of size and insertion loss in various microwave filter technologies [11]. 6

Figure 2-3: Lumped-element resonator [12] 7

Figure 2-4: Basic microstrip structure [1] 8

Figure 2-5: Hairpin-line filter [13] 8

Figure 2-6: Microstrip open-loop (SIR) [13] 8

Figure 2-7: Structure of a five-order hairpin diplexer [17] 9

Figure 2-8: Structure of a microstrip diplexer with a joint T-shaped resonator [18] 10

Figure 2-9: A 10-pole HTS filter at 800 MHz [19] 11

Figure 2-10: Layout of the eight-pole quasi-elliptic filter [20] 11

Figure 2-11: Layout of the designed superconducting diplexer [25] 12

Figure 2-12: (a) Interdigital filters (b) Combline filters [12] 13

Figure 2-13: Combline resonator 14

Figure 2-14: The geometric structure of the fifth-order combline diplexer [35] 14

Figure 2-15: Rectangular waveguide resonator 15

Figure 2-16: (a) Schematic structure of the designed diplexer; (b) comparison between diplexers using or not using the resonant Y-junction as first-stage input [37] 16

Figure 2-17: The typical DR with support structure [19] 17

Figure 2-18: (a) A typical $TE_{01\delta}$ filter for cellular base-station and (b) measured performance [39] 18

Figure 2-19: Dual-mode dielectric resonator loaded cavity filter structure [41] 18

Figure 2-20: 3-D view of the triple-mode diplexer [42] 19

Figure 2-21: Prototype manufactured dielectric resonators, combline resonators and hybrid model [43] 20

Figure 2-22: Electromagnetic model of the fourth-order filter with mixed dielectric and coaxial resonators [45] 20

Figure 2-23: Photograph of the fourth-order filter with mixed coaxial and microstrip resonators [45] 21

Figure 3-1: A three-port network 22

Figure 3-2: A four-port network.. 23
Figure 3-3: Schematic diagram of the four-port diplexer using two back-to-back three-port diplexers with amplitude and 180° phase cancellation technique between Rx and Tx channels.................... 25
Figure 3-4: Simulated Tx/Rx isolation versus phase differences between ports 2 and 4 of two diplexers (Path 1 and Path 2) with the same Q-factors. The best Tx/Rx signal isolation is achievable at a 180° phase shift... 26
Figure 3-5: Simulated Tx/Rx signal isolation versus attenuation of two diplexers with different Q-factors. The reasonable Tx/Rx signal isolation of better than 40 dB is obtained when the attenuation difference between the two diplexers is less than 0.1 dB 27
Figure 3-6: Design steps of the insertion loss method.......................... 27
Figure 3-7: Equivalent circuit of impedance inverter 30
Figure 3-8: inverter coupled bandpass filter layout at 1.73 and 2.13 GHz... 31
Figure 3-9: The simulated second-order filter at 1.73 GHz 31
Figure 3-10: The simulated second-order filter at 2.13 GHz 32
Figure 3-11: Second-order inverter coupled diplexer layout at 1.73 and 2.13 GHz.. 33
Figure 3-12: The simulated second-order inverter coupled diplexer at 1.73 GHz and 2.13 GHz 34
Figure 3-13: The simulated isolation of the inverter coupled diplexer . 34
Figure 3-14: Simulated wide-band response of the second-order inverter coupled 3-port diplexer 35
Figure 3-15: Four-port diplexer topology and its equivalent circuit based on a second-order filter consisting of external coupling, internal coupling coefficients and element values of resonators with a 180° phase shift between ports 2 and 4 37
Figure 3-16: Simulation results of S-parameters of the four-port diplexer design at Tx=2.13 GHz, Rx=1.73 GHz................................ 38
Figure 3-17: Simulated wide-band response of the second-order inverter coupled four-port diplexer 38
Figure 3-18: Simulation results of phases of S_{13} and S_{24} with a 180° phase difference at 2.13 GHz 39
Figure 3-19: Simulation results of isolation of the four-port diplexer design at Tx=2.13 GHz, Rx=1.73 GHz 40
Figure 3-20: Isolation results compared to mismatched antenna port. 40
Figure 4-1: Equivalent circuit of the impedance inverter....................... 43
Figure 4-2: Capacitively coupled filter layout 45

Figure 4-3: Capacitively coupled lumped-element filter response at 1.95 GHz 46
Figure 4-4: Capacitively coupled lumped-element filter response at 2.14 GHz 47
Figure 4-5: TXLINE tool for calculating length and width of the microstrip line of dielectric constant 6.15 at 1.95 GHz 52
Figure 4-6: Microstrip open-loop resonator with coupled-feed for extracting the external quality factor 53
Figure 4-7: Response of S_{21} of the microstrip with coupled-feed 53
Figure 4-8: Q_e factor versus the distance of coupling line to the resonator 54
Figure 4-9: Two microstrip open-loop lines for extracted coupling coefficient 55
Figure 4-10: A typical frequency response of a decoupled resonator structure for extracting the coupling coefficient 55
Figure 4-11: The coupling coefficient K versus the spacing(s) between two resonators 56
Figure 4-12: Second-order microstrip open-loop resonator filter with coupled-feed 57
Figure 4-13: The second-order microstrip filter simulated at 1.95 GHz 57
Figure 4-14: The second-order microstrip filter simulated at 2.14 GHz 58
Figure 4-15: Second-order microstrip diplexer with coupled-feed 59
Figure 4-16: The simulated response of the second-order diplexer at 1.95 GHz and 2.14 GHz 60
Figure 4-17: The isolation of the microstrip diplexer with coupled-feed 60
Figure 4-18: Wide-band response of the second-order microstrip diplexer with coupled-feed 61
Figure 4-19: Second-order four-port diplexer with coupled-feed line [53] 63
Figure 4-20: The simulated response of the second-order four-port diplexer with coupled-feed line at 1.95 GHz and 2.14 GHz 64
Figure 4-21: Simulated isolation of the four-port diplexer compared to the three-port diplexer 64
Figure 4-22: Simulated phases of S_{31} and S_{24} with 179.56° phase difference at 2.14 GHz 65
Figure 4-23: Wide-band response of the second-order microstrip open-loop diplexer with coupled-feed line 65
Figure 4-24: TXLINE tool for calculating length and width of the microstrip line of a dielectric constant 10.2 at 1.95 GHz 66

Figure 4-25: Microstrip resonator with tapped-feed for extracted external quality factor 67

Figure 4-26: Response of S_{21} of the microstrip with tapped-feed 67

Figure 4-27: External quality factor Q_e versus the distance of the coupling line to the resonator 68

Figure 4-28: Two microstrip open-loop resonators for extracted coupling coefficient 69

Figure 4-29: A typical frequency response of a decoupled resonator structure for extracting the coupling coefficient........ 70

Figure 4-30: The coupling coefficient K versus the spacing between two resonators (s) 70

Figure 4-31: Second-order microstrip open-loop resonator filter with tapped-feed 71

Figure 4-32: The microstrip filter with tapped-feed simulated at 1.95 GHz 72

Figure 4-33: The microstrip filter with tapped-feed simulated at 2.14 GHz 72

Figure 4-34: Geometry of the microstrip open-loop diplexer with tapped-feed 73

Figure 4-35: Simulated response of the microstrip open-loop diplexer with tapped-feed design at 1.95 GHz and 2.14 GHz 74

Figure 4-36: Simulated response of signal isolation of the diplexer 75

Figure 4-37: Wide-band response of the second-order microstrip diplexer 75

Figure 4-38: Second-order four-port diplexer with tapped-feeds.......... 77

Figure 4-39: Simulated results of the microstrip four-port diplexer with tapped-feed 77

Figure 4-40: Comparison of simulated results of isolation (S_{32}) between three-port diplexer and four-port diplexer 78

Figure 4-41: Simulated phase responses of S_{31} and S_{24} with 179.92° phase difference at 2.14 GHz 78

Figure 4-42: Wide-band response of the microstrip four-port diplexer 79

Figure 5-1: Equivalent circuit of impedance inverter 82

Figure 5-2: Equivalent circuit of the second-order combline filter with the introduction of the input transformer 83

Figure 5-3: Simulated response of the combline filter at 1.73 GHz....... 84

Figure 5-4: Simulated response of the combline filter at 2.13 GHz....... 85

Figure 5-5: Combline resonator by using metallic rod 87

Figure 5-6: The magnitude and vector of E-field distribution of the combline resonator ... 89

Figure 5-7: The magnitude and vector of H-field distribution of the combline resonator ... 89

Figure 5-8: Combline resonator for extracted external quality factor .. 90

Figure 5-9: Response of S_{21} for extracted external quality factor ... 91

Figure 5-10: External quality factor Q_e versus the distance of the input transformer to the resonator ... 91

Figure 5-11: Two combline resonators for extracted coupling coefficient ... 92

Figure 5-12: A typical frequency response of the decoupled resonator structure for extracting the coupling coefficient ... 93

Figure 5-13: The coupling coefficient K versus the spacing between two resonators (sp) ... 93

Figure 5-14: Two combline resonators for extracted coupling coefficient ... 94

Figure 5-15: The coupling coefficient K versus the length of metallic wire ... 94

Figure 5-16: Geometrical structure of the positive coupling combline resonator filter ... 95

Figure 5-17: Geometrical structure of the negative coupling combline resonator filter ... 96

Figure 5-18: Simulated response of the second-order combline filter at 1.73 GHz ... 96

Figure 5-19: Simulated responses of the positive and negatively coupled filters simulated by HFSS program at 2.13 GHz ... 97

Figure 5-20: Simulated responses of comparison of the phase between the positive and negatively coupled filters at 2.13 GHz . 97

Figure 5-21: Geometrical structure of the second-order combline diplexer ... 99

Figure 5-22: Simulated response of the second-order three-port diplexer simulated by HFSS program at 1.73 GHz and 2.13 GHz.. 99

Figure 5-23: Simulation of signal isolation of the three-port diplexer 100

Figure 5-24: Wide-band response of the second-order combline diplexer ... 100

Figure 5-25: Geometrical structure of the second-order four-port diplexer with equal Q-factors ... 102

Figure 5-26: Simulation results of S-parameters of the four-port diplexer with the same Q-factors at Rx=1.73 GHz, Tx= 2.13 GHz 103

Figure 5-27: Simulation results of signal isolation, S_{32}, of the four-port diplexer with similar Q-factors and the three-port diplexer......... 103

Figure 5-28: Simulation results of phase of S_{31} and S_{24} at 2.13 GHz .. 104

Figure 5-29: Simulations of wide-band response of the four-port diplexer with the same Q-factors.. 104

Figure 5-30: Photographs of the four-port diplexer with the same Q-factors 106

Figure 5-31: Measurement results of S-parameters of the four-port diplexer with similar Q-factors where Q_1=Q_2=1800 at Tx=2.13 GHz, Tx=1.73 GHz 106

Figure 5-32: Measurement results of signal isolation, S_{32}, of the four-port diplexer with similar Q_1-factors (35.15 dB) and the three-port diplexer (26.28 dB) 107

Figure 5-33: Measurement results of phases of S_{13} and S_{24} with 177.65° phase difference at 2.13 GHz 107

Figure 5-34: Combline resonator by using metallic rod 108

Figure 5-35: The magnitude and vector of E-field distribution of the combline resonator... 109

Figure 5-36: The magnitude and vector of E-field distribution of the combline resonator... 109

Figure 5-37: Combline resonator for extracted external quality factor 109

Figure 5-38: External quality factor Q_e versus the distance of input transformer to the resonator... 110

Figure 5-39: Two combline resonators for extracted coupling coefficient 111

Figure 5-40: The coupling coefficient K versus the spacing between two resonators (sp).. 111

Figure 5-41: Two combline resonators for extracted coupling coefficient 112

Figure 5-42: The coupling coefficient K versus the length of metallic wire (cp) 112

Figure 5-43: Geometrical structure of the positive coupling combline resonator filter.. 113

Figure 5-44: Geometrical structure of the negative coupling combline resonator filter.. 114

Figure 5-45: Simulated response of the combline filter at 1.73 GHz... 114

Figure 5-46: Simulated responses of the positive and negatively coupled filters at 2.13 GHz 115

Figure 5-47: Simulated responses comparing the phases between the positive and negatively coupled filters at 2.13 GHz 115

Figure 5-48: Geometrical structure of the second-order four-port diplexer with dissimilar Q-factors.. 117

Figure 5-49: Simulation results of S-parameters of the four-port diplexer with dissimilar Q-factors at Rx=1.73 GHz, Tx= 2.13 GHz.. 118

Figure 5-50: Simulation results of signal isolation, S_{32}, of the four-port diplexer with dissimilar Q-factors and three-port diplexer.......... 118

Figure 5-51: Simulation results of phase of S_{31} and S_{24} with 178.35 phase difference at 2.13 GHz 119

Figure 5-52: Simulations of wide-band response of the four-port diplexer with different Q-factors 119

Figure 5-53: Photographs of the four-port diplexer with different Q-factors 120

Figure 5-54: Measurement results of S-parameters of the four-port diplexer with dissimilar Q-factors where Q_1=1800, Q_2=3600 at Tx=2.13 GHz, Tx=1.73 GHz 121

Figure 5-55: Measurement results of signal isolation, S_{32}, of the four-port diplexer with the dissimilar Q-factors (40.11 dB) and three-port diplexer (26.28 dB) 121

Figure 5-56: Measurement results of phases of S_{31} and S_{24} with 178.33° phase difference at 2.13 GHz 122

Figure 6-1: Typical I/O coupling structures for open-loop resonator filters (a) Coupled-line coupling (b) Tapped-line feed 125

Figure 6-2: Typical coupling structures for open-loop resonator filters (a) Mixed coupling (b) Electric coupling 126

Figure 6-3: Combline resonator 127

List of Tables

Table 2-1: Comparison between various modes of operation [11] 17

Table 3-1: Specifications of the bandpass filter design 28

Table 3-2: Element values of second-order inverter coupled filters 31

Table 4-1: Specifications of the microstrip bandpass filter design 42

Table 4-2: Element values of the second-order Chebyshev filters at 1.95 and 2.14 GHz 45

Table 4-3: Specifications of the microstrip bandpass filter design 48

Table 4-4: Simulated dimensions of the microstrip open-loop resonator filter with coupled-feed 56

Table 4-5: Simulated dimensions of the microstrip diplexer with coupled-feed 59

Table 4-6: Simulated dimensions of the four-port microstrip diplexer with coupled-feed 62

Table 4-7: Simulated dimensions of the microstrip open-loop resonator filter with tapped-feed 71

Table 4-8: Simulated dimensions of the three-port diplexer with tapped-feeds 73

Table 4-9: Simulated dimensions of the four-port diplexer with tapped-feeds 76

Table 5-1: Specifications of the combline bandpass filter design 80

Table 5-2: Element values of the second-order combline filters at 1.73 and 2.13 GHz 83

Table 5-3: Specifications of the combline diplexer design 85

Table 5-4: Eigen modes and Q factors of metallic combline resonator 88

Table 5-5: Simulated dimensions of the combline resonator filter 95

Table 5-6: Simulated dimensions of the second-order combline resonator diplexer 98

Table 5-7: Simulated dimensions of the combline diplexer 101

Table 5-8: Eigen modes and Q factors of metallic combline resonator 108

Table 5-9: Simulated dimensions of the combline resonator filter 113

Table 5-10: Simulated dimensions of the four-port combline resonator diplexer with different Q-factors 116

Table 5-11: Comparison of four-port diplexer with the state-of-the-art diplexer 123

Abbreviations

DSRs	Dual-resonance spiral resonators
DRs	Dielectric resonators
GHz	Gigahertz
HTS	High Temperature Superconducting
IL	Insertion loss
MMICs	Microwave monolithic integrated circuits
PCB	Printed circuit board
RL	Return loss
RF	Radio frequency
Rx	Receive
SIR	Stepped-impedance resonator
SSRs	Single-resonance spiral resonators
Tx	Transmit
TE	Transverse electric
TEM	Transverse electromagnetic
TM	Transverse magnetic

Notations

$K_{r,r1}$	Coupling coeffiecient between resonator r and r+1
Y	Admittance
C	Capacitor
K	Characteristic impedance
L	Inductor
N	Order of the filter
Q	Quality factor
Q_e	External quality factor
R	Resistance
S	Ratio of stopband to passband bandwidth
V	Speed of light
F	Frequency
$\tan\delta$	Dielectric loss tangent
Z_c	Characteristic impedance
λ_g	Guided wavelength
β	Propagation constant
v_p	Phase velocity
Θ	Electrical length
c	Velocity of light
ε_{re}	Effective dielectric constant
α_c	Attenuation due to conductor loss
R_s	Surface resistivity of the conductor
μ_0	Permeability of free space
σ	Conductivity of copper
α_c	Attenuation due to conductor loss
α_d	Attenuation due to dielectric loss

Chapter 1
Introduction

1.1 Motivation

Filters play important roles in many RF/microwave applications. They are used to separate or combine different frequencies. The electromagnetic spectrum is limited and has to be shared. Filters are used to select or confine the RF/microwave signals within assigned spectral limits. Emerging applications such as wireless communications continue to challenge RF/microwave filters with ever more stringent requirements with higher performance, smaller size, lighter weight, and lower cost [1]. A few decades ago, a variety of materials were developed to fabricate the bandpass filter, e.g. lumped-elements (LC circuit), microstrip configurations, coaxial configurations, dielectric filters, cavity filters and high temperature superconductors [1, 2]. As the main design considerations of microwave resonators are the resonator size, Q-factor, spurious performance, and power handling capability. The Q-factor represents the inherent losses in the resonator. The higher the losses are, the lower is the Q value. It is therefore desirable to use resonators with high Q factors. Therefore, it is challenging to design a filter at low cost and high performance using a variety of materials.

1.2 Application of microwave filters

Diplexers, which are usually set in the form of filters, are three-port networks and are commonly used to combine or separate different signal frequencies. The RF front end in a radio cellular network uses bandpass filters to discriminate two different frequency bands for transmitting (Tx) and receiving (Rx) channels when a single antenna is shared in the base station, as shown in Figure 1-1. Generally, relative high-power signals, with an order of 30W, are generated and flow in the Tx channel. These high-power signals generated in the Tx branch can easily interfere with the Rx channel and can even destroy some Rx components, e.g. low-noise amplifiers, etc., if the signal isolation between Tx and Rx channels is not sufficiently high [3]. Therefore, a design technique to increase signal isolation while offering ease of design and superior figure-of-merit, e.g. low signal losses as well as low cost and small size, is required.

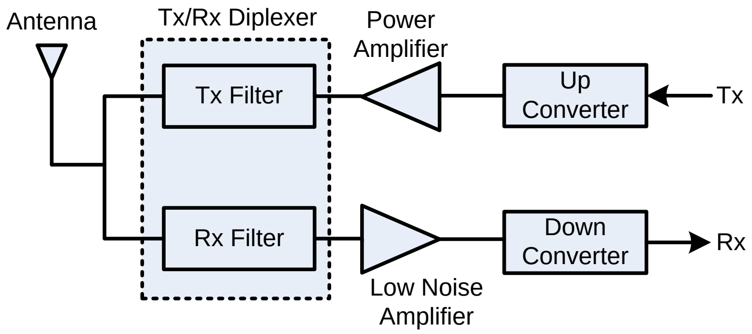

Figure 1-1: RF front end of a cellular base station [3]

Normally, the most common diplexer structure is to combine bandpass filters through a three-port impedance matching network. Most diplexer designs with high Tx/Rx isolation require high order filters, resulting in a very complicated filter design and fabrication. Consequently, these complicated higher-order filter architectures increase overall signal losses as well as having a high fabrication cost and large diplexer size. Diplexer designs based on microstrip structure can achieve low cost, small filter size and ease of integration but provide low power handling and high signal losses due to dielectric and ohmic losses [4-7]. An alternative technology to reduce overall signal losses and increase power handling with the same or better isolation compared to the microstrip technology is combline coaxial resonator structures [8, 9]. However, the main drawback of this design technique is that the degree of the filters increases linearly when higher signal isolation is required because this conventional diplexer structure design is still based on three-port networks. To achieve higher signal isolation, a higher-order conventional diplexer design technique can be used but at the costs of higher signal losses, complexity, cost and bigger size.

1.3 Objectives

The objectives of this thesis are as follows:

1) To propose a microwave interference cancellation technique for high Tx/Rx signal isolation.

2) To design a four-port diplexer that is small in size and lightweight by using a low Q-factor diplexer compared to the previous solutions.

3) To consider possible solutions for filters and diplexer with low cost, low loss and high power by using a combline resonator with similar and dissimilar Q-factor diplexers.

1.4 Scope of the study

The aim of this project is to design a diplexer structure for high Tx/Rx signal isolation with relatively low-order filter topology. Because the main drawback of conventional diplexer is that the degree of the filters increases linearly when higher signal isolation is required and the conventional diplexer is still based on three-port components. The new design technique is based on two back-to-back second-degree diplexers, which are combined to form a four-port diplexer. The design technique is based on amplitude and phase cancellation between two diplexer branches of the four-port diplexer. Therefore, the best Tx/Rx signal isolation can be obtained by using four-port diplexer structure. The majority of this project focuses on the realization of the physical structure using AWR Microwave Office and 3D HFSS simulator.

1.5 Organisation of the thesis

The project organisation is as follows. Chapter 1 introduces the motivation to design a filter for RF and microwave communications. Applications of microwave filters in cellular base stations are also introduced here. The objectives and scope of the study are also defined in this chapter.

Chapter 2 introduces microwave resonator filters and a literature review of related previous structures in the topic of microwave resonator filters and diplexer.

Chapter 3 analyses three-port and four-port diplexers. The second-order lumped-element Chebyshev filter for diplexer and four-port diplexer is explained in details. Then, design examples and results are presented.

Chapter 4 presents the filters and diplexer design of a low-Q four-port diplexer. The microstrip filter and diplexer are discussed in detail. Then, the microstrip resonator filters and diplexer using coupled-feed and tapped-feed are presented.

Chapter 5 introduces the filters and diplexer design of a high-Q four-port diplexer. The combline filter and diplexer are simulated and fabricated. Then, the combline resonator filters and diplexer using the same Q-factors and dissimilar Q-factors are also successfully proved.

Lastly, Chapter 6 introduces the major conclusion of this work and the contributions from this work to suggest possible future work.

Chapter 2

Literature Review of the Microwave Resonator Filter and Diplexer

2.1 Introduction

In this chapter, the general types of filter and their definitions are described. A review of implemented filter and diplexer structures is also discussed here. The various types of microwave filter and diplexer technologies are explained, such as lumped-element resonator, microstrip resonator filter, coaxial resonator filter, waveguide resonator filter, superconductor structure and dielectric resonator filter, as well as other types and shapes of dielectric resonators.

2.2 General types of filter and definitions

The filter's frequency response is widely discussed in filter design because it is the filter's basic characteristic. Filters are mainly classified into four types: lowpass filter, highpass filter, bandpass filter and bandstop filter. The relationship between attenuation coefficient and normalised angular frequency of the four general types of filter is shown in Figure 2-1 [10].

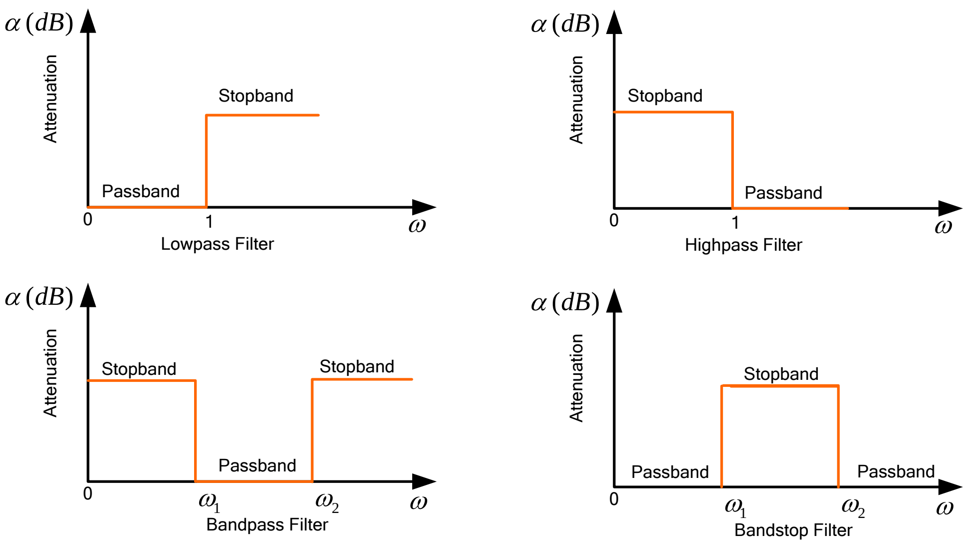

Figure 2-1: Four general types of ideal filters [10]

Firstly, the lowpass filter is defined as one where a frequency band lower than the cut-off frequency can pass through the circuit. In other word, the high frequency band is rejected from the circuit. Secondly, the highpass filter will permit high frequencies to pass through the circuit when the frequency band is higher than the cut-off frequency. Thirdly, the bandpass filter allows certain types of frequency to pass through the circuit. In another aspect, the bandpass filter also combines the lowpass and highpass filters to create the bandpass filter. Finally, the band reject or bandstop filter is explained where the frequency band in the bandwidth cannot pass into the circuit.

2.3 Microwave resonators

A resonator is a component that is capable of storing both electric and magnetic energy in certain frequencies where inductor L stores the magnetic energy and capacitor C stores the electric energy. It can be described by stating that the simple model of a resonator at resonant frequency is exchanged energy between capacitor and inductor, where resonant frequency is defined as $f = 1/\,2\pi\sqrt{LC}$. At resonant frequency of a resonator, the energy stored in the electric field equals the energy stored in the magnetic field. Consequently, the field distribution in materials at the resonant frequency can also be determined by the various shapes and forms of physical microwave structures. There are different implemented resonators which are formed as lumped-elements (LC resonators), planar resonators, coaxial combline resonators, dielectric combline resonators and waveguide resonators. Microwave resonators can support an infinite number of frequency modes which are not the same as lumped-elements. The latter only have one resonant frequency. Furthermore, the main considerations of microwave filter design are size reduction, unloaded Q-factor, spurious performance and their power-handling capability. The unloaded Q can be used to define the inherent losses in their resonators. The lower the losses, the higher the Q value [11].

2.4 Implementation of microwave filters

As mentioned before, certain types of structure and technologies are designed in microwave resonators and filters such as lumped-element, planar (microstrip, CPW), coaxial, waveguide, dielectric and superconductor technology. Each type of microwave technology has its specific advantages and disadvantages.

As illustrated in Figure 2-2, comparisons between size and insertion loss in various microwave resonator filters are discussed. The lumped-element resonators have a small size but they offer low Q-factor. The Q-factor represents the inherent losses in the resonator. The higher the losses are, the lower is the Q value. However, lumped element realizations of microwave filters are not often use because the wavelength is so short compared with the dimensions of circuit elements. Microstrip resonators or planar resonators have a higher Q-factor than the Q-factor in lumped-element ones but have a lower Q-factor than in three-dimensional (3D) cavity-type resonators [11]. The dielectric resonators offer high Q-factor as well as waveguide resonators. However, waveguide resonators are bigger in size. The coaxial resonators have a lower Q-factor and bigger volume compared to the dielectric resonators. Moreover, in wireless base station applications considering filter design with low loss and high power handling, the cavity-type resonator (coaxial, dielectric and waveguide resonator) is more interesting than planar technologies and it is also more interesting to use in microwave technologies than superconductor filters, which require more complex technologies in the realisation process to achieve high Q values.

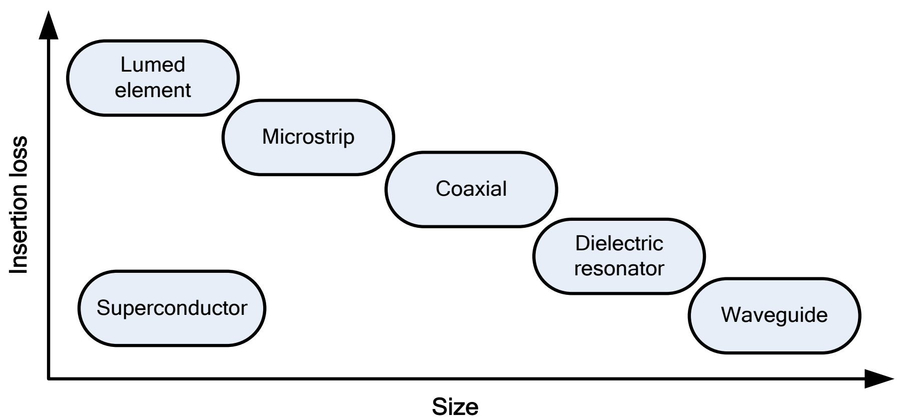

Figure 2-2: A comparison of size and insertion loss in various microwave filter technologies [11].

2.5 Lumped-element resonator

Figure 2-3 represents a lumped-element resonator that can be printed on a dielectric substrate in the form of inductor and capacitor. Lumped-element resonators have a large reduction in size and wide spurious free window. Typically, lumped-element filters are employed in low frequency applications which are suitable for integration in microwave monolithic integrated circuits (MMICs) or RFIC circuits [11]. However, lumped-element resonators offer low Q value between 10 and 50 at 1 GHz.

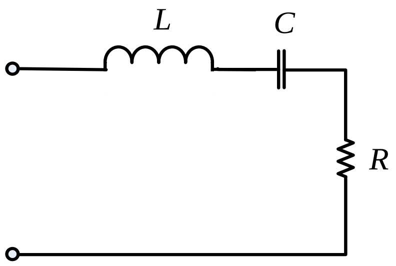

Figure 2-3: Lumped-element resonator [12]

2.6 Microstrip resonator filter and diplexer

The microstrip line structure is shown in Figure 2-4. It is used for fabricating microwave circuits that are low cost, small size and easy to integrate into other microwave devices. Its structure consists of three layers: the top layer is a conducting strip that is presented as *W* (width) and *t* (thickness). This layer has a significant role in fabricating the circuit pattern of the microstrip structure. The middle layer is a dielectric substrate layer. This layer is defined as h (height) and ε_r (dielectric constant). The bottom layer is a ground plane. In addition, the microstrip structure is called the 'printed circuit board' (PCB), which is used in the fabrication microwave equipment.

For this reason, based on microstrip structure or planar resonator, the filter can be fabricated on this structure. Generally, power losses in the microstrip structure will be affected by conductor loss, dielectric loss and radiation loss [1]. The microstrip structure typically offers a Q value in the range of 50-300 at 1 GHz. If the planar filters are needed to implement with high Q values, it is necessary to use the superconductor technology, and the planar resonators can offer Q values ranging from 20,000 to 50,000 at 1 GHz. However, very low temperature, below 90K, is needed to cool down the structure [11]. An example of microstrip filter design is folded parallel-coupled-line filters, known as hairpin filters. They are purposed to reduce the size of parallel-coupled-line filters, as shown in Figure 2-5. Furthermore, In order to reduce interference by keeping out-of-band signals from reaching a sensitive receiver, a wider upper stopband, including $2f_0$, where f_0 is the midband frequency of a bandpass filter, may also be required. However, many planar bandpass filters that are comprised of half-wavelength resonators inherently have a spurious passband at $2f_0$. A cascaded lowpass filter or bandstop filter may be used to suppress the spurious passband at a cost of extra insertion loss and size. Although quarter-wavelength resonator filters have the first spurious passband at $3f_0$, they require short-circuit (grounding) connections with via holes, which is not quite compatible with planar fabrication techniques. Lumped-element filters ideally do not have any spurious passband at all, but they suffer from higher loss and poorer power handling capability. Bandpass filters using stepped impedance resonators is able to control spurious response with a compact filter size because of the effects of a slow wave. The configuration is composed of a microstrip line with both ends loaded with folded open-stubs as Figure 2-6. The folded arms of open-stubs are not only for increasing the loading capacitance to ground but also for the purpose of wide upper stopband.

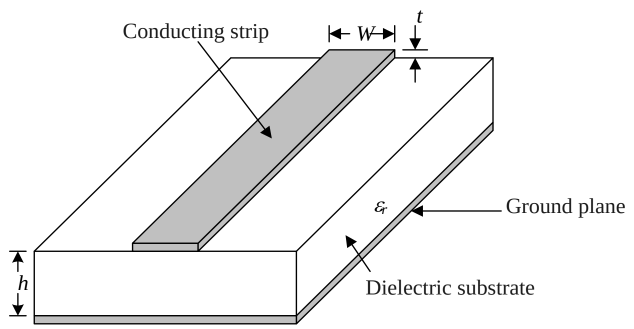

Figure 2-4: Basic microstrip structure [1]

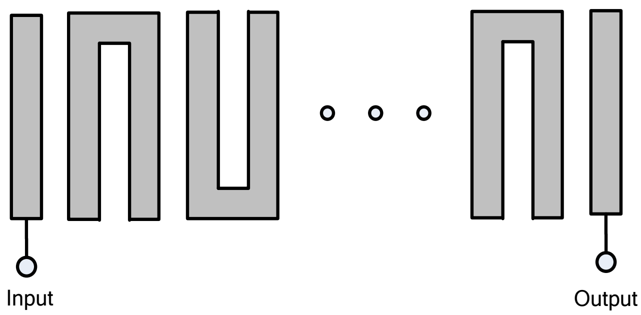

Figure 2-5: Hairpin-line filter [13]

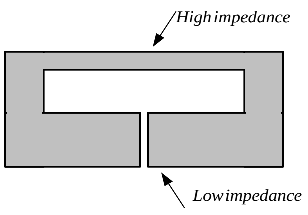

Figure 2-6: Microstrip open-loop (SIR) [13]

To design the microstrip diplexer structure, the microstrip T-junction is used to combine two filters with the antenna as shown in [14], the transmission zero of the upper sideband of lower-frequency channel and lower sideband of higher-frequency channel is designed and T-junction is used to combine two filters. Therefore, very high diplexer output isolation can be achieved. Another design technique by using microstrip T-junctions with open stubs is also introduced in [15], a very compact duplexer based on miniaturized loaded-close-loop dual resonators is introduced and two different dual resonators are used to establish the two bands by using T-junction with open stub at common junction. Moreover, a stepped impedance transformer matching is used to reduce the required microstrip line length between two channels [16]. The proposed planar diplexer is designed on the basis of a dual-mode resonator approach in order to achieve the required specifications (compact size with high performance). Furthermore, a tapped-stub has also been introduced to combine the TX port and the RX port in [17]. The tapped open stub is added in the lower frequency because an upper attenuation pole is required to suppress it, as shown in Figure 2-7. In order to reduce the size of the diplexer, both common feed and resonator can be used in the microstrip diplexer with a joint T-shaped resonator presented in [18]. The simulated isolation of the diplexer is around 39 dB. Schematic layout of the diplexer structure using the T-shaped resonator combines two second-order bandpass filters, as shown in Figure 2-8. Port 1 uses coupled feeding, whilst ports 2 and 3 use tapped-feeding. All in all, as the diplexer consists of two filters, the simplest way to design a diplexer that is small in size is to reduce the size of the resonator in both filters, and the high signal isolation achieves when high order of the filters is required.

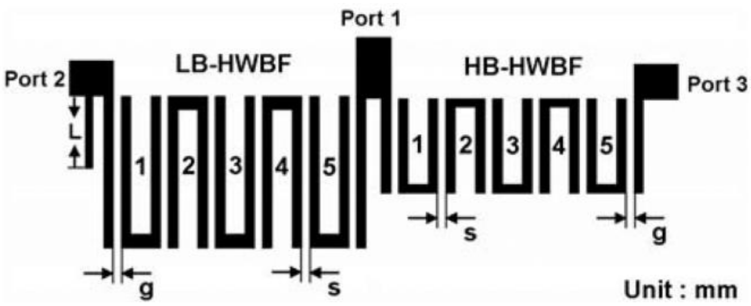

Figure 2-7: Structure of a five-order hairpin diplexer [17]

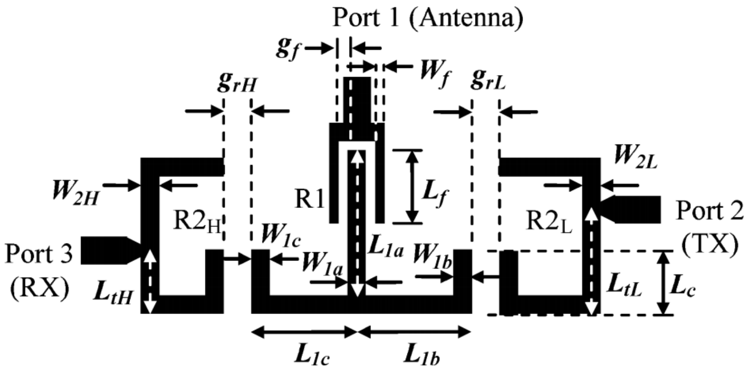

Figure 2-8: Structure of a microstrip diplexer with a joint T-shaped resonator [18]

2.7 High-temperature superconductivity (HTS) filter and diplexer

Nowadays, it is very interesting to design compact low-loss microwave filters using High-Temperature Superconducting (HTS). The operated temperature of HTS could be in the 60–80K range. However, this cooling system is made with special material and technologies such as liquid nitrogen, and also the use of small practical electromechanical 'cryocoolers'. Most HTS microwave filters are made of microstrips which are formed by using a thin-film HTS ground plane at the bottom of the substrate and HTS circuit lines are patterned on the top, the substrate being mounted in a normal metal housing. [12]. Superconductor films are deposited on a low loss dielectric substrate. The substrates widely used are lanthanum aluminates (LaALO3) with a dielectric constant of εr = 24 and magnesium oxides (MgO) with εr = 9.5. Therefore, planar microstrip filter configurations can be realised in HTS technology by replacing metal films with HTS films. The Q-value of the filter can be increased to a high value. For instance, a half-wave length microstrip resonator made of gold film on a LaALO3 substrate would typically have an unloaded Q value of 400. Replacing the gold films with HTS films would provide the HTS resonator with an unloaded Q value of around 30,000 while using the same substrate [19]. Figure 2-9 shows an example of a 10-pole HTS planar filter built using superconductor technologies.

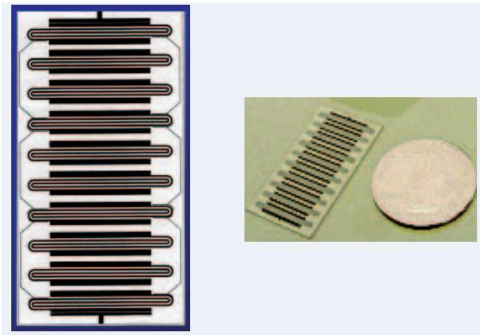

Figure 2-9: A 10-pole HTS filter at 800 MHz [19]

In another example, the filter is fabricated on a 0.5 mm thick MgO substrate with 600 nm thickness and YBCO HTS thin films are put on both sides. The line patterns are made on one side, and the ground is on the other side. The relative dielectric constant (ε_r) is 9.65 at low temperature. The HTS filter is designed at 610 MHz with very sharp cut-off response and low insertion loss at 0.3 dB [20]. The layout of the eight-pole HTS filter is shown in Figure 2-10.

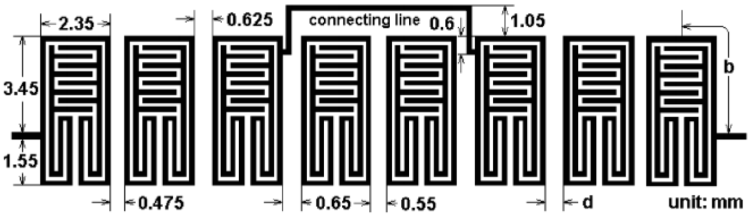

Figure 2-10: Layout of the eight-pole quasi-elliptic filter [20]

Moreover, the HTS diplexer can be implemented by using HTS filters. A compact L-band microstrip HTS manifold-coupled input diplexer has been presented for satellite communication application [21]. To improve the out-of-band rejection at a spurious frequency band, the HTS bandstop filter has been added to the diplexer structure. The optimised HTS spiral diplexers and multiplexers can also be realised, as in [22, 23]. A compact HTS diplexer with low insertion loss and wide stopband is presented in [24]. Each frequency band of the diplexer is composed of single-resonance spiral resonators (SSRs) and dual-resonance spiral resonators (DSRs).

According to the research paper [25], a small High-Temperature Superconducting (HTS) diplexer for mobile (1.8 GHz) and wireless local area (2.4 GHz) networks presents a stub-loaded spiral resonator as a signal splitter and a common resonator for both channels. Both transmission lines are used to create a cross coupling between the common port and fourth resonator of the lower and higher frequency bands. The diplexer is fabricated on a YBa2Cu3Oy (YBCO) thin film and polished MgO substrate wafer, as can be seen in Figure 2-11.

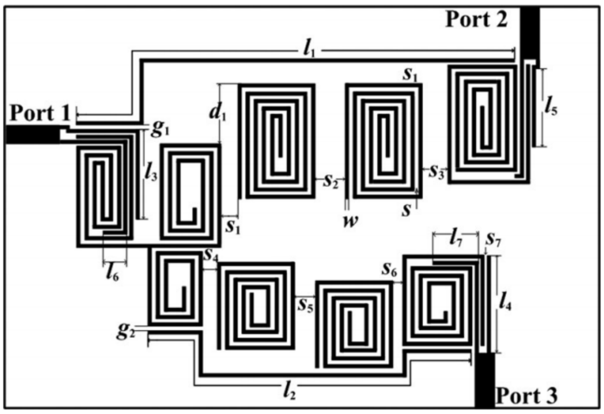

Figure 2-11: Layout of the designed superconducting diplexer [25]

2.8 Coaxial resonator filter and diplexer

One of the most typical TEM transmission-line resonator filters utilising transverse electromagnetic modes (TEM) or quasi-TEM modes is the coaxial resonator. Coaxial TEM filters are regularly combline or interdigital structures. The combline resonators are all short-circuited at the same end but the opposite ends of the resonators are mounted by capacitors which are connected to the ground [3]. In the case of the interdigital filters, they are normally designed when wider bandwidth is needed. The interdigital filters have quite a similar configuration to the combline filters but have inverted resonators. Generally, combline resonator structure can be used in design of filter with bandwidth from 1-50% in wireless base stations [19]. The structure of interdigital and combline resonators is shown in Figure 2-12.

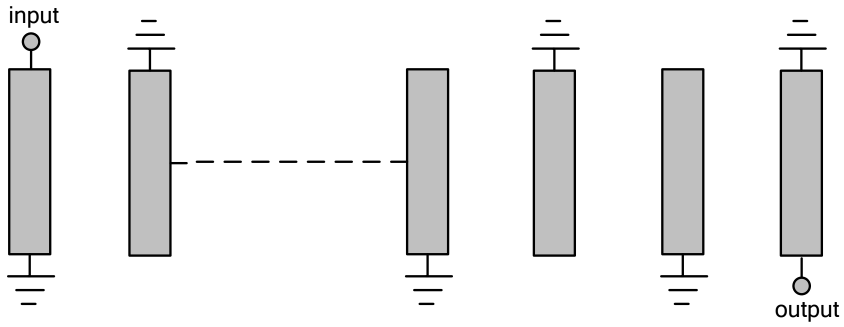

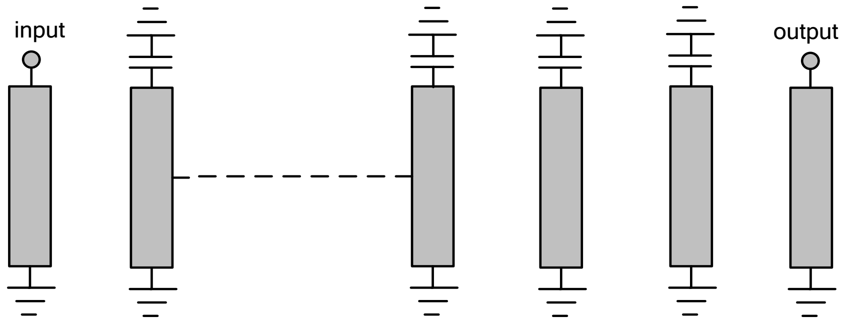

Figure 2-12: (a) Interdigital filters (b) Combline filters [12]

In 1963, the first combline filters were presented by G. Matthaei [26]. Arrays of parallel resonators are arranged in the form of short-circuited at one end and they have a lumped capacitance between the opposite end and the ground. Combline resonator filters are a widely used type of coaxial filters owing to their compactness and wide spurious free window. They also have an electrical length of less than λg/4 wavelength. From Figure 2-13, it is based upon the fact that the realised capacitance gap occurs when there is a gap between the resonator and the ground plane spacing; meanwhile, the other end of resonator is short circuited with ground spacing. The conventional combline structures have a nominal Q factor because of their inner conductor rod. They offer a Q factor in the range of 3,000–5,000 at 1,800 MHz [19]. The Q factor of combline resonators can be increased by using different techniques such as base rounding [27] and periodic 6-disk loaded combline resonator [28]. In addition, the power handling of the combline resonator filter can achieve a 15% improvement compared with the power-handling capability of traditional combline resonators while having the same size and the same Q of the traditional combline resonator designed by using the mushroom-shaped post. The cylindrical-shaped post has a diameter of the half sphere on the top of the post [29].

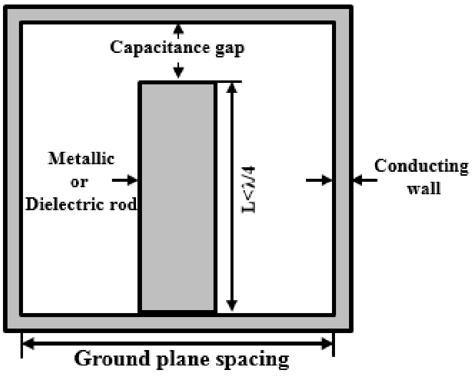

Figure 2-13: Combline resonator

There are high losses in conventional coaxial combline resonators, which can be minimised by replacing the metallic rod with a high permittivity dielectric rod. The advantage of the dielectric combline resonator filter is that it can increase the 50% of Q factor in conventional combline resonator filters while maintaining the same overall size [19]. Therefore, the use of the dielectric combline resonator not only achieves a higher Q than that of the conventional combline resonator but also keeps all the advantages of the conventional combline resonator, such as good spurious performance and low cost [30-34].

Moreover, the folded combline diplexer is able to minimise the diplexer's overall size, as presented in [35]. The two bandpass filters are combined with a coaxial feed input. The isolation is lower than -65 dB over the whole passband. The geometric structure of the fifth-order combline diplexer is shown in Figure 2-14.

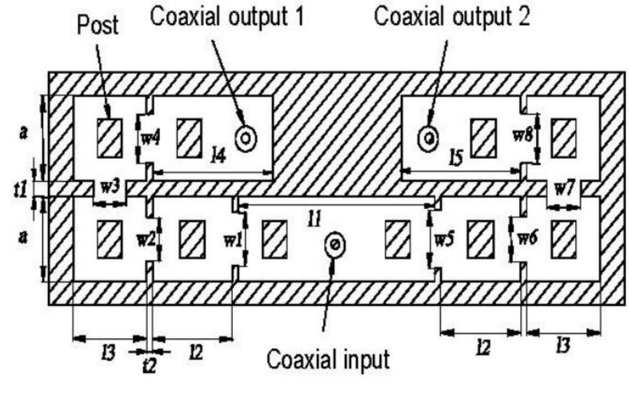

Figure 2-14: The geometric structure of the fifth-order combline diplexer [35]

2.9 Waveguide resonator filter and diplexer

A waveguide structure is used to guide electromagnetic energy in a particular direction. Typically, the waveguides are formed in rectangular and circular shapes. The short-circuited walls from both ends form a closed box waveguide structure that is called a cavity resonator. The cavity can store electric and electromagnetic energy dissipated power in metallic walls. The cavity resonator can be coupled with a small aperture or a small probe or loop. The TEM mode cannot exist in the waveguide because it is of a single conductor. The simplest modes in the waveguide are TE_{mn}, TM_{mn}. Where m and n represent the half-wave variations of field in the ‘x’, and ‘y’, direction of rectangular waveguide, the fundamental dominant mode is typically TE_{101} [3, 36]. Normally, the aspect ratio of a rectangular waveguide is a=2b and is mostly used at microwave frequencies. They offer very high Q values ranging from 10,000 to 50,000 suitable for designing low loss devices but the filter construction still suffers from being large in size, which is significant when designing a communications system. The rectangular waveguide resonator is illustrated in Figure 2-15.

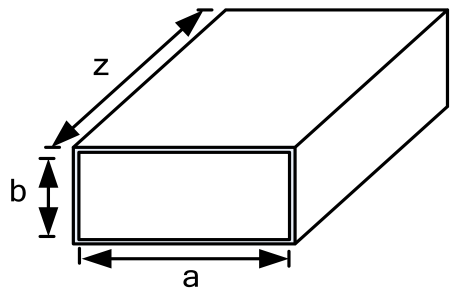

Figure 2-15: Rectangular waveguide resonator

An example of a waveguide diplexer is the compact fifth-order rectangular waveguide diplexer using a resonant Y-junction proposed in [37]. An elliptic ridge resonator is a resonator that behaves as a common dual-mode resonator for two common channel filters. The first block of rectangular waveguide diplexers uses the Y-junction with elliptic ridge resonator as it integrates the first resonators of both channel filters. Therefore, size reduction of the conventional diplexer can be achieved. The Tx/Rx signal isolation is lower than 65 dB. The schematic structure of a Y-junction waveguide diplex is shown in Figure 2-16.

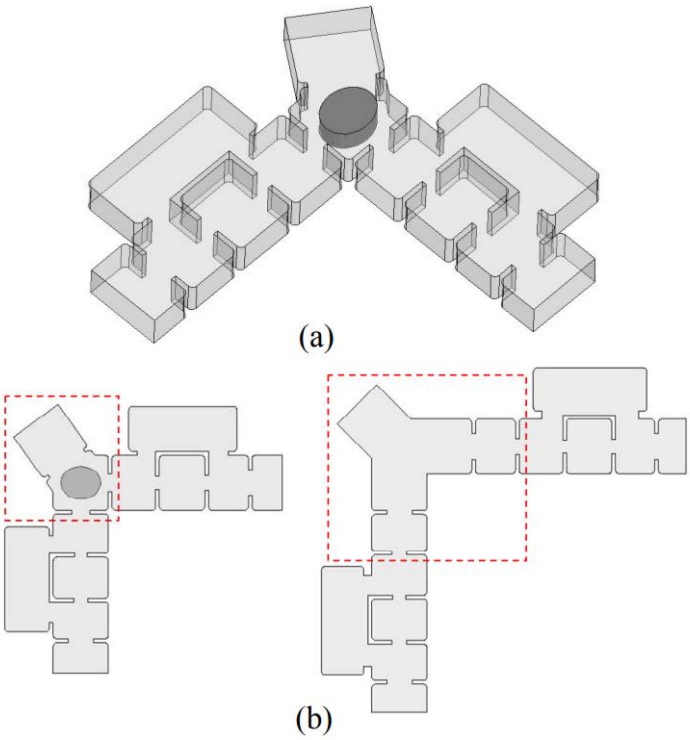

Figure 2-16: (a) Schematic structure of the designed diplexer; (b) comparison between diplexers using or not using the resonant Y-junction as first-stage input [37]

2.10 Dielectric resonator filter and diplexer

As per the trade-off between size and Q factor mentioned before, dielectric resonators (DRs) have shown a significant size reduction and high Q compared to waveguide technologies. DR filters are useful to employ in satellite and base station systems, where a high Q filter (low insertion loss) is needed with narrow bandwidth filter specifications [11]. In general, when the designed filter is at the same frequency, DR filters will miniaturise the waveguide filter size because of the cavity loaded with the dielectric resonator, and decrease the wavelength of the resonant frequency by a factor of $1/\sqrt{\varepsilon_r}$. Therefore, it can be seen that using a dielectric resonator can meet the specification of reducing the footprint of these filters in both volume and weight.

In the 1960s, Cohn [38] introduced dielectric resonators. A cylindrical dielectric resonator is known as a puck. It is placed inside the conducting enclosure and supported by a low dielectric resonator, as shown in Figure 2-17. At its resonant frequency, the majority of the electric and magnetic energy is stored within the resonator and the fields outside the ceramic puck decays and vanishes rapidly when the fields are further away from the puck. The conduction enclosure is used to stop the radiated field going outside [3]. Table 2-1 provides a summary of various modes of DR used in microwave components.

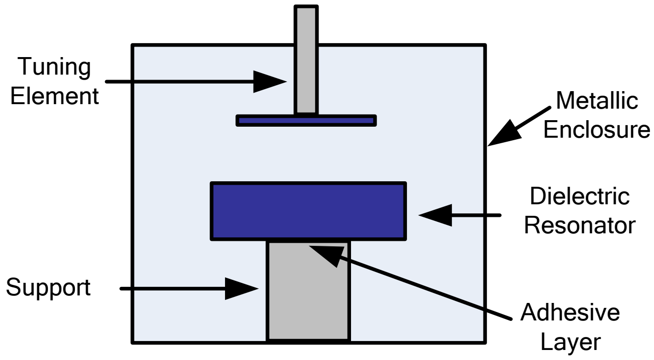

Figure 2-17: The typical DR with support structure [19]

Table 2-1: Comparison between various modes of operation [11]

Parameters	Single-Mode	Dual-Mode	Triple-Mode
Size	Large	Medium	Small
Spurious Performance	Good	Fair	Fair
Unloaded Q	High	Medium	Medium
Power-Handling capability	High	Medium	Medium
Design Complexity	Low	Medium	High

Normally, the resonant modes in microwave resonators exist in the form of a single mode representing one electric resonant or in the form of degenerate modes. These degenerate modes allow the realization of two electric resonators within the same physical resonator (dual-mode resonators) or three electric resonators within the same physical resonator (triple-mode resonators). The key advantage of operating in dual-mode or triple-mode configurations is size reduction. However, these modes have an impact on the Q-factor, spurious performance and power handling capability of the resonator.

The modified cylindrical resonator with a hole at the centre of the conventional resonator used in cellular base-station applications is reported in [39], as shown in Figure 2-18. This aims to increase the free space window between the fundamental mode ($TE_{01\delta}$ mode) and the second mode ($HE_{11\delta}$ mode).

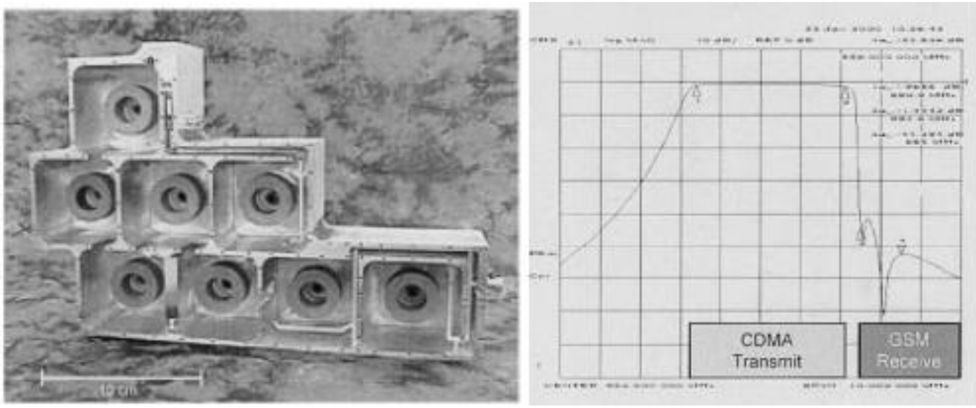

(a) (b)

Figure 2-18: (a) A typical $TE_{01\delta}$ filter for cellular base-station and (b) measured performance [39]

Moreover, a method to design $TE_{01\delta}$ mode DR filters with transmission zeros is proposed to improve the selectivity of filters in sidebands [40]. The feeding probes are extended along ring DRs and they are used to excite the $TE_{01\delta}$ mode and introduce transmission zeros. When the angle of the feeding position is rotated, transmission zeros can be shifted to the lower or the upper stopband. Based on this method, second- and fourth-order filters with different responses are designed and fabricated.

In 1982, the first introduction for size reduction was presented by Fiedziuszko. A dual-mode dielectric resonator loaded cavity was considered to offer significant advantages in size reduction and temperature performance [41]. The modes within a single cavity are coupled by using a screw located at 45° with respect to orthogonal tuning screws. Cruciform irises were used between inter-cavity couplings. The dual-mode dielectric resonator loaded cavity filter structure is shown in Figure 2-19.

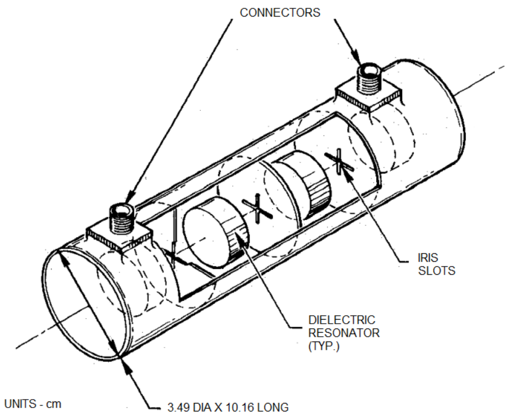

Figure 2-19: Dual-mode dielectric resonator loaded cavity filter structure [41]

Triple-mode dielectric-loaded cylindrical cavities are proposed and employed for the design of a small-size diplexer for base station applications. Two different frequency bands (Tx and Rx) are designed in each metal cavity as three resonant modes of a single cavity. The fabricated diplexer does not require any tuning screws, irises or corner cuts, and it offers a precise performance, simple tuning capability and low processing cost [42]. The isolation performance is better than 20 dB. The schematic of this triple-mode diplexer is shown in Figure 2-20.

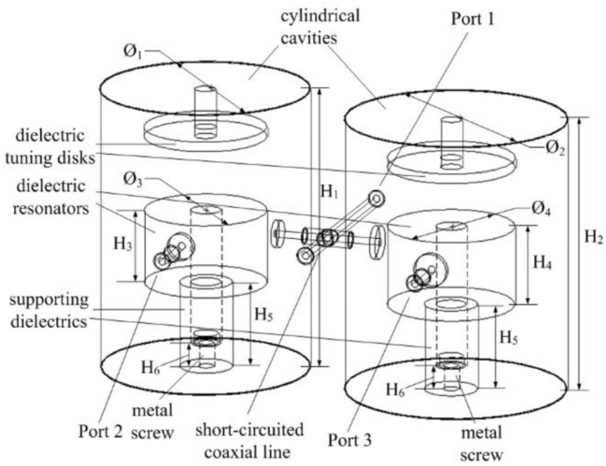

Figure 2-20: 3-D view of the triple-mode diplexer [42]

2.11 Other types and shapes of dielectric resonators

In this section, the combination of other technologies and DR filters is discussed. The different technologies have different Q-factors, which lead to cost reduction and improved insertion loss in the band as well as out of band rejection. However, the advantages of mixed technologies trade-off size, cost and frequency response. Hunter et al. [43] presented the use of non-uniform Q with first and last resonators by using a combline resonator. This method can help to improve the free spurious window and also reduce problems of realising input couplings. The configuration is shown in Figure 2-21.

Figure 2-21: Prototype manufactured dielectric resonators, combline resonators and hybrid model [43]

An integrated combline and $TE_{01\delta}$ mode dielectric filter is presented in [44]. The use of a wideband combline filter is combined with a narrowband dielectric filter. The integrated design results in a filter with spurious suppression and good in-band performance.

In addition, mixed material technologies are still interesting in designing filters, as shown in [45]. The authors have introduced a circuit realised by the fourth-order filter with mixed dielectric and coaxial resonators, as shown in Figure 2-22.

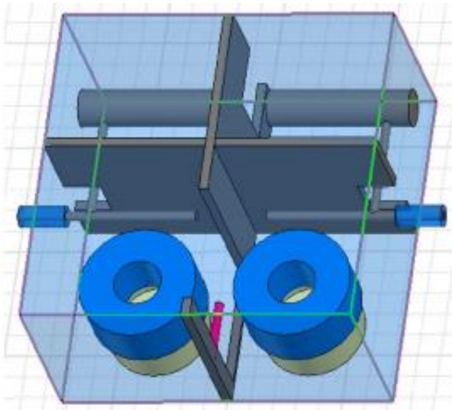

Figure 2-22: Electromagnetic model of the fourth-order filter with mixed dielectric and coaxial resonators [45]

Furthermore, the circuit could also be realised by a combined coaxial and microstrip technology. The final parallel network is then realised by connecting the branches using a microstrip T junction [45], as illustrated in Figure 2-23. The substrate used is Rogers Duroid 6010 with a thickness of 1.27 mm. The Q factor for the coaxial resonator and the microstrip resonator are 4000 and 220, respectively. The microstrip lines connecting each subnetwork to the T junction need to be tuned to match the phase of the two parallel connected networks.

Therefore, the alternative design technique based on dissimilar Q factors for each filter can be adapted to three-port diplexer branch and this technique can decrease the overall size and cost of the diplexer system, while still offering superior figure-of-merits, e.g. losses and high Tx/Rx signal isolation.

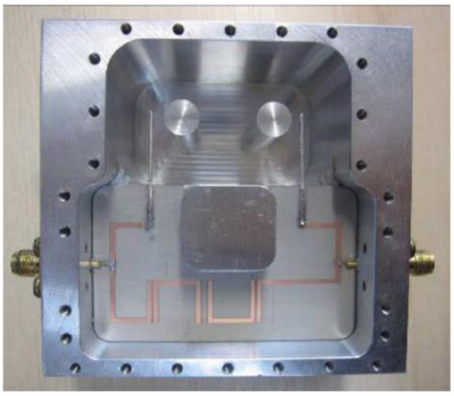

Figure 2-23: Photograph of the fourth-order filter with mixed coaxial and microstrip resonators [45]

2.12 Summary

This chapter has presented a background on filters and diplexers in different technologies, such as lumped-element, planar (microstrip, CPW), coaxial, waveguide, dielectric, superconductor technology and mixed material technologies. Each type of microwave technology has its specific advantages and disadvantages, such as cost, loss, size and power handling. To design a conventional diplexer, all diplexer structures are based on the three-port diplexer. However, the main drawback of this design technique is that the degree of the filters increases linearly when higher signal isolation is required. If the degree of filters increases, the size and losses of filters also increase. Moreover, high order filters increase the complicated structure because many coupling components have to consider such as external coupling and inter resonator coupling. Therefore, the new technique to achieve high TX/Rx isolation with relatively low degree filters is introduced in the next chapter. High signal isolation between Tx and Rx module is achievable by only using second-order filter topology and the design technique is based on amplitude and phase cancellation between two back to back three-port diplexers with a 180° phase shift in one branch.

Chapter 3
Four-port Diplexer Analysis

3.1 Introduction

In this chapter, three and four-port diplexers are intensively analysed and synthesised for solving S-parameter equations. The mathematical model was developed and some analytical and simulation results were obtained to verify the model. A second-order admittance inverter Chebyshev bandpass filter is designed for diplexer prototype. Then, the diplexer designed by connecting the two independent filters together is presented. The four-port diplexer circuit based on two back-to-back second-order diplexers with dissimilar Q-factors is simulated to verify the new design technique. Finally, an investigation of phase and mismatched antenna is presented.

3.2 Four-port diplexer analysis and synthesis

For a lossless and reciprocal network, the unitary condition of the network can be shown as [3]:

$$[S][S^*]\text{=}[1] \tag{3.1}$$

Consider the three-port network shown in Figure 3-1; the scattering matrix can be described:

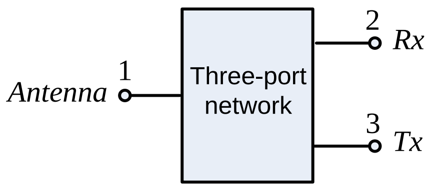

Figure 3-1: A three-port network

$$\begin{bmatrix} S_{11} & S_{12} & S_{13} \\ S_{21} & S_{22} & S_{23} \\ S_{31} & S_{32} & S_{33} \end{bmatrix} \begin{bmatrix} {S_{11}}^* & {S_{12}}^* & {S_{13}}^* \\ {S_{21}}^* & {S_{22}}^* & {S_{23}}^* \\ {S_{31}}^* & {S_{32}}^* & {S_{33}}^* \end{bmatrix} \text{=}[1] \tag{3.2}$$

$$S_{12}{S_{13}}^* + S_{22}{S_{23}}^* + S_{23}{S_{33}}^* = 0 \tag{3.3}$$

We wish $S_{23}\text{=}\epsilon \ll 1$ in Tx band and we also consider $S_{13} \cong 1$ for low loss. From equation (3.3), when S_{13} is equal to 1, the equation (3.3) will then be $S_{12} \cdot 1 + S_{22} \cdot \epsilon^* + \epsilon \cdot {S_{33}}^* = 0$. Now we give the reflection in Tx band at port 2, $S_{22} \cong 1$. Therefore, $S_{12} + \epsilon^* + \epsilon \cdot {S_{33}}^* = 0$, then $S_{12}\text{=}\ll 1$.

Hence, the only solution for a three-port network would be a conventional diplexer. However, we then examine a four-port network, as shown in Figure 3-2.

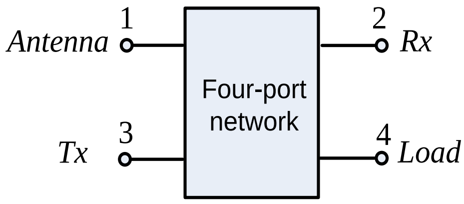

Figure 3-2: A four-port network

Let $S_{11},\ S_{22},\ S_{33},\ S_{44} = 0$ All frequency ($\forall\omega$)

Let $S_{23} = 0$ All frequency ($\forall\omega$)

Again, we consider in Tx band,

By setting γ and ϵ, which are arbitray numbers, then

We define S_{12}=γ $\ll$1, $S_{13} = \Delta \cong 1$, S_{34}=ϵ $\ll$1, S_{14}=0 (3.4)

In order to determine S_{24}, we consider from four-port S-parameters

$$\begin{bmatrix} 0 & \gamma & \Delta & 0 \\ \gamma & 0 & 0 & S_{24} \\ \Delta & 0 & 0 & \epsilon \\ 0 & S_{24} & \epsilon & 0 \end{bmatrix} \begin{bmatrix} 0 & \gamma^* & \Delta^* & 0 \\ \gamma^* & 0 & 0 & {S_{24}}^* \\ \Delta^* & 0 & 0 & \epsilon^* \\ 0 & {S_{24}}^* & \epsilon^* & 0 \end{bmatrix} = [1] \tag{3.5}$$

And then

$$|\gamma|^2+|\Delta|^2=1 \tag{3.6}$$

$$|\gamma|^2+|S_{24}|^2=1 \tag{3.7}$$

$$|\Delta|^2+|\epsilon|^2=1 \tag{3.8}$$

$$|S_{24}|^2+|\epsilon|^2=1 \tag{3.9}$$

Hence

$$|S_{24}|=|\Delta| \tag{3.10}$$

$$|\epsilon|=|\gamma| \tag{3.11}$$

$$\gamma \cdot {S_{24}}^* + \Delta \cdot \epsilon^* = 0 \tag{3.12}$$

$$\gamma \cdot \Delta^* + S_{24} \cdot \epsilon^* = 0 \tag{3.13}$$

A solution is

$$S_{24} = -\Delta^* \text{ and } \gamma = \epsilon^* \tag{3.14}$$

For real quantities

$$\Delta = \sqrt{1-\epsilon^2}, \quad \gamma = \epsilon, \quad S_{24} = -\sqrt{1-\epsilon^2} \tag{3.15}$$

When $\epsilon \ll 1$

Therefore, the scattering of the four-port network at Tx frequency can be given as [46]

$$[S] = \begin{bmatrix} 0 & \epsilon & \sqrt{1-\epsilon^2} & 0 \\ \epsilon & 0 & 0 & -\sqrt{1-\epsilon^2} \\ \sqrt{1-\epsilon^2} & 0 & 0 & \epsilon \\ 0 & -\sqrt{1-\epsilon^2} & \epsilon & 0 \end{bmatrix} \tag{3.16}$$

And at Rx frequency

$$[S] = \begin{bmatrix} 0 & \sqrt{1-\epsilon^2} & \epsilon & 0 \\ \sqrt{1-\epsilon^2} & 0 & 0 & -\epsilon \\ \epsilon & 0 & 0 & \sqrt{1-\epsilon^2} \\ 0 & -\epsilon & \sqrt{1-\epsilon^2} & 0 \end{bmatrix} \tag{3.17}$$

In (3.16) and (3.17), S_{13} is equal to $-S_{24}$, i.e. the same value but different sign or 180° out of phase. Therefore, it is noticeable that, between ports 2 and 4, exactly a 180° phase shift must be introduced while keeping the signal amplitudes equal in order to obtain an infinite Tx/Rx signal isolation The schematic of the four-port diplexer is shown in Figure 3-3. It can be explained that the high power-signal generate form Tx branch can easily interfere the Rx channel in two paths (Path1 and 2). Therefore, to achieve the best Tx/Rx signal isolation, the two sinusoidal signals in Paths 1 and 2 must have the same amplitude and out of phase.

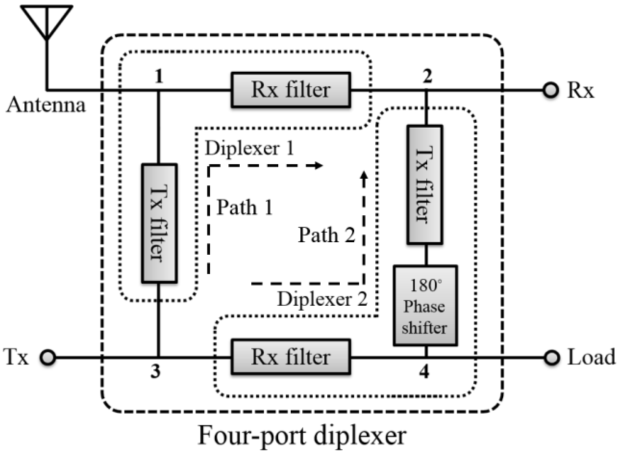

Figure 3-3: Schematic diagram of the four-port diplexer using two back-to-back three-port diplexers with amplitude and 180° phase cancellation technique between Rx and Tx channels

To investigate the signal from Tx to Rx, we consider two sinusoidal signals propagating in two paths: Path 1 and Path 2, as shown in Figure 3-3. The superposition of these two sine waves with the same amplitude, *A*, but different phases between points 2 and 4 can be expressed as $A\sin\theta + A\sin(\theta + \emptyset)$, where θ is the phase of sinusoidal signals and ∅ is the phase difference between these two signals. Then, the relationship between signal phases of these two sinusoidal signals and Tx/Rx signal isolation is simulated and plotted, as shown in Figure 3-4. To obtain the best Tx/Rx isolation, the two sinusoidal signals in paths 1 and 2 must have the same amplitude and the signal phases between ports 2 and 4 must be out of phase, 180° difference. To fulfil these requirements, therefore, two diplexer resonators are used with equal Q-factors (Q_1=Q_2) and added an additional 180° phase shift in diplexer designs, which is shown in Figure 3-4.

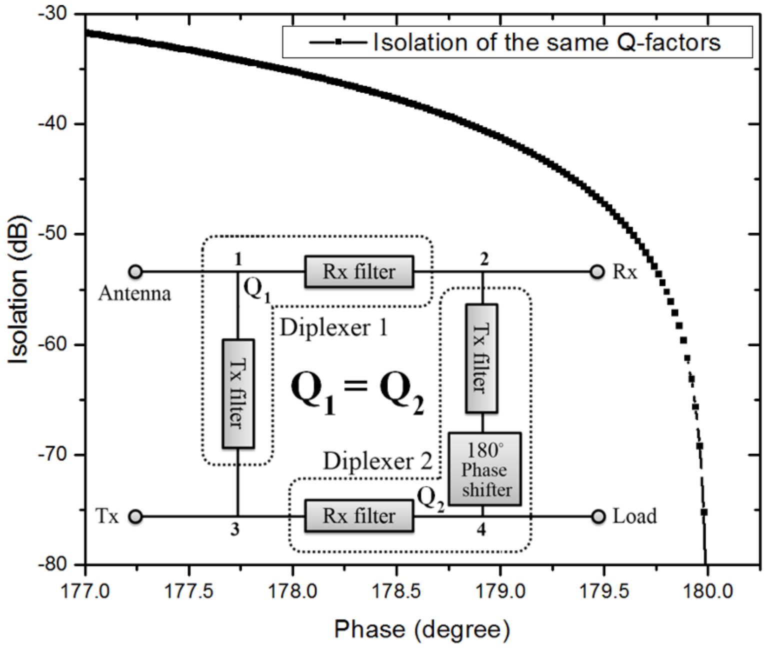

Figure 3-4: Simulated Tx/Rx isolation versus phase differences between ports 2 and 4 of two diplexers (Path 1 and Path 2) with the same Q-factors. The best Tx/Rx signal isolation is achievable at a 180° phase shift

To decrease the overall size of the four-port diplexer, resonators with dissimilar Q-factors between paths 1 and 2 may be used. For the resonators with dissimilar Q-factors, $Q_1 \neq Q_2$, we also consider the superposition of two sinusoidal signals with different amplitudes and phase difference of 180° as $A \sin\theta + B\sin(\theta + 180°)$, where *A* and *B* are the signal amplitudes in both signal paths and we assume *A*<*B* ($Q_1 < Q_2$). The relationship between signal attenuation, differences between B and A, and the Tx/Rx signal isolation is calculated and plotted in Figure 3-5. To maintain a reasonable Tx/Rx signal isolation, e.g. better than 40 dB, the amplitude attenuation between the two diplexers must be kept smaller than 0.1dB.

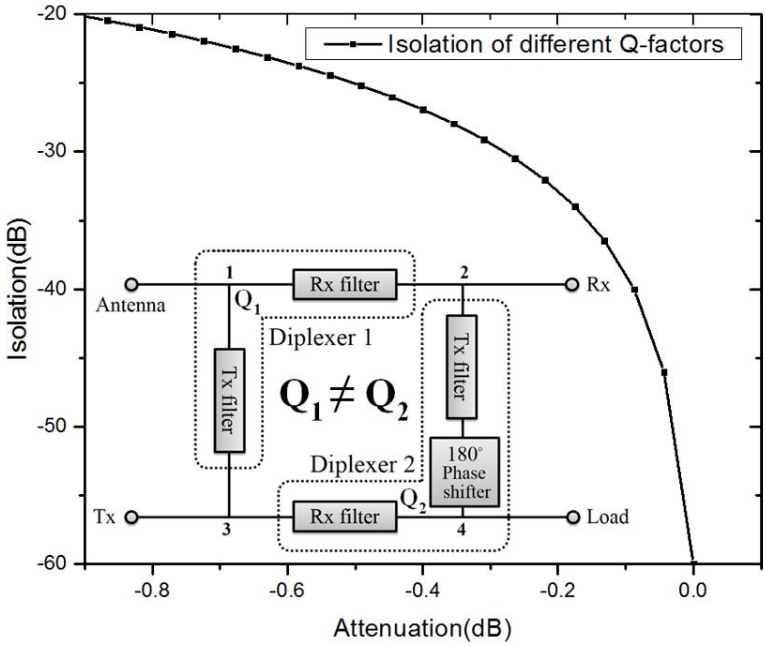

Figure 3-5: Simulated Tx/Rx signal isolation versus attenuation of two diplexers with different Q-factors. The reasonable Tx/Rx signal isolation of better than 40 dB is obtained when the attenuation difference between the two diplexers is less than 0.1 dB

3.3 Lumped-element model of the four-port diplexer

The microwave filter design steps using the insertion loss method are followed. First of all, the filter specifications are determined, such as centre frequency, pass band bandwidth, stop band insertion loss, maximum pass band insertion loss, order of filter and filter type. A normalised lumped-element for a low pass prototype filter is defined and it is then transformed to bandpass by using frequency and scaling impedance. The insertion method design steps are shown in Figure 3-6.

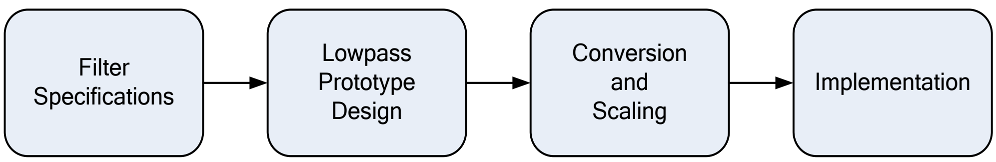

Figure 3-6: Design steps of the insertion loss method

3.3.1 Second-order lumped-element impedance inverter filters

The design of the admittance inverter Chebyshev bandpass filter according to the following specifications is shown in the table below.

Table 3-1: Specifications of the bandpass filter design

Centre frequency (f_0)	Rx=1.73 GHz and Tx=2.13 GHz
Passband bandwidth, '(ΔF)'	50 MHz (FBW=2.89% and 2.34%)
Stopband insertion loss 'L_A'	>40 dB at $f_0 = \pm 1000\ MHz$
Return loss, 'RL'	> 20 dB
Insertion loss, 'IL'	< 0.5 dB
System Impedance, 'Z_0'	50 Ω

Firstly, the order of the filter can be calculated in [3].

$$N \geq \frac{L_A+L_R+6}{20\ log_{10}[S+(S^2-1)^{1/2}]} \tag{3.18}$$

Where N is the order of the filter

When

$$L_A\text{=40 and } L_R\text{=20} \tag{3.19}$$

Where L_A is the stopband insertion loss

R_L is the return loss

S is the selectivity and S is the ratio of stopband to passband bandwidth. Hence

$$S = \frac{Stopband\ insetion\ loss}{\text{Passband bandwidth}} = \frac{2000}{50} = 40 \tag{3.20}$$

$$N \geq = 1.734 \tag{3.21}$$

Therefore, the order of the filter required to meet the specification is second order.

The ripple level ε is

$$\varepsilon = (10^{L_R/10} - 1)^{-1/2} \tag{3.22}$$

$$=0.1005$$

The doubly loaded normalised lowpass prototype filter element values (g_i) can be calculated as [6]

$$g_1 = \frac{2a_1}{\gamma} \tag{3.23}$$

$$g_i = \frac{4a_{i-1}a_i}{b_{i-1}g_{i-1}} \ , \qquad i = 2,3, \dots N \tag{3.24}$$

$$g_{N+1} = 1 \ \ for\ N\ odd$$
$$= coth^2\left(\frac{\beta}{4}\right) \ \ for\ N\ even \tag{3.25}$$

Where

$$\beta = ln\left(\coth\frac{L_R}{L17.37}\right) \tag{3.26}$$

$$\gamma = sinh\left(\frac{\beta}{2N}\right) \tag{3.27}$$

$$a_i = sin\left[\frac{(2_i-1)\pi}{2N}\right], \ i = 1,2, \dots N \tag{3.28}$$

And

$$b_i = \gamma^2 + sin^2\left(\frac{i\pi}{N}\right), \ i = 1,2, \dots N \tag{3.29}$$

Therefore, the calculated element values of a second order Chebyshev filter are given as g_0=1, g_1=0.6682, g_2=0.5462 and g_3=1.2222. The coefficient for the normalised external couplings is calculated as

$$k_e = \frac{1}{g_0 g_1} = \frac{1}{g_{N,N+1}} \tag{3.30}$$

$$k_e = 1.5047$$

And the internal couplings are calculated as

$$k_{i,i+1} = \frac{1}{\sqrt{g_i g_{i+1}}}, \ i = 1, \dots, N-1 \tag{3.31}$$

$$k_{1,2} = 1.6614$$

The normalised coupling coefficient can be represented in terms of coupling bandwidths. The bandwidth of the filter is 0.05 GHz. Then, the coupling bandwidth of the filter becomes

$$K_e = \frac{1}{g_0 g_1} * Bandwidth\ (GHz) \tag{3.32}$$

$$K_e = 0.0752$$

$$K_{i,i+1} = \frac{1}{\sqrt{g_i g_{i+1}}} * Bandwidth\ (GHz) \tag{3.33}$$

$$K_{1,2} = 0.08307$$

The inductor used to realise the external inverter of the bandpass filter can be calculated from the relation [47].

$$L_e = \frac{Z_0}{\pi\sqrt{2\pi f_{0(GHz)} \ \ K_{e(GHz)}}} nH \tag{3.34}$$

At 1.73 GHz, $L_e = 17.61nH$

At 2.13 GHz, $L_e = 15.87nH$

The inductor is used to form the inverter between adjacent resonators of the bandpass filter, as shown in Figure 3-7. It can be calculated from [47].

$$L_{ij} = \frac{Z_0}{\pi^2 K_{ij(GHz)}} nH \qquad (3.35)$$

At 1.73 GHz, $L_{12} = 61.047nH$

At 2.13 GHz, $L_{12} = 61.047nH$

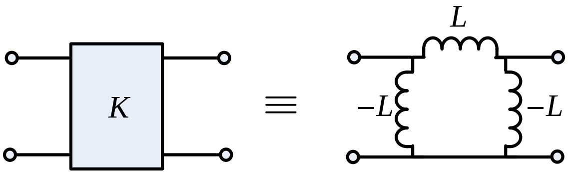

K=1/ωL

Figure 3-7: Equivalent circuit of impedance inverter

The element values of a shunt resonator with centre frequency and a system impedance level of 50 Ω can be calculated as [48].

$$\mathrm{C} = \frac{1}{4\mathrm{f}_{0(\mathrm{GHz})}\mathrm{Z}_0} \mathrm{pF} \qquad (3.36)$$

At 1.73 GHz, $C = 2.89pF$

At 2.13 GHz, $C = 2.35pF$

And $$\mathrm{L} = \frac{\mathrm{Z}_0}{\pi^2 \mathrm{f}_{0(\mathrm{GHz})}} \mathrm{nH} \qquad (3.37)$$

At 1.73 GHz, $L = 2.93nH$

At 2.13 GHz, $L = 2.38nH$

The loss is given by [49]

The Insertion loss $$(\mathrm{IL}) = \frac{4.343\ \mathrm{f0} \sum g}{\mathrm{BW} * \mathrm{Q}} \qquad (3.38)$$

An example of the resonator Q of 1800 would lead to a loss of 0.101 dB at 1.73 GHz and 0.124 dB at 2.13 GHz. The second-order inverter coupled filter is shown in Figure 3-8.

Table 3-2: Element values of second-order inverter coupled filters

Elements	Rx=1.73 GHz	and Tx=2.13 GHz
K_{R1}	0.0752	0.0752
K_{R12}	0.08307	0.08307
C_{11}	2.89 pF	2.35 pF
L_{11}	2.93 nH	2.38 nH

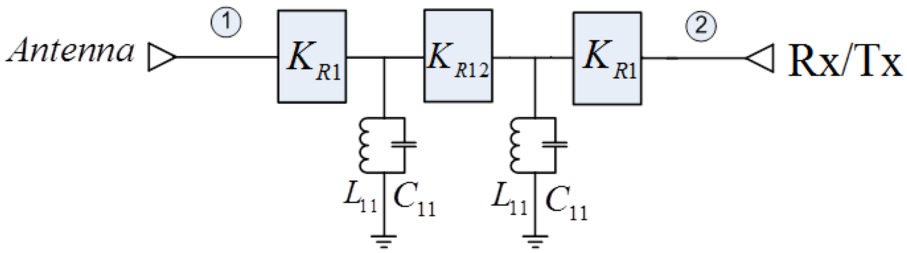

Figure 3-8: inverter coupled bandpass filter layout at 1.73 and 2.13 GHz

The simulated response of the inverter coupled filter at 1.73 GHz by AWR Microwave Office is portrayed in Figure 3-9. The 20-dB bandwidth is 50 MHz. The passband IL in the Rx band is less than 0.118 dB. The RL is better than 20 dB in the passband. It can be seen that the simulated IL result in Rx frequency shows a good agreement with the calculation (0.101dB).

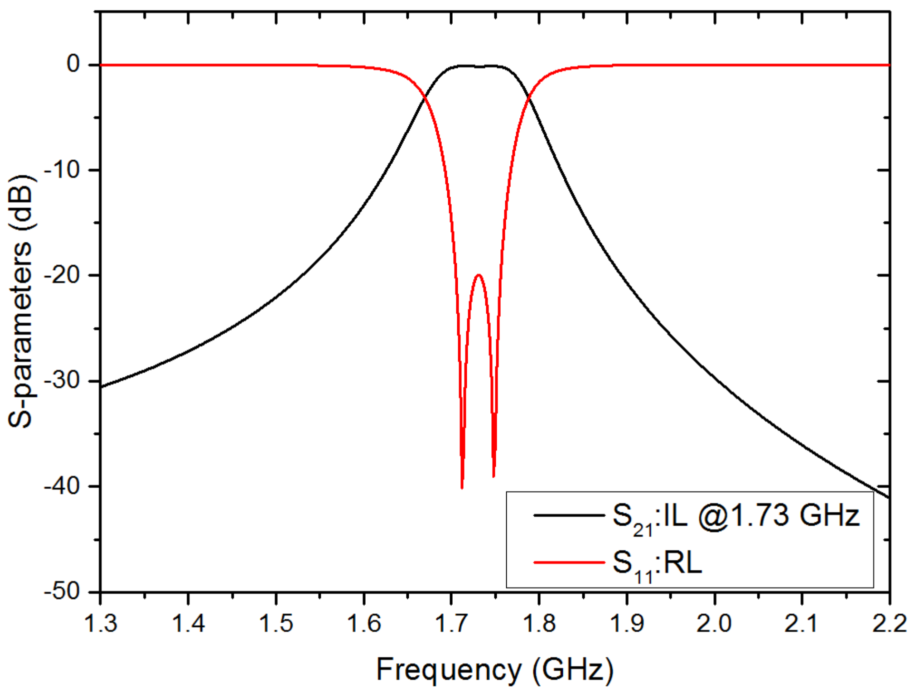

Figure 3-9: The simulated second-order filter at 1.73 GHz

The simulated response of the inverter-coupled filter at 2.13 GHz is portrayed in Figure 3-10. The 20-dB bandwidth is 50 MHz. The passband IL in the Tx band is less than 0.181 dB. The RL is better than 20 dB in the passband. It can be verified that the simulated IL result in the Tx frequency also shows a good agreement with the calculation (0.124dB).

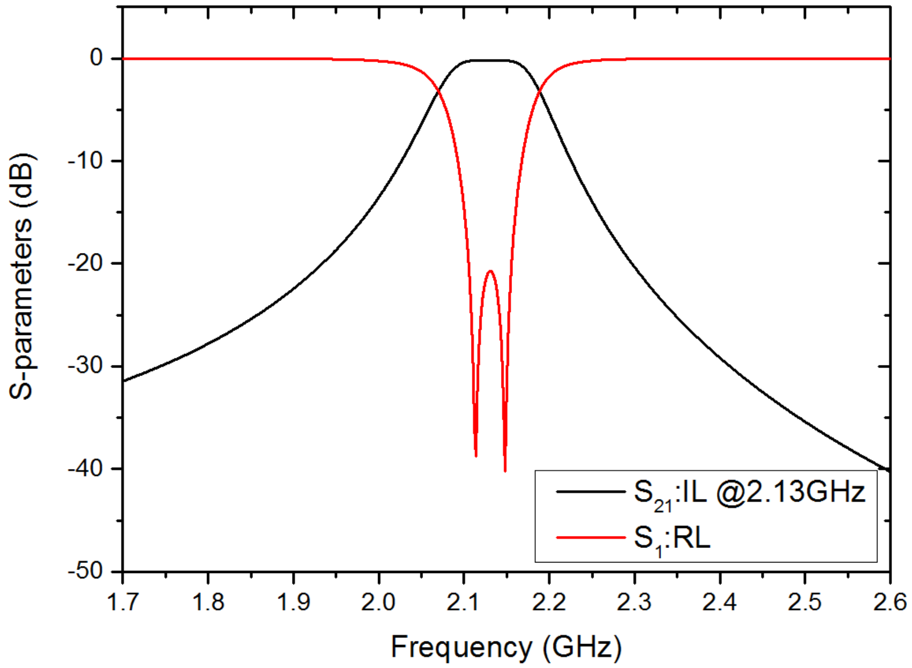

Figure 3-10: The simulated second-order filter at 2.13 GHz

3.3.2 Second-order inverter coupled diplexer

The diplexer (three-port) design is based on the independent design of two bandpass filters as per the following steps [50]:

Step 1: design the filter in Rx between ports 1 and 3 at a centre frequency of 1.73 GHz with 50 MHz bandwidth.

Step 2: calculate the external and internal coupling coefficients as equations (3.32) and (3.33).

Step 3: calculate the shunt resonator elements as equations (3.36) and (3.37).

Step 4: design the filter in Tx between ports 1 and 2 at a centre frequency of 2.13 GHz with 50 MHz bandwidth, which is the same step as in Rx.

Then, the two independent bandpass filters are connected together. The circuit of the inverter coupled diplexer network is shown in Figure 3-11. The external coupling coefficients are K_{T1}= 0.0752 and K_{R1}= 0.752. The internal coupling coefficients are K_{T12}= 0.08307, K_{R12}= 0.08307. The element values of the shunt resonator are L_{11}= 2.93 nH, L_{22}= 2.38 nH, C_{11}= 2.89 pF, C_{22}= 2.35 pF.

The simulated response of the diplexer is portrayed in Figure 3-12. The fractional bandwidth is 2.89% and 2.34% .The passband IL in the Rx band is less than 0.144 dB and, in the Tx band, 0.186 dB. The RL in both channels is better than 20 dB in the passband. The simulated isolation between Rx and Tx bands is better than 35.66 dB in transmit and receive bands, as shown in Figure 3-13. Figure 3-14 shows the wide-band simulation of the second-order diplexer. It can also be seen that the simulated wideband has no spurious response because the lumped-element only has one resonant mode, which is not the same as in other resonators.

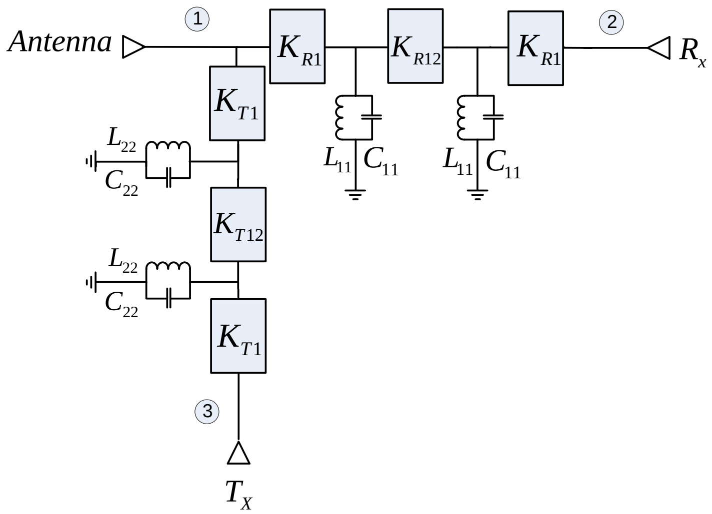

Figure 3-11: Second-order inverter coupled diplexer layout at 1.73 and 2.13 GHz

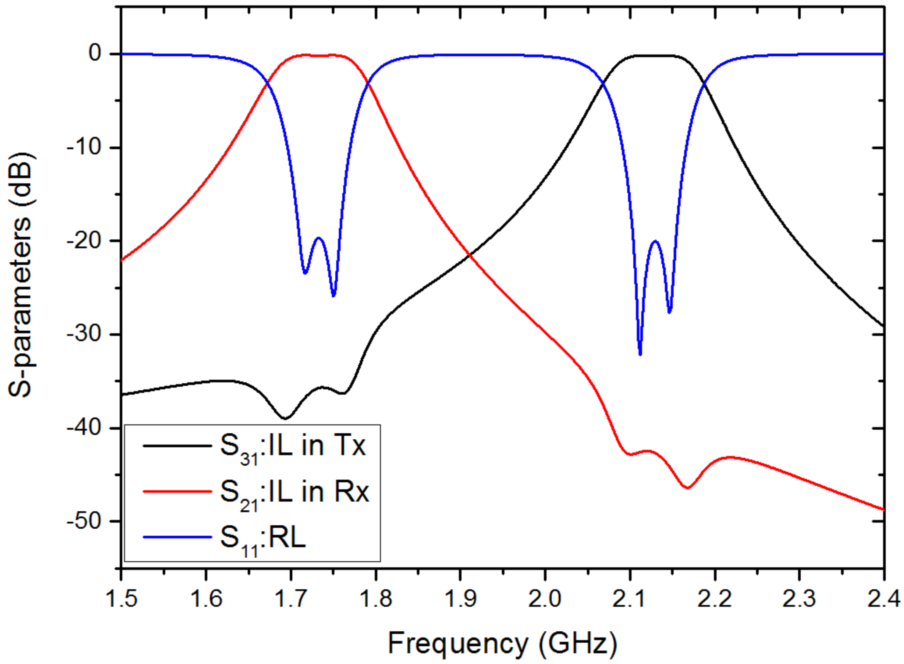

Figure 3-12: The simulated second-order inverter coupled diplexer at 1.73 GHz and 2.13 GHz

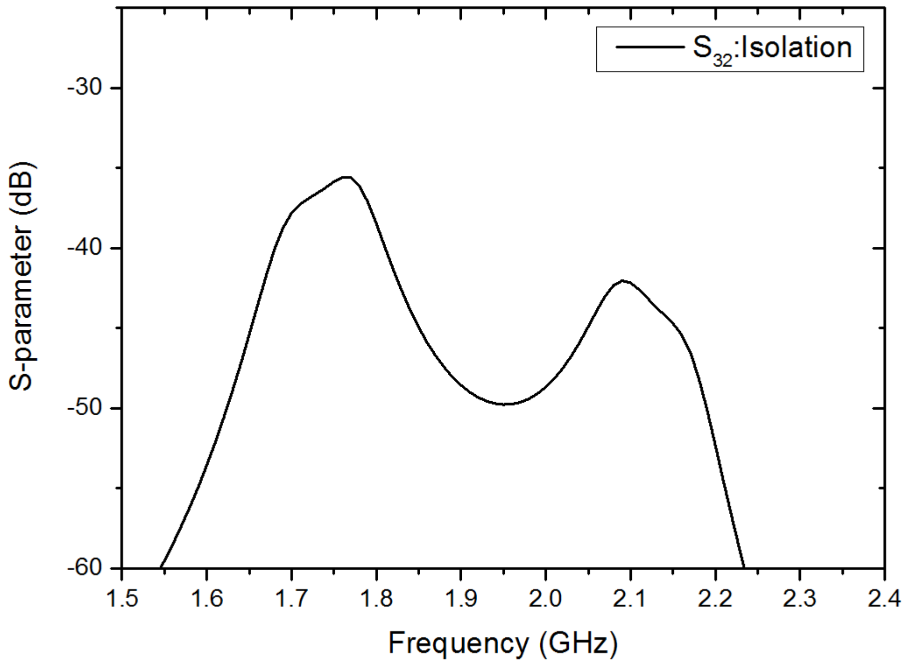

Figure 3-13: The simulated isolation of the inverter coupled diplexer

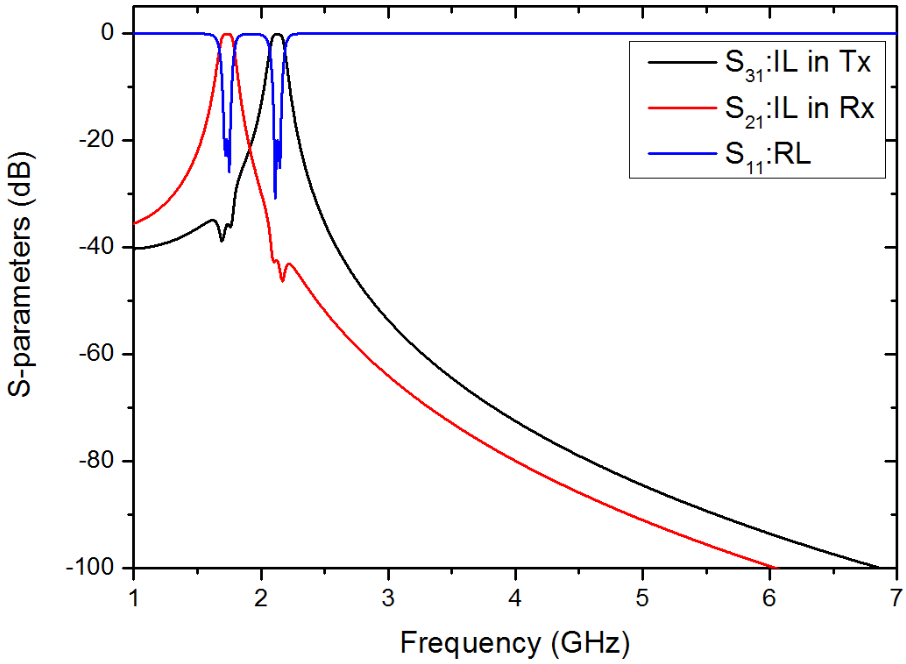

Figure 3-14: Simulated wide-band response of the second-order inverter coupled 3-port diplexer

3.3.3 Second-order inverter coupled four-port diplexer

The key design parameters of the lumped-element Chebyshev four-port diplexer are specified as the centre frequency, passband bandwidth, stopband attenuation, passband insertion loss and passband return loss. Both four-port diplexers with equal Q (Q_1=Q_2=1800) and dissimilar Q-factors (Q_1=1800, Q_2=3600) are designed at the centre frequency of 1.73 GHz and 2.13 GHz for Rx and Tx module, respectively, with 20-dB bandwidth of 50 MHz. The equivalent circuit of the four-port diplexer, for both equal and dissimilar Q-factors, is shown in Figure 3-15. The loaded normalised lowpass prototype filter element values (g_i) can be calculated as in [1]. The calculated design element values of the equal Q and dissimilar Q-factors are given as g_0=1, g_1=0.6682, g_2=0.5462 and g_3=1.2222. The external coupling coefficients are K_{T1}= 0.0752 and K_{R1}= 0.0752. The internal coupling coefficients are K_{T12}= 0.08307, K_{R12}= 0.08307. The element values of the shunt resonator are L_{11}= 2.93 nH, L_{22}= 2.38 nH, C_{11}= 2.89 pF, C_{22}= 2.35 pF. Both equal Q and dissimilar Q factor diplexer designs have exactly the same parameters as the key design parameters and the only difference between these two designs is the Q factors. If we allow the antenna impedance to change, we can tune the load impedance at port 4 to compensate for the antenna mismatch and recover the isolation back again.

From Figure 3-15, two diplexers, which can have either similar or dissimilar Q-factors, with a phase difference of 180° are combined together by using the back-to-back technique to achieve an optimum Tx/Rx signal isolation. The simulation results of the four-port diplexer circuit analysis simulated by AWR Microwave Office are plotted in Figure 3-16. For the similar Q-factor diplexer design, diplexers 1 and 2 are designed with the same Q-factor of 1800. The simulation results show that the passband insertion loss (IL) in the Tx band is less than 0.19 dB while, in Rx band, it is less than 0.14 dB. For the dissimilar Q-factor diplexer design, Diplexer 1 is designed with a Q factor of 1800 while the second diplexer, Diplexer 2, is designed with a Q factor of 3600. From the simulation results, the passband IL in the Tx band is less than 0.08 dB and the passband IL in the Rx band is less than 0.12 dB. The return loss (RL) of the diplexer design for both similar and dissimilar Q-factors in both Tx and Rx channels is better than 20 dB in the passband. Figure 3-17 shows the wide-band simulation of the second-order 4-port diplexer. It can also be seen that the simulated wideband has no spurious response.

According to equations (3.16) and (3.17), the phase responses of S_{21} and S_{34} have the same phase but, for S_{31} and S_{24}, phase differences between these parameters are 180° or out of phase. Figure 3-18 depicts the phase responses of S_{31} and S_{24}. To achieve an optimum Tx/Rx isolation, the phases of S_{31} and S_{24} are designed to be 93.92° and -86.11°, respectively, and thus the phase difference between them is 180° at f0 =2.13 GHz, which fulfils the requirements as stated in (3.16) and (3.17).

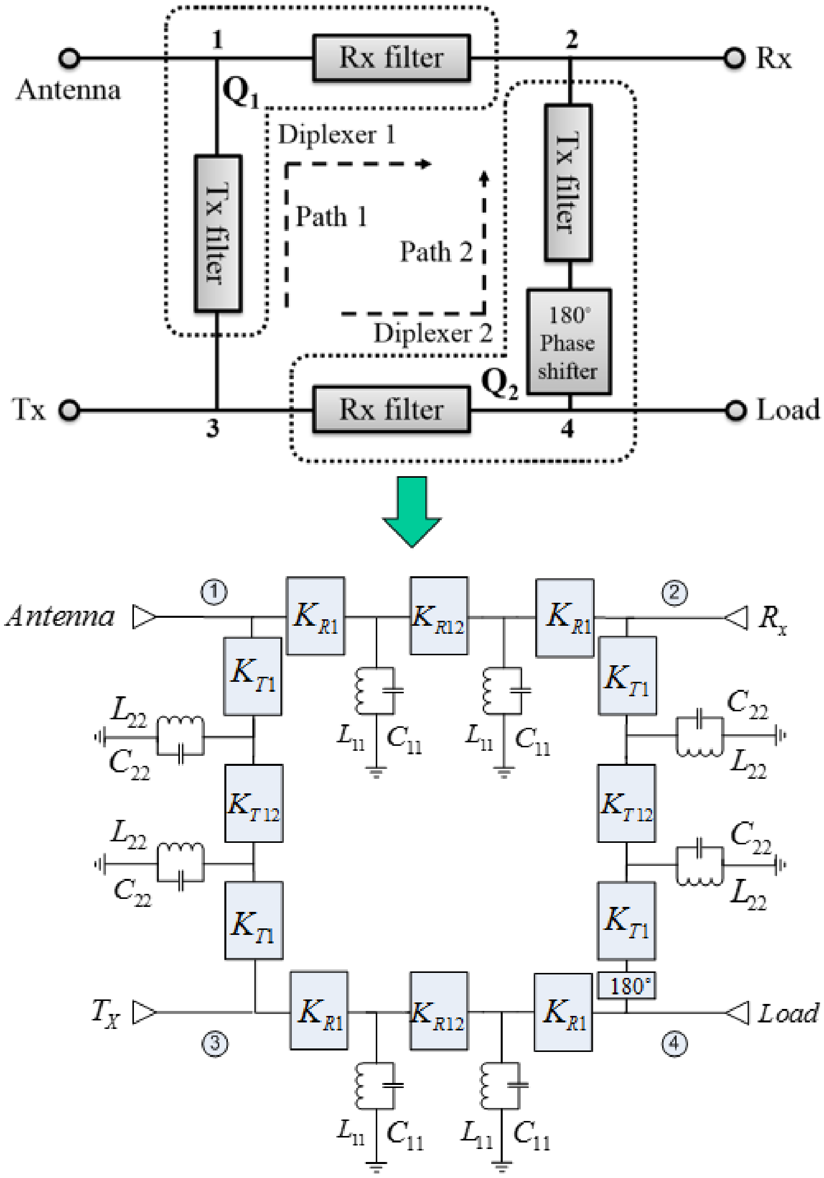

Figure 3-15: Four-port diplexer topology and its equivalent circuit based on a second-order filter consisting of external coupling, internal coupling coefficients and element values of resonators with a 180° phase shift between ports 2 and 4

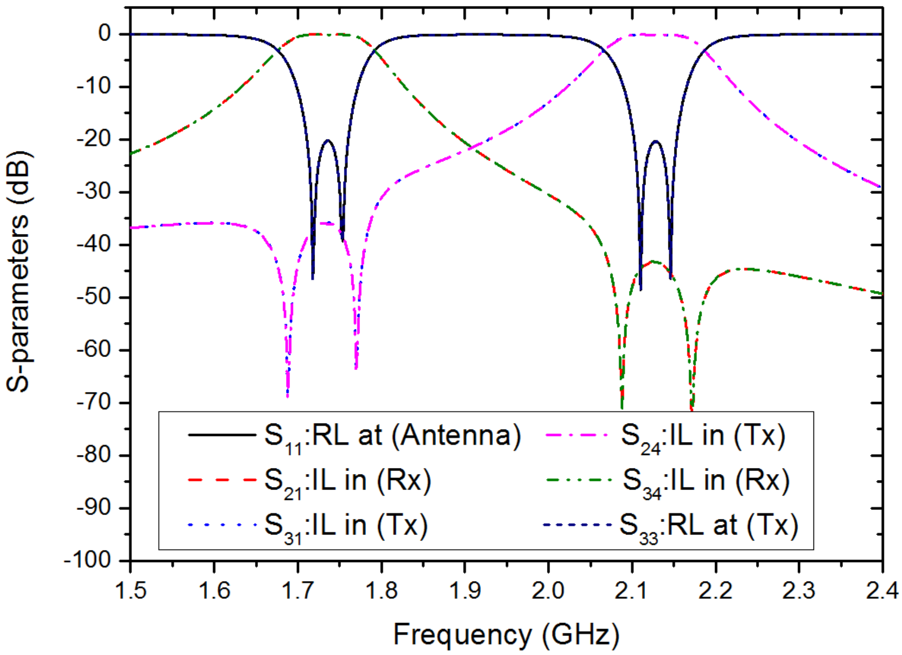

Figure 3-16: Simulation results of S-parameters of the four-port diplexer design at Tx=2.13 GHz, Rx=1.73 GHz

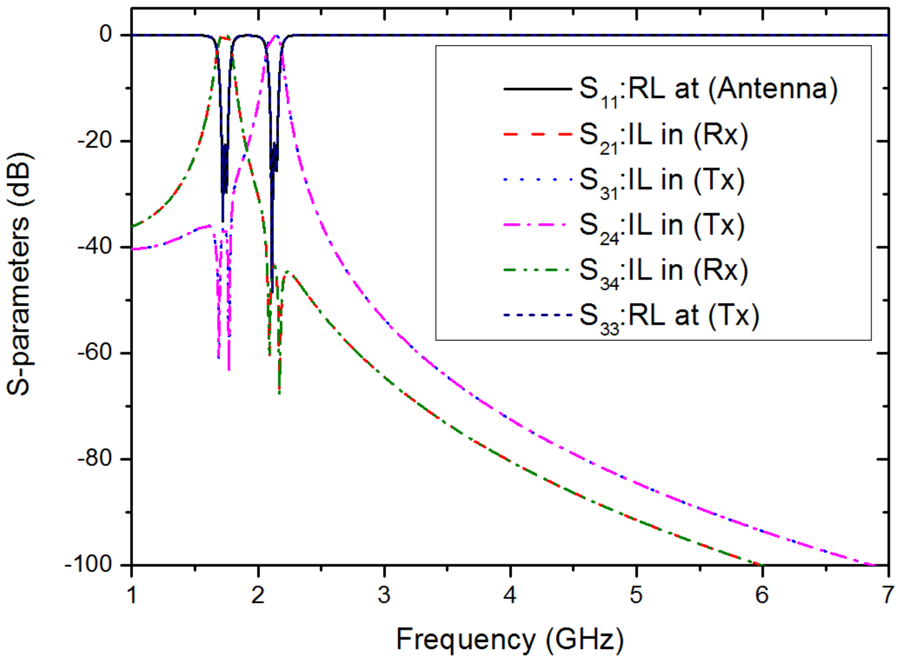

Figure 3-17: Simulated wide-band response of the second-order inverter coupled four-port diplexer

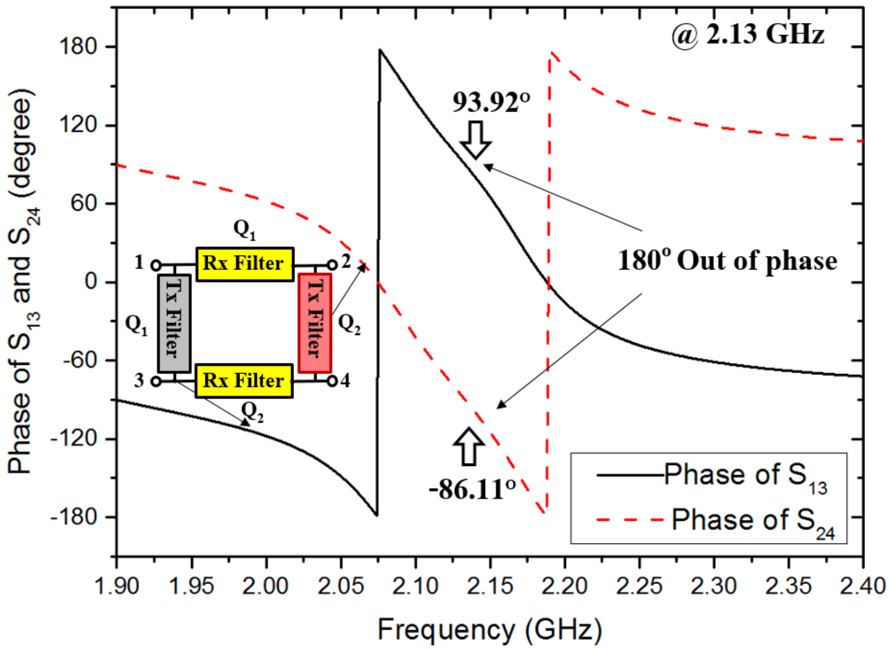

Figure 3-18: Simulation results of phases of S_{13} and S_{24} with a 180° phase difference at 2.13 GHz

The comparison of isolation (S_{32}) between the three-port and four-port is shown in Figure 3-19. The simulated isolation of the diplexer network is 35.66 dB and 79.11 dB in the four-port. From Figure 3-19, it can be seen that the phase shift between 177° and 180° of the four-port network still has a better signal isolation (S_{32}) than the existing diplexer.

Moreover, if we allow the antenna impedance to change, we can tune the load impedance to compensate for the antenna mismatch and recover the isolation back again. Thus, the effects of a mismatched antenna port are considered. Clearly, if the antenna port impedance is not 50 Ω, then the isolation reduces. Figure 3-20 shows the isolation (S_{32}) of the four-port diplexer with different Q-factors and allowing the antenna impedance to change between 25 and 75 ohms. The isolation varies between 46.67 dB and 79.11 dB.

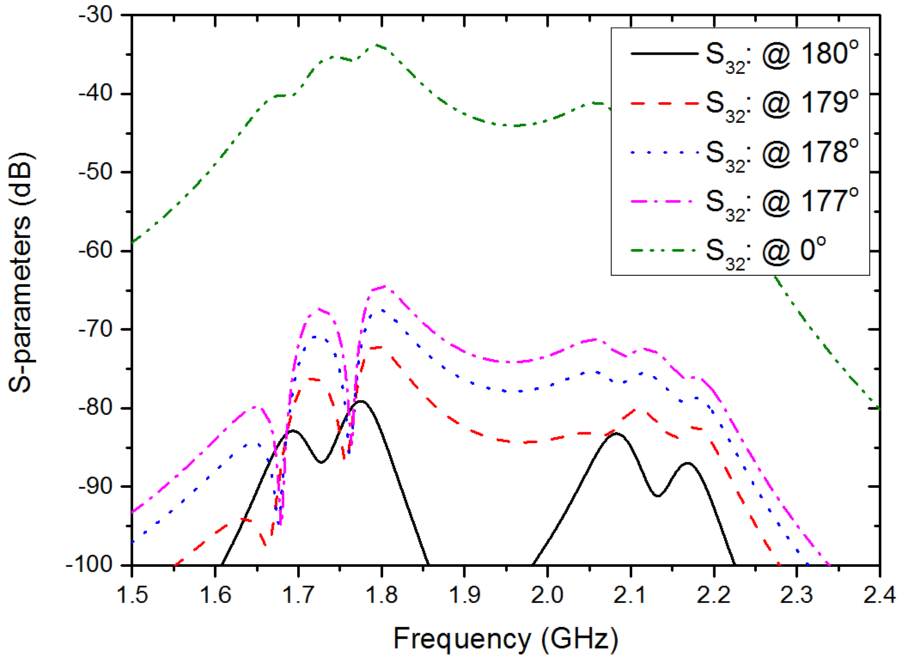

Figure 3-19: Simulation results of isolation of the four-port diplexer design at Tx=2.13 GHz, Rx=1.73 GHz

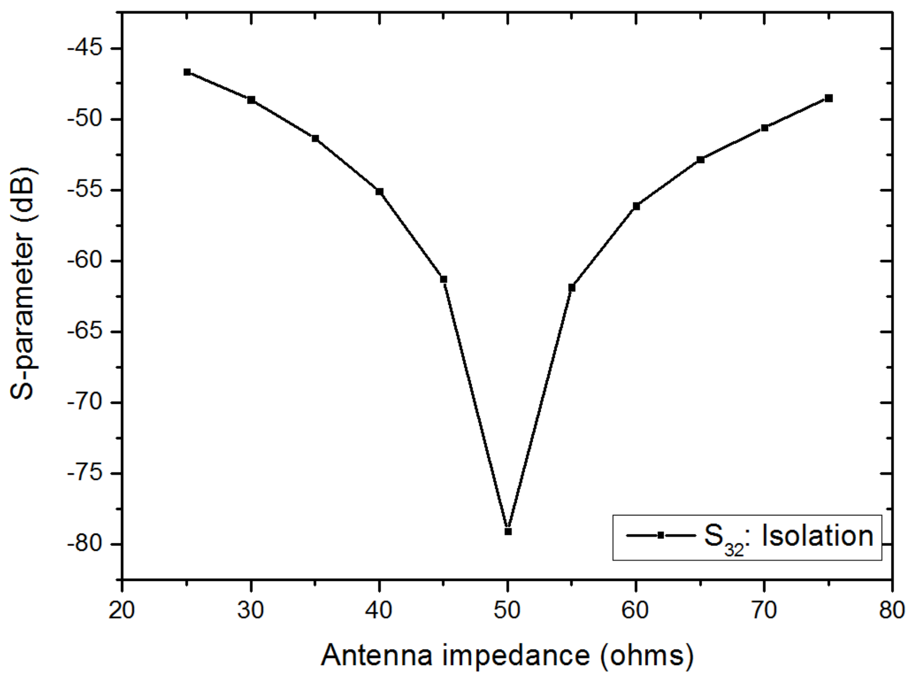

Figure 3-20: Isolation results compared to mismatched antenna port

3.4 Summary

A novel method for achieving high Tx/Rx isolation using a four-port diplexer has been presented in this chapter. Three and four-port diplexers have been intensively analysed and synthesised for solving S-parameter equations. The mathematical model was developed and some analytical and simulation results were obtained to verify the model. The new technique achieves high isolation with two back-to-back low degree diplexers. However, one diplexer can have significantly lower Q than the other and the phase and mismatched antenna have been investigated. The next chapter, a second-order capacitively coupled Chebyshev bandpass filter is an example designed with a low Q-factor. Then, the four-port diplexer using a microstrip open-loop resonator with coupled-feed is presented as low Q-factor material. Finally, another alternative solution of a microstrip four-port diplexer by using a tapped-feed is introduced.

Chapter 4

Modelling and Development of a Low-Q Four-port Diplexer

4.1 Introduction

After three and four-port networks are intensively analysed and synthesize solving S-parameter equations, the analytical solution is verified by Microwave Office simulation. Therefore, the four-port diplexer can be designed by using two diplexers with 180° different phase. This technique offers higher Tx/Rx signal isolation compared to conventional three-port diplexer. To verify the new design technique, both microstrip open-loop resonator with coupled-feed and tapped-feed are presented in this chapter.

4.2 Chebyshev filter design

This section describes the design of the second-order Chebyshev filter. The specifications of the required filter are shown below:

Table 4-1: Specifications of the microstrip bandpass filter design

Centre frequency (f_0)	R_X=1.73 GHz and T_X=2.13 GHz
Passband bandwidth, '(ΔF)'	50 MHz (FBW=2.6% and 2.3%)
Stopband insertion loss 'L_A'	>40 dB at $f_0 = \pm 1000\ MHz$
Return loss, 'RL'	> 20 dB
Insertion loss, 'IL'	< 0.5 dB
System Impedance, 'Z_0'	50 Ω

Firstly, the order of the filter can be calculated in [3].

$$N \geq \frac{L_A + L_R + 6}{20\, log_{10}[S + (S^2 - 1)^{1/2}]} \tag{4.1}$$

Where N is the order of the filter

When

$$L_A = 40 \text{ and } L_R = 20 \tag{4.2}$$

Where L_A is the stopband insertion loss

R_L is the return loss

S is the selectivity and S is the ratio of stopband to passband bandwidth. Hence

$$S = \frac{Stopband\ insetion\ loss}{\text{Passband bandwidth}} = \frac{2000}{50} = 40 \quad (4.3)$$

$$N \geq = 1.734 \quad (4.4)$$

Therefore, the order of the filter required to meet the specification is second order.

The ripple level ε is

$$\varepsilon = (10^{L_R/10} - 1)^{-1/2} \quad (4.5)$$

$$= 0.1005$$

Hence

$$\eta = \sinh[\frac{1}{N} sinh^{-1}(1/\varepsilon) \quad (4.6)$$

$$= 2.1213$$

And the shunt capacitive element value of the capacitive element Chebyshev lowpass prototype is

$$C_r = \frac{2}{\eta}\sin[\frac{(2r-1)\pi}{2N}] \quad (4.7)$$

Where r=1,…, N

$$C_1 = C_2 = 0.6667$$

The element value of the normalised inverter coupled Chebyshev lowpass prototype is

$$K_{r,r+1} = \frac{[\eta^2 + sin^2(r\pi/N)]^{1/2}}{\eta} \quad (4.8)$$

Where r=1,…, N-1

Therefore, the inverter value is

$$K_{12} = 1.1055$$

The normalised Chebyshev inverter coupled lowpass prototype is represented in Figure 4-1.

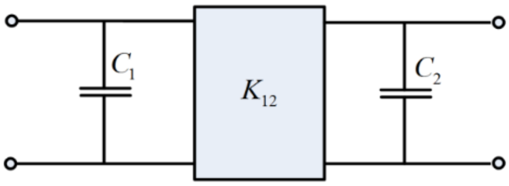

Figure 4-1: Equivalent circuit of the impedance inverter

At a centre frequency of 1.95 GHz and 2.14 GHz and Z=50 ohm

$$\omega = 2\pi f \tag{4.9}$$

at 1.95 GHz, ω = 12.25x10^9 and at 2.14 GHz, ω = 13.45x10^9

and $$\alpha = \frac{f}{\mathrm{BW}} \tag{4.10}$$

at 1.95 GHz, α =39 and at 2.14 GHz, α =42.8

The element values of a lowpass to bandpass frequency and impedance scaled capacitively coupled network can be calculated as

$$C_{01} = C_{N,N+1} = \frac{1}{\omega Z(\alpha-1)^{1/2}} \tag{4.11}$$

and

$$C_{r,r+1} = \frac{Kr,r+1}{Z\alpha\omega} \tag{4.12}$$

Where r=1,…, N-1

The shunt element values can be calculated as

And

$$C_{11} = \frac{\left[\frac{C_1}{\omega} - \frac{(\alpha-1)^{\frac{1}{2}}}{\omega\alpha} - C_{12}\right]}{Z} \tag{4.13}$$

And

$$C_{NN} = \frac{\left[\frac{C_N}{\omega} - \frac{(\alpha-1)^{\frac{1}{2}}}{\omega\alpha} - C_{N-1,N}\right]}{Z} \tag{4.14}$$

And

$$C_{rr} = \frac{\left[\frac{C_r}{\omega} - \frac{(\alpha-1)^{\frac{1}{2}}}{\omega\alpha} - C_{r-1,r} - C_{r,r+1}\right]}{Z} \tag{4.15}$$

Where r=2,…, N-1

$$L_{r,r} = \frac{Z}{C_r\omega} \tag{4.16}$$

Where r=1,…, N

The loss is given by [49]

The insertion loss (IL) $= \frac{4.343 \text{ f0} \sum g}{\text{BW} * \text{Q}}$ (4.17)

When design filter with low Q-factor is about 186.5, it would lead to a loss of 1.1 dB at 1.95 GHz.

When design filter with low Q-factor is about 191, it would lead to a loss of 1.07dB at 2.14 GHz.

The element values of the second-order Chebyshev diplexer are shown in Table 4-2.

Table 4-2: Element values of the second-order Chebyshev filters at 1.95 and 2.14 GHz

Elements	Tx=1.95 GHz	Rx=2.14 GHz
C_{01}= C_{23}	0.2648pF	0.2301 pF
C_{12}	0.0463pF	0.0384 pF
C_{11}= C_{22}	0.7840 pF	0.7285 pF
L_{11}= L_{22}	6.1213 nH	5.5779 nH

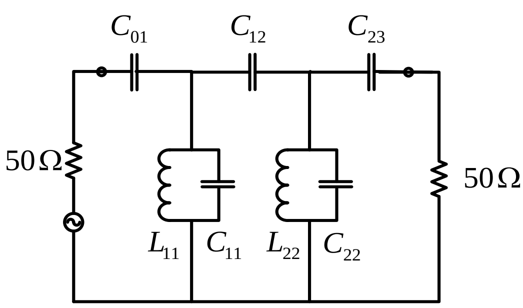

Figure 4-2: Capacitively coupled filter layout

The simulated response of the capacitively coupled filter at 1.95 GHz is portrayed in Figure 4-3. The 20-dB bandwidth is 50 MHz. The passband IL in the Tx band is less than 1.14 dB. The RL is better than 20 dB in the passband.

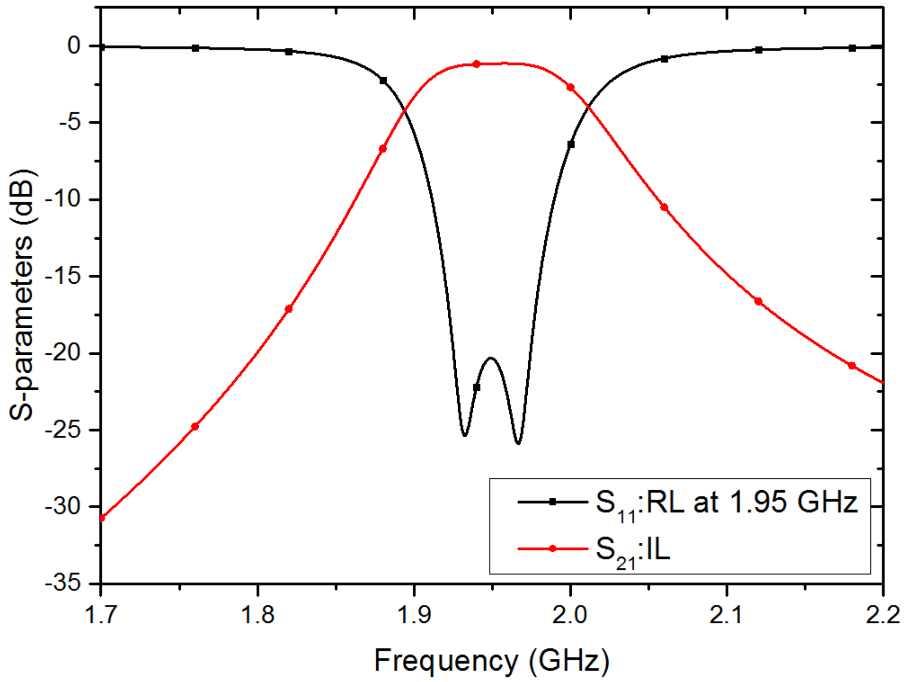

Figure 4-3: Capacitively coupled lumped-element filter response at 1.95 GHz

The simulated response of the capacitively coupled filter at 2.14 GHz by AWR Microwave Office is shown in Figure 4-4. The 20-dB bandwidth is 50 MHz. The passband IL in the Tx band is less than 1.09 dB. The RL is better than 20 dB in the passband.

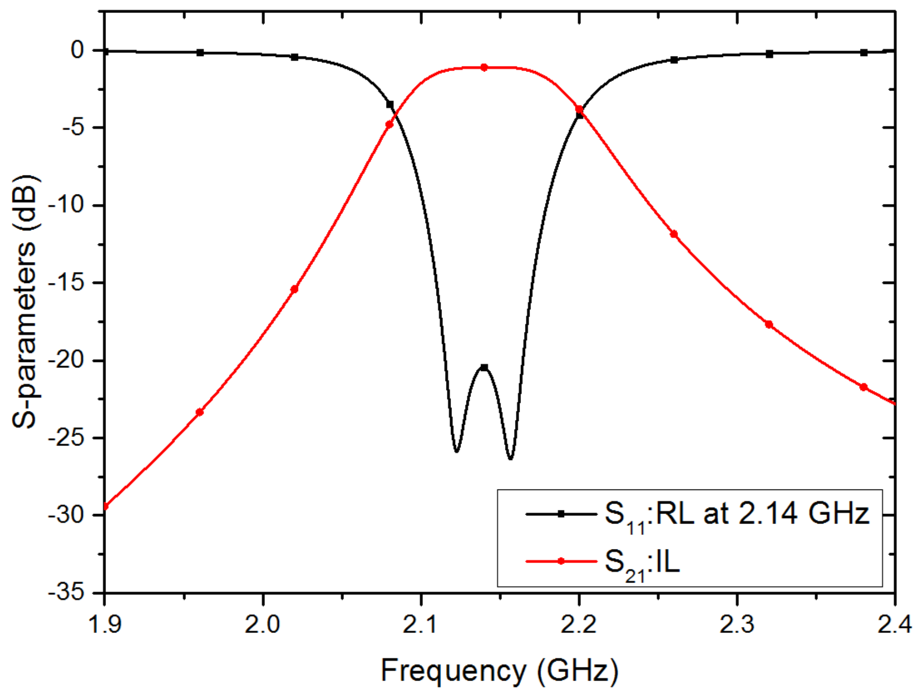

Figure 4-4: Capacitively coupled lumped-element filter response at 2.14 GHz

4.3 Microstrip resonator filter design

It would seem that planar filter structures which can be fabricated using printed-circuit technologies would be preferred whenever they are available and are suitable because of smaller sizes and lighter weight. In this section, the microstrip open-loop resonator is introduced as small size, light weight and low Q-factor. The filters are comprised of microstrip open-loop resonators. Each resonator has a perimeter about a half-wavelength. The design of the second-order Chebyshev microstrip resonator filter is provided. The specifications of the required filters are shown below.

Table 4-3: Specifications of the microstrip bandpass filter design

Centre frequency (f_0)	Rx=1.95 GHz and Tx=2.14 GHz
Passband bandwidth, '(ΔF)'	50 MHz (FBW=2.6%, 2.3%)
Stopband insertion loss	>40 dB
Return loss, 'RL'	> 20 dB
Insertion loss, 'IL'	< 1.5 dB
System impedance, 'Z_0'	50 Ω

The doubly loaded resonator normalised lowpass prototype filter element values (g_i) can be calculated as [48],

$$g_0 = 1$$

$$\beta = \ln\left(\coth\left(\frac{L}{17.37}\right)\right)$$

$$\gamma = \sinh\left(\frac{\beta}{2n}\right)$$

$$a_k = \sin\left[\frac{(2k-1)\pi}{2n}\right], \quad k = 1, 2, ..., n$$

$$b_k = \gamma^2 + \sin^2\left(\frac{k\pi}{n}\right), \quad k = 1, 2, ..., n$$

$$g_1 = \frac{2a_1}{\gamma}$$

$$g_k = \frac{4a_{k-1}a_k}{b_{k-1}g_{k-1}}, \quad k = 2, 3, ..., n$$

$$g_{n+1} = \begin{cases} 1 & n \text{ odd} \\ \coth^2\left(\frac{\beta}{4}\right) & n \text{ even} \end{cases} \tag{4.18}$$

Then, the element values of the second-order Chebyshev filter operating at the centre frequencies of 1.95 GHz and 2.14 GHz are given as

g_0=1, g_1= 0.6682, g_2= 0.5462, g_3= 1.2222

The design parameters of the bandpass filter, i.e., the coupling coefficients and external quality factors, as referring to the general coupling structure can be determined by the formulas.

The external values can be calculated by

$$Q_e = \frac{g_0 g_1}{FBW} \tag{4.19}$$

At 1.95 GHz, Q_e= 25.9

At 2.14 GHz, Q_e= 28.44

The coupling coefficient can be calculated by

$$K_{i,i+1} = \frac{FBW}{\sqrt{g_1 g_2}} \qquad \text{for i=1 to n-1} \tag{4.20}$$

At 1.95 GHz, K_{12}=0.0426

At 2.14 GHz, K_{12}=0.0387

4.4 Half-wavelength microstrip resonator and Q-factor

Microstrip transmission line is chosen as an example of the low Q-factor of the four-port diplexer as it is low in cost, small in size and easy to integrate into other microwave devices. The general structure consists of w (width), t (thickness), h (height) and ε_r (dielectric constant). The propagation in a microstrip is assumed to be quasi-TEM [1]. The two parameters used to describe the transmission characteristics are the effective dielectric constant (ε_{re}) and characteristic impedance (Z_c).

The effective dielectric constant (ε_{re}) is given approximately by [36]

$$\varepsilon_{re} = \frac{\varepsilon_r+1}{2}+\frac{\varepsilon_r-1}{2}\left(1+12\frac{h}{w}\right)^{-0.5} \tag{4.21}$$

Characteristic impedance (Z_c).

For w/h≤1

$$Z_c = \frac{60}{\sqrt{\varepsilon_{re}}} ln\left(\frac{8h}{w} + 0.25\frac{w}{h}\right) \quad (4.22)$$

For w/h≥1

$$Z_c = \frac{120\pi}{\sqrt{\varepsilon_{re}}}\left\{\frac{w}{h} + 1.393 + 0.677ln\left(\frac{w}{h} + 1.444\right)\right\}^{-1} \quad (4.23)$$

The guided wavelength of the microstrip is given by

$$\lambda_g = \frac{300}{f(GHz)\sqrt{\varepsilon_{re}}} \quad \text{mm} \quad (4.24)$$

Where λ_g is the guided wavelength at operation frequency $f(GHz)$.

The propagation constant β and phase velocity v_p can be determined by

$$\beta = \frac{2\pi f}{v_p} = \frac{2\pi}{\lambda_g} = \frac{2\pi f\sqrt{\varepsilon_{re}}}{c} = k_0\sqrt{\varepsilon_{re}} \quad (4.25)$$

$$v_p = \frac{\omega}{\beta} = \frac{c}{\sqrt{\varepsilon_{re}}} \quad (4.26)$$

Where c is the velocity of light (c≈ 3×10^8 m/s).

The relationship between electrical length θ and physical length l of the microstrip line is given by

$$\theta = \beta l \quad (4.27)$$

when $\theta = \pi$ and $l = \lambda_g/2$; this is called the half-wavelength microstrip line.

If a half-wavelength microstrip line of 50Ω impedance is designed at 1.95 GHz and 2.14 GHz, the Q-factors can be calculated as follows. The filters are designed on a RT/Duroid substrate having a thickness h = 1.27mm with relative dielectric constant εr =6.15. Loss tangent ($\tan\delta$) is 0.0027.

The width of a 50Ω microstrip line is estimated to be

W=1.87 mm

From equation (4.21), the effective dielectric constant (ε_{re}) is

ε_{re} =4.43

At 1.95 GHz, the resonant length can be calculated as

$$l = \frac{\lambda_g}{2} = \frac{v_p}{2f} = \frac{c}{2f\sqrt{\varepsilon_{re}}} = \frac{3\times10^8}{2(1.95\times10^9)\sqrt{4.43}} = 36.6 \text{ mm}$$

At 2.14 GHz, the resonant length (l) is 33.3 mm

At 1.95 GHz, the propagation constant is

$$\beta = \frac{2\pi f\sqrt{\varepsilon_{re}}}{c} = \frac{2\pi(1.95\times10^9)\sqrt{4.43}}{3\times10^8} = 85.9 \text{ rad/m}$$

At 2.14 GHz, the propagation constant (β) is 94.28 rad/m

The attenuation due to conductor loss is calculated approximately by [51]

$$\alpha_c = \frac{R_s}{Z_c W} \qquad \text{Np/m} \tag{4.28}$$

Where$R_s = \sqrt{\frac{\omega\mu_0}{2\sigma}}$ is the surface resistivity of the conductor

$\mu_0 = 4\pi \times 10^{-7}$ is permeability of free space

$\sigma = 5.8 \times 10^7\ S/m$ is the conductivity of copper

At 1.95 GHz, the attenuation due to conductor loss is

$$\alpha_c = \frac{R_s}{Z_c W} = \frac{0.0115}{50(0.00187)} = 0.123 \qquad \text{Np/m} \tag{4.29}$$

At 2.14 GHz, the attenuation due to conductor loss (α_c) is 0.129 Np/m

At 1.95 GHz, the attenuation due to dielectric loss is

$$\alpha_d = \frac{k_0\varepsilon_r(\varepsilon_{re}-1)\tan\delta}{2\sqrt{\varepsilon_{re}}(\varepsilon_r-1)} = \frac{40.33(6.15)(3.43)(0.0027)}{2\sqrt{4.43}(5.15)} = 0.107 \qquad \text{Np/m} \tag{4.30}$$

Where $k_0 = \frac{\beta}{\sqrt{\varepsilon_{re}}}$

At 2.14 GHz, the attenuation due to dielectric loss (α_d) is 0.118 Np/m

At 1.95 GHz, the Q-factor is

$$Q = \frac{\beta}{2(\alpha_c+\alpha_d)} = \frac{85.9}{2(0.123+0.107)} = 186.5 \tag{4.31}$$

At 2.14 GHz, the Q-factor is 191.

From (4.17), the second-order filter with low Q-factor is about 186.5, which would lead to a loss of 0. 1.1 dB at 1.95 GHz.

The filter designed with a low Q-factor is about 191, which would lead to a loss of 1.07dB at 2.14 GHz.

4.5 Second-order microstrip resonator with coupled-feed

The open-loop microstrip design is designed by the total line length of the microstrip line at a half-wavelength long at the resonant frequency [1]. The proposed microstrip diplexer is designed on a RT/Duroid substrate having a thickness h = 1.27mm with relative dielectric constant ε_r =6.15. The microstrip resonator filter was simulated by AWR Microwave Office. The basic parameters can be given by using the TXLINE tool, as shown in Figure 4-5.

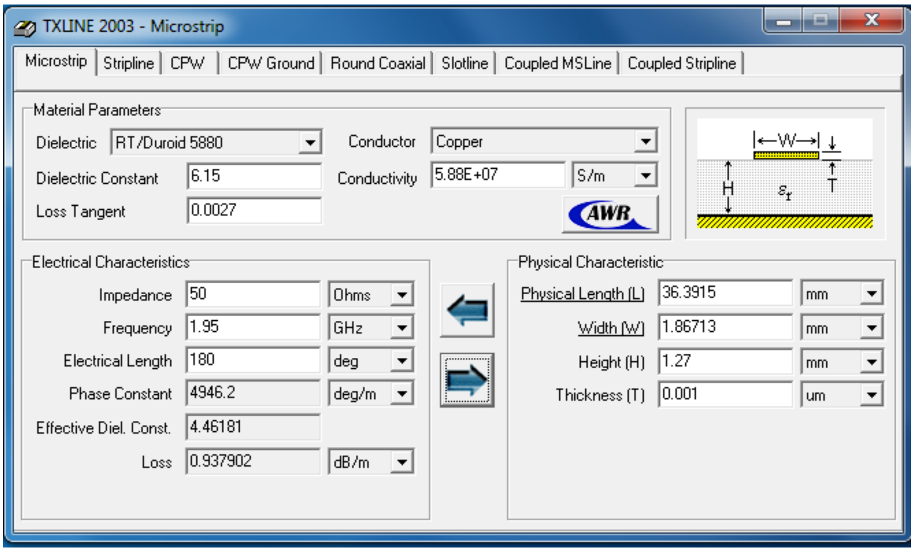

Figure 4-5: TXLINE tool for calculating length and width of the microstrip line of dielectric constant 6.15 at 1.95 GHz

4.5.1 External coupling

EM simulation tools can accurately model a wide range of RF/microwave structures and can be more efficiently used if the user is aware of sources of error. One principle error, which is common to most all the numerical methods, is due to the finite cell or mesh sizes. These EM simulators divide a RF/microwave filter structure into subsections or cells with 2D or 3D meshing, and then solve Maxwell's equations upon these cells. Larger cells yields faster simulations, but at the expense of larger errors. Errors are diminished by using smaller cells, but at the cost of longer simulation times. It is important to learn if the errors in the filter simulation are due to mesh-size errors. This can be done by repeating the EM simulation using different mesh sizes and comparing the results. The open-loop microstrip resonator is designed by Microwave Office circuit design software. The software can optimize any planar microstrip filter that can be defined in Microwave Office element catalog. In addition, S-parameter files imported from any planar can be port tuned. First of all, the external coupling is calculated because it is used to couple the filter with other devices in the system, which is expressed as Q values or it is called external loaded Q_e. The external loaded Q of the resonator is coupled to the input/output port by a coupling feed, as shown in Figure 4-6. The Q_e values can be extracted by changing the gap (g) between the coupled-feed and open-loop resonator. The calculation for extracting the external quality factor (Q_e) can be obtained as [1].

$$Q_e = f_0/\Delta f_{3dB} \tag{4.32}$$

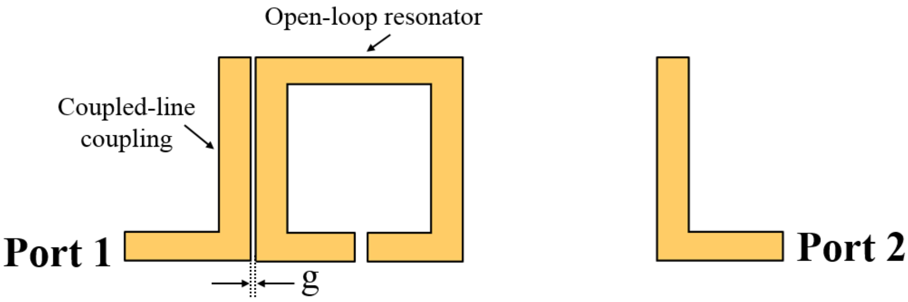

Figure 4-6: Microstrip open-loop resonator with coupled-feed for extracting the external quality factor

The external coupling is found by measuring at the 3 dB bandwidth of the resonant curve of the S_{21} magnitude fallen to 0.707 (-3dB) of maximum value, as shown in Figure 4-7.

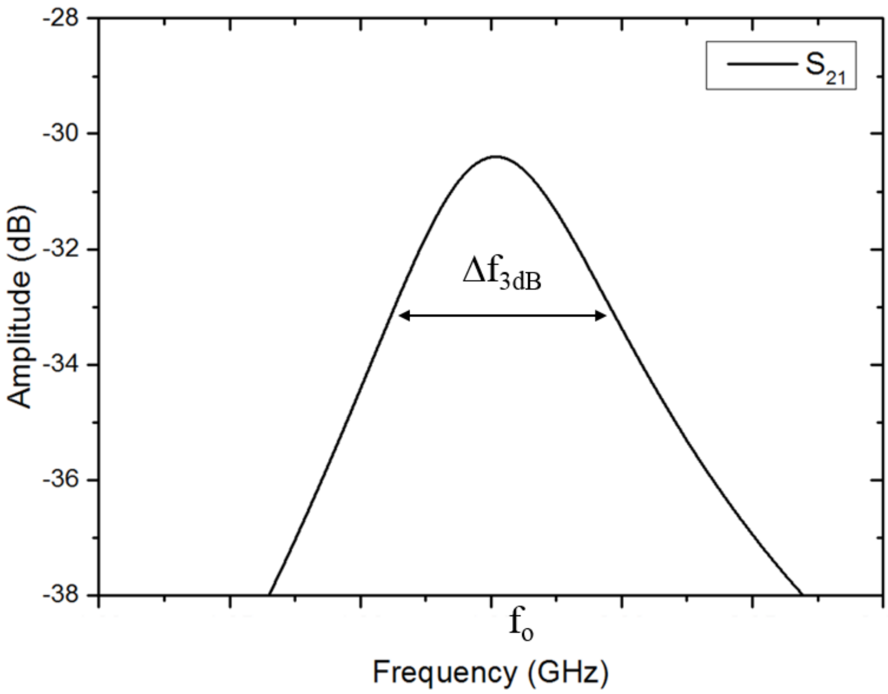

Figure 4-7: Response of S_{21} of the microstrip with coupled-feed

Figure 4-8 shows the relationship between the external quality factor (Q_e) of microstrip open-loop resonator and coupled-feed gap. The microstrip line width (w) = 1.87mm for 50Ω transmission line. The distance of external coupling line to resonator operating at the centre frequency of 1.95 GHz with Q_e= 25.9 is equal to 0.075 mm and of 2.14 GHz with Q_e= 28.44 is equal to 0.16 mm, respectively.

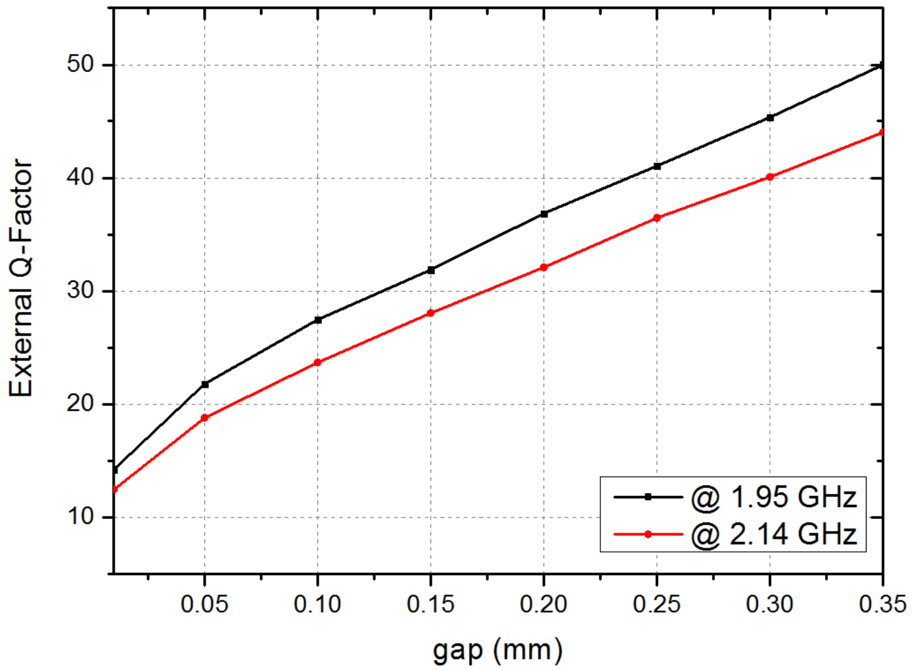

Figure 4-8: Q_e factor versus the distance of coupling line to the resonator

4.5.2 Inter-resonator coupling

To extract the coupling coefficient of two microstrip open-loop lines, the geometric structure can be presented as shown in Figure 4-9. The coupling coefficients between adjacent resonators can be given as equation (4.33). By varying the space between the two resonators, the coupling coefficient is dependent on the spacing between them [52]. It can then be calculated by

$$K = \pm \frac{f_{p2}^2 - f_{p1}^2}{f_{p2}^2 + f_{p1}^2} \tag{4.33}$$

Where f_{p1} and f_{p2} are the lower and higher spilt resonant frequencies of a pair of coupled resonators. The frequency response of a decoupled resonator structure for extracting the coupling coefficient can be represented in Figure 4-10 and the coupling coefficient (K) values between the two resonators can be plotted in Figure 4-11. By using equation (4.20), the coupling coefficient (K) between two resonators at 1.95 GHz, K_{12}=0.0426 and at 2.14 GHz, K_{12}=0.0387 are 1.74 and 1.89 mm, respectively.

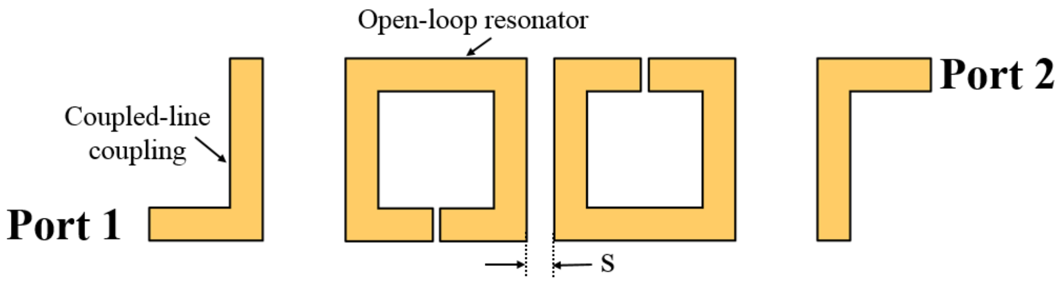

Figure 4-9: Two microstrip open-loop lines for extracted coupling coefficient

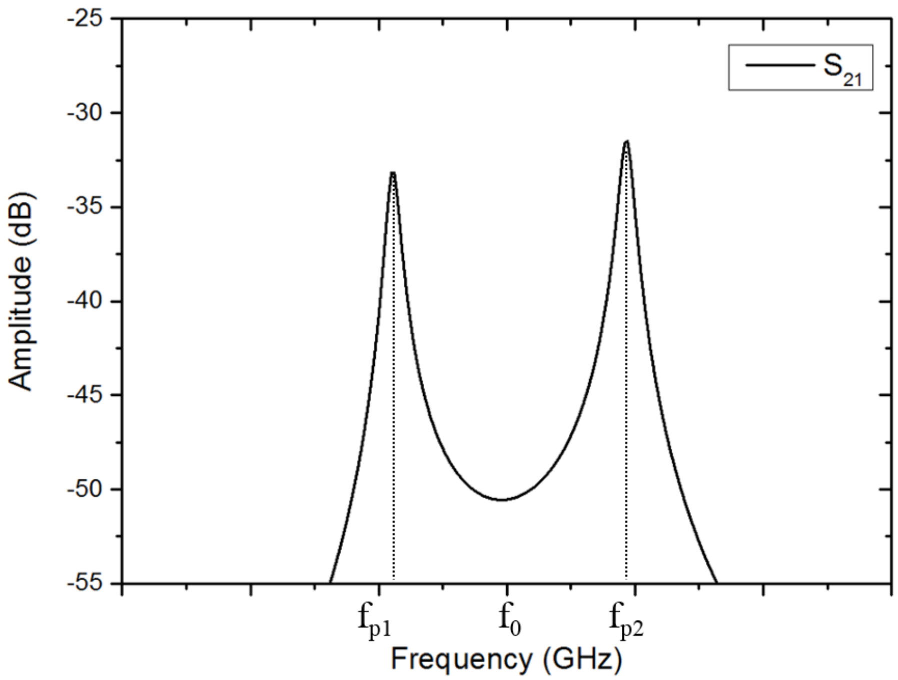

Figure 4-10: A typical frequency response of a decoupled resonator structure for extracting the coupling coefficient

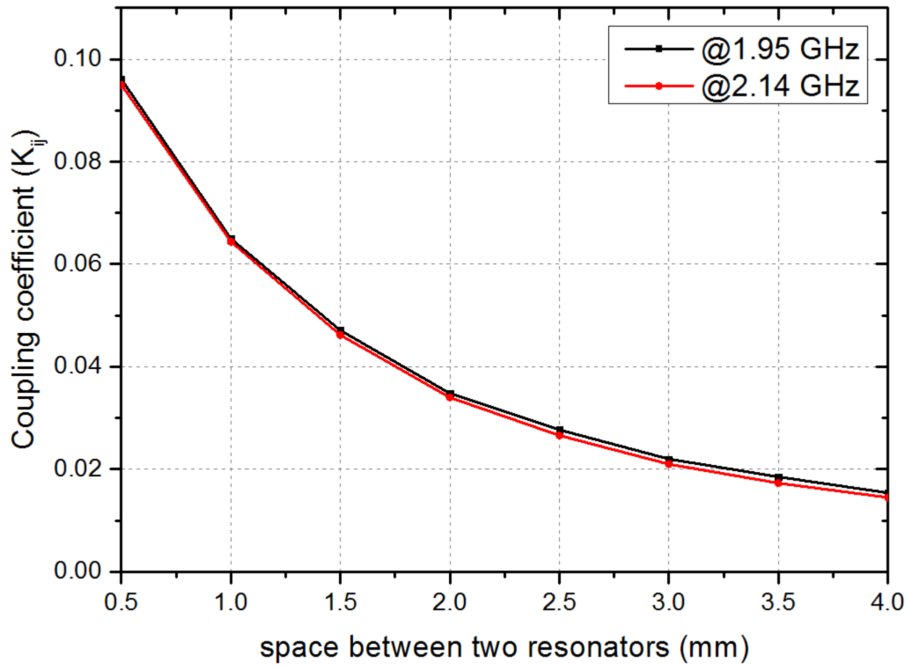

Figure 4-11: The coupling coefficient K versus the spacing(s) between two resonators

4.5.3 Physical simulation microstrip filter with coupled-feed

The simulation of bandpass filters can be achieved using a microstrip open-loop resonator with tapped-feed. The dimensions of the second-order microstrip resonator are shown in Table 4-4. The geometry of the proposed filters can be achieved as shown in Figure 4-12.

Table 4-4: Simulated dimensions of the microstrip open-loop resonator filter with coupled-feed

Dimensions	**R_X=1.95 GHz**	**T_X=2.14 GHz**
Microstrip width (w)	1.87 mm	1.87 mm
Space between two resonators (s)	1.74 mm	1.89 mm
Coupling feed gap (g)	0.075 mm	0.16 mm
Resonator length (a)	7.8 mm	7.8 mm
Open-loop length (b)	3.68 mm	1.92 mm
Feed length (f)	5 mm	5 mm

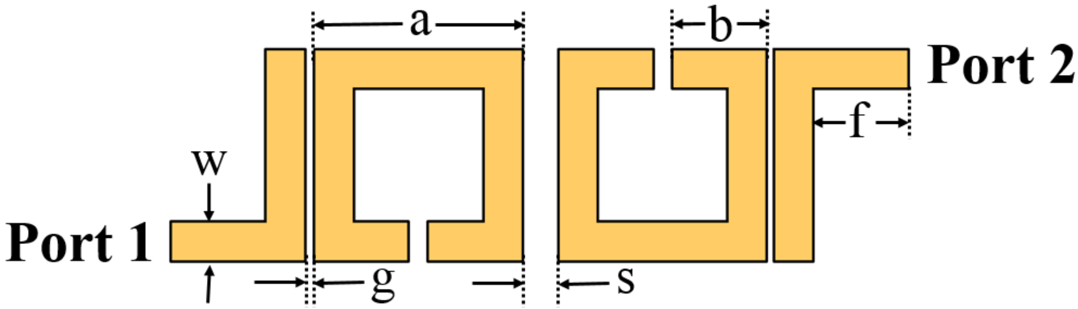

Figure 4-12: Second-order microstrip open-loop resonator filter with coupled-feed

The simulated second-order microstrip open-loop resonator with coupled-feed at the centre frequency of 1.95 GHz is portrayed in Figure 4-13. The fractional bandwidth is 2.6% (50 MHz at 1.95 GHz). The passband IL is less than 1.22 dB and the RL is better than 20.48 dB in the passband. Figure 4-13 shows the wide-band simulation of this second-order resonator.

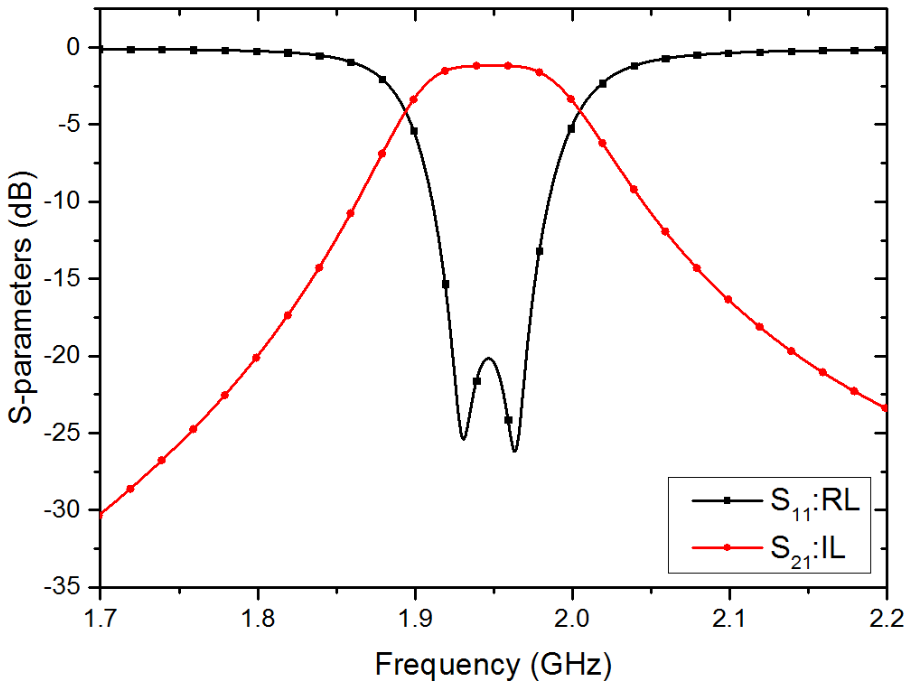

Figure 4-13: The second-order microstrip filter simulated at 1.95 GHz

The simulated response of the second-order microstrip open-loop resonator with coupled-feed at the centre frequency of 2.14 GHz is portrayed in Figure 4-14. The fractional bandwidth is 2.3% (50 MHz at 2.14 GHz). The passband IL is less than 1.09 dB and the RL is better than 20 dB in the passband.

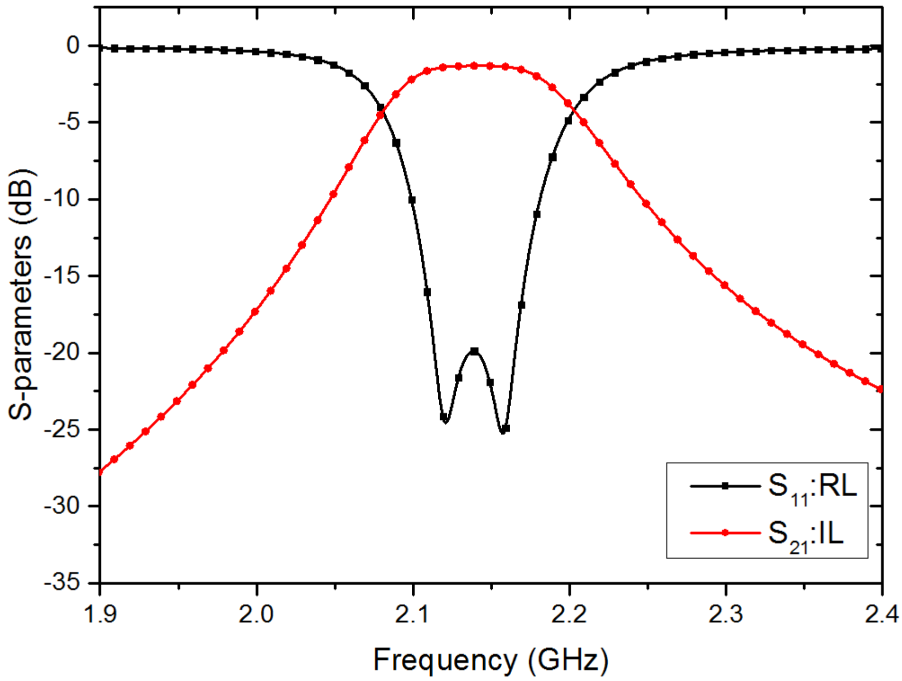

Figure 4-14: The second-order microstrip filter simulated at 2.14 GHz

4.5.4 Second-order microstrip resonator diplexer with coupled-feed

The diplexer design is based on the design of the two bandpass filters independently: one of them meeting the desired frequency band in the Rx band at 1.95 GHz and the other desired frequency band in the Tx band at 2.14 GHz. Then, the T-junction is used to connect the two independent bandpass filters together. The dimensions of the geometric microstrip diplexer with coupled-feed are shown in Table 4-5. The geometry of the proposed diplexer is designed at 1.95 and 2.14 GHz, as shown in Figure 4-15.

Table 4-5: Simulated dimensions of the microstrip diplexer with coupled-feed

Dimensions	**Rx=1.95 GHz**	**Tx=2.14 GHz**
Microstrip width (w)	1.87 mm	1.87 mm
Space between two resonators (s)	1.89 mm	1.74 mm
Coupling feed gap (g)	0.075 mm	0.10 mm
Resonator length (a)	7.8 mm	7.8 mm
Open-loop length (b)	3.68 mm	1.92 mm
Feed length (f)	5 mm	5 mm
Tap feed length (t)	37.44 mm	

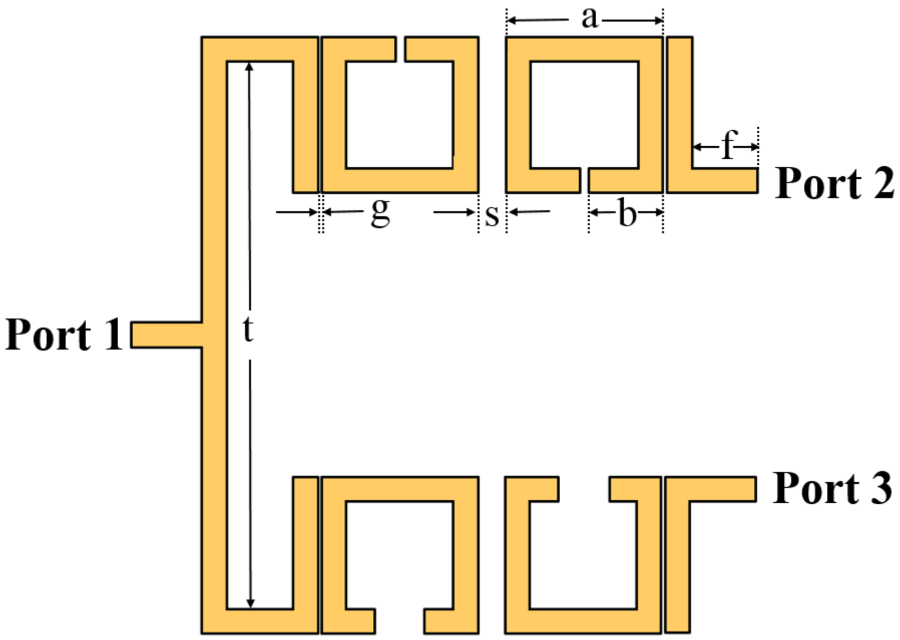

Figure 4-15: Second-order microstrip diplexer with coupled-feed

The simulated response of the diplexer is portrayed in Figure 4-16. The fractional bandwidth is 2.6% and 2.3% .The passband IL in the Rx band is less than 1.25 dB and, in the Tx band, 1.3 dB. The RL in both channels is better than 20 dB in the passband. The simulated isolation between Rx and Tx bands is better than 23.55 dB in transmit and receive bands as shown in Figure 4-17. Figure 4-18 shows the wide-band simulation of this second-order diplexer. It can also be seen that the simulated wideband has a spurious response at 3.95 GHz and 4.33 GHz because the first higher mode of the λ/2 microstrip line resonate at around two times of fundamental mode.

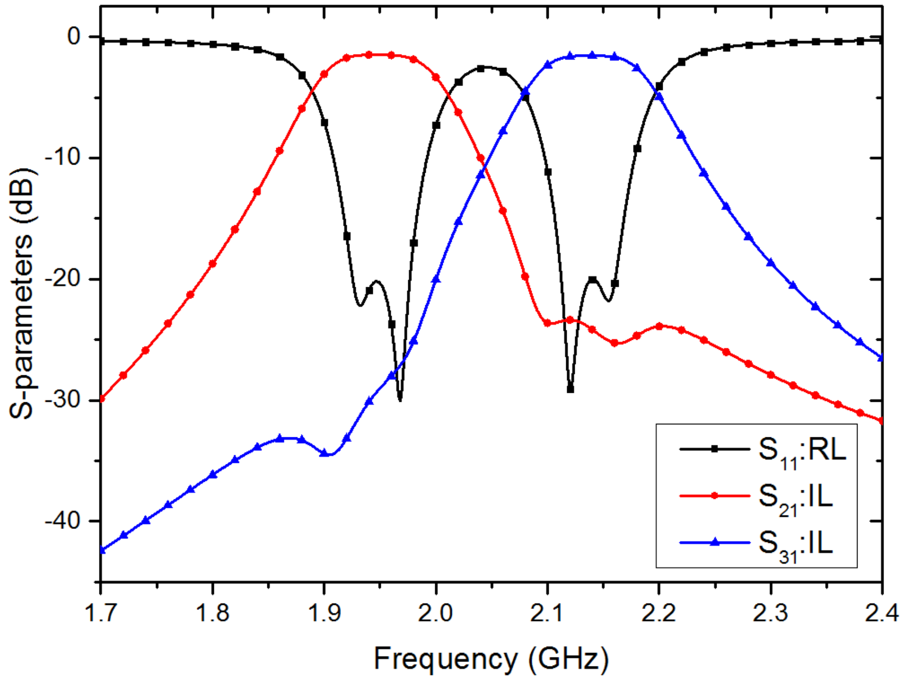

Figure 4-16: The simulated response of the second-order diplexer at 1.95 GHz and 2.14 GHz

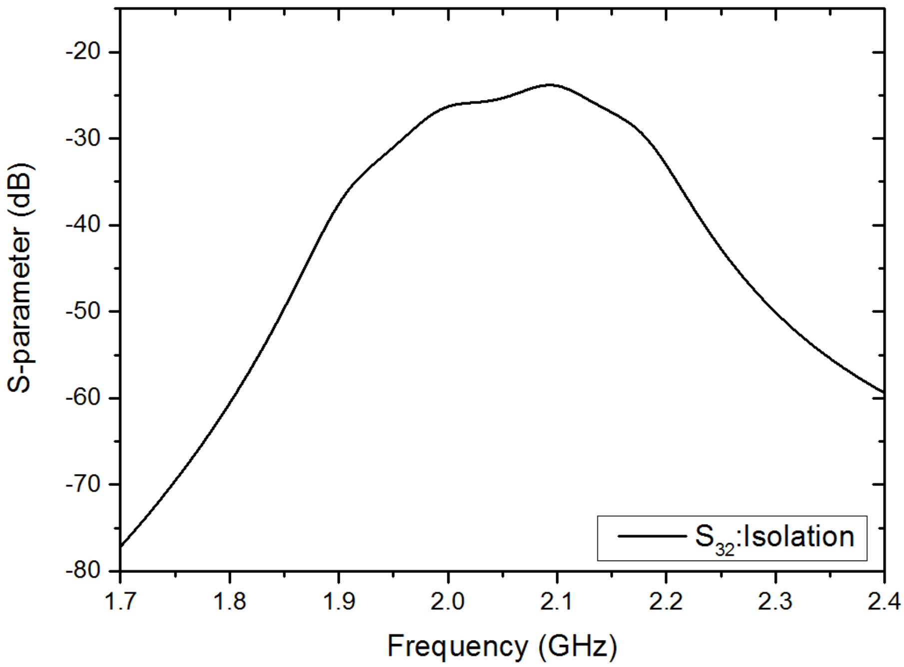

Figure 4-17: The isolation of the microstrip diplexer with coupled-feed

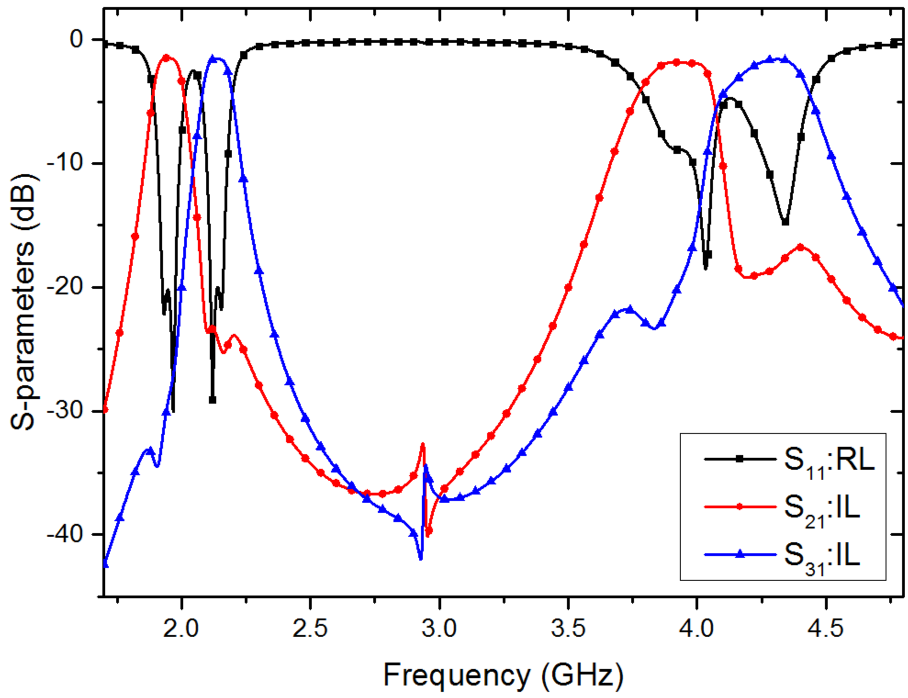

Figure 4-18: Wide-band response of the second-order microstrip diplexer with coupled-feed

4.5.5 Second-order microstrip four-port diplexer with coupled-feed

The microstrip four-port diplexer is based on two back-to-back second-degree microstrip-open loop diplexers with coupled-feeders, which are combined to form a four-port diplexer. The delayed-line is used to tune the phase between ports 2 and 4 to achieve a 180° phase shift. The dimensions of the microstrip four-port diplexer are shown in Table 4-5. The geometry of the proposed four-port diplexer is designed at 1.95 and 2.14 GHz, as shown in Figure 4-19.

Table 4-6: Simulated dimensions of the four-port microstrip diplexer with coupled-feed

Dimensions	**R_X=1.95 GHz**	**T_X=2.14 GHz**
Microstrip width (w)	1.87 mm	1.87 mm
Space between two resonators (s)	1.89 mm	1.74 mm
Coupling feed gap (g)	0.075 mm	0.10 mm
Resonator length (a)	7.8 mm	7.8 mm
Open-loop length (b)	3.68 mm	1.92 mm
Feed length (f)	5 mm	5 mm
Tap feed length (t)	37.44 mm	
Microstrip line (j)	21.6 mm	
Microstrip line m)	5.4 mm	
Microstrip line (k)	16.4 mm	
Microstrip line (n)	7.415 mm	
Microstrip line feed (ft)	20 mm	

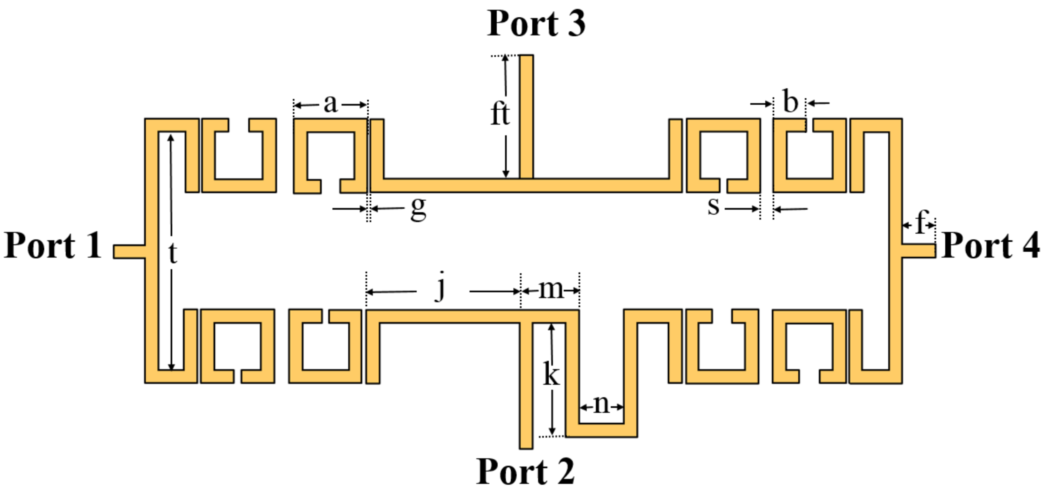

Figure 4-19: Second-order four-port diplexer with coupled-feed line [53]

The simulated response of the four-port diplexer is portrayed in Figure 4-20. The passband IL in the Rx band is less than 1.46 dB and, in the Tx band, 1.47 dB. The RL in both channels is better than 20 dB in the passband. The simulated isolation between Rx and Tx bands is better than 53.57 dB in transmit and receive bands, as shown in Figure 4-21. The phases of S_{31} and S_{24} are 128.6° and -50.96°, respectively, resulting in a phase difference of 179.56°, as shown in Figure 4-22. Figure 4-23 shows the wide-band simulation of this second-order diplexer. It can also be seen that the simulated wideband has a spurious response at 3.95 and 4.33 GHz.

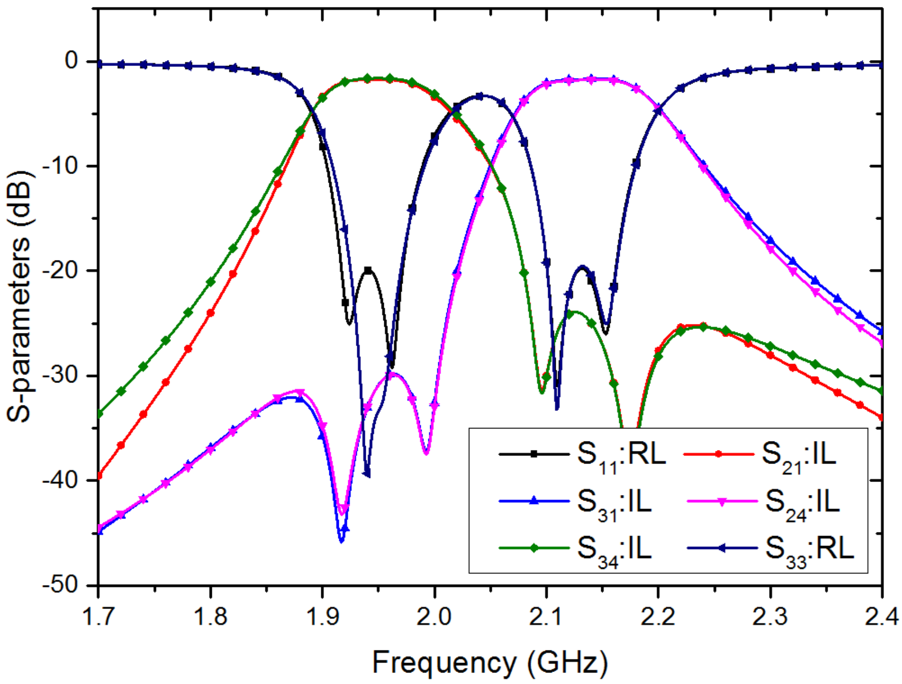

Figure 4-20: The simulated response of the second-order four-port diplexer with coupled-feed line at 1.95 GHz and 2.14 GHz

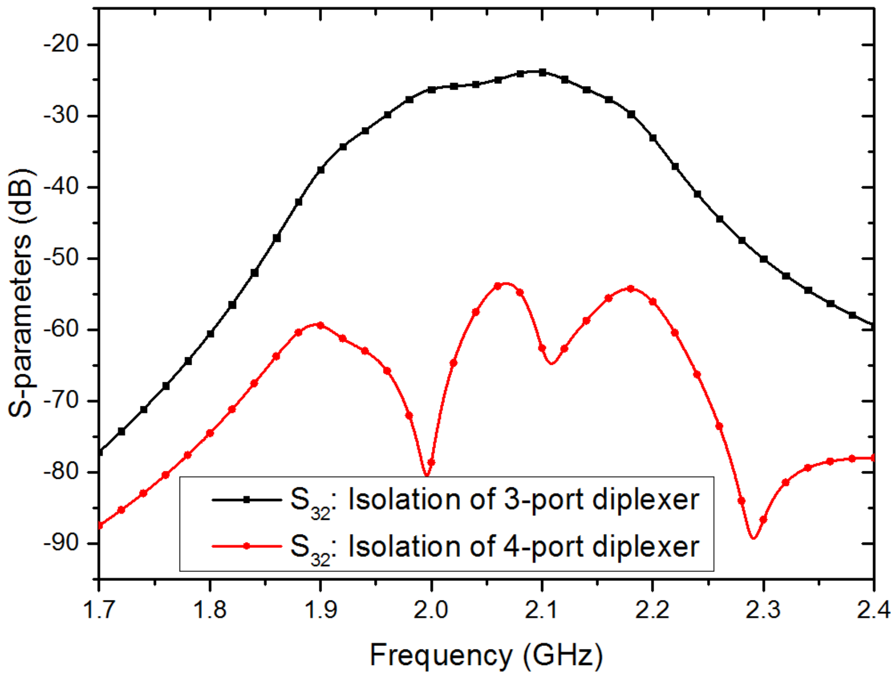

Figure 4-21: Simulated isolation of the four-port diplexer compared to the three-port diplexer

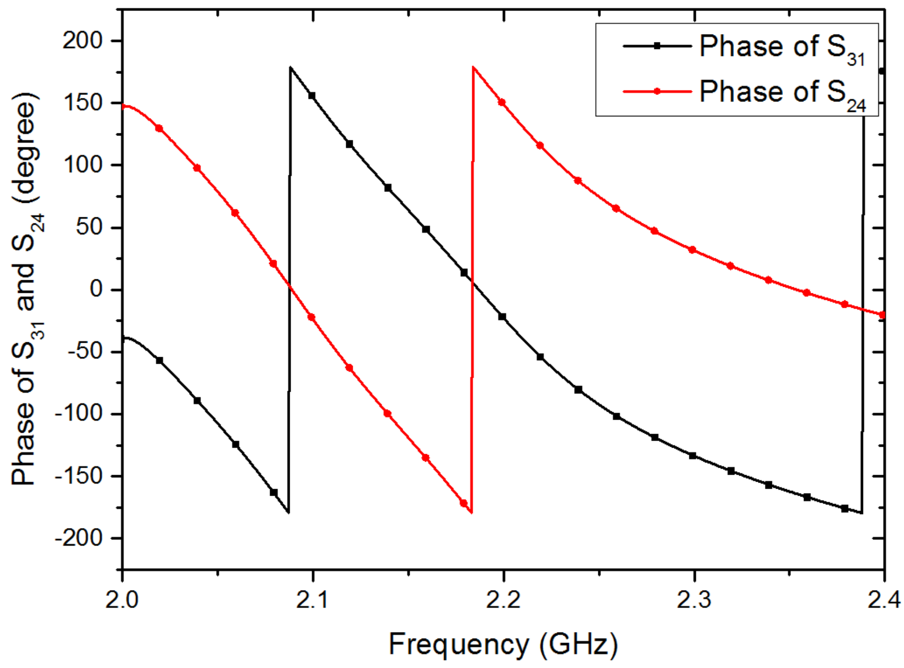

Figure 4-22: Simulated phases of S31 and S24 with 179.56° phase difference at 2.14 GHz

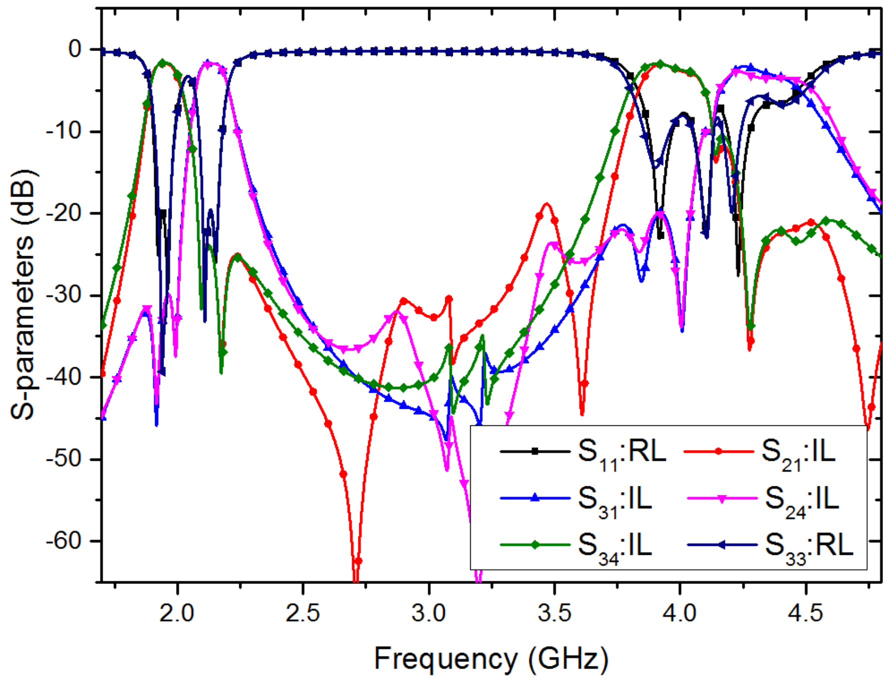

Figure 4-23: Wide-band response of the second-order microstrip open-loop diplexer with coupled-feed line

4.6 Second-order microstrip resonator with tapped-feed

A half-wavelength microstrip line of 50Ω impedance is designed at 1.95 GHz and 2.14 GHz. The filters are designed on a RT/Duroid substrate having a thickness h = 1.27mm with relative dielectric constant εr =10.2. Loss tangent $(\tan\delta)$ is 0.0023. From equation (4.31), the calculated Q-factor at 1.95 GHz is 160. At 2.14 GHz, the Q-factor is 165.2.

From equation (4.17), the second-order filter with low Q-factor is about 160, which would lead to a loss of 1.28 dB at 1.95 GHz.

The filter designed with a low Q-factor is about 165.2, which would lead to a loss of 1.24dB at 2.14 GHz.

The basic parameters can be given by using the TXLINE tool, as shown in Figure 4-24.

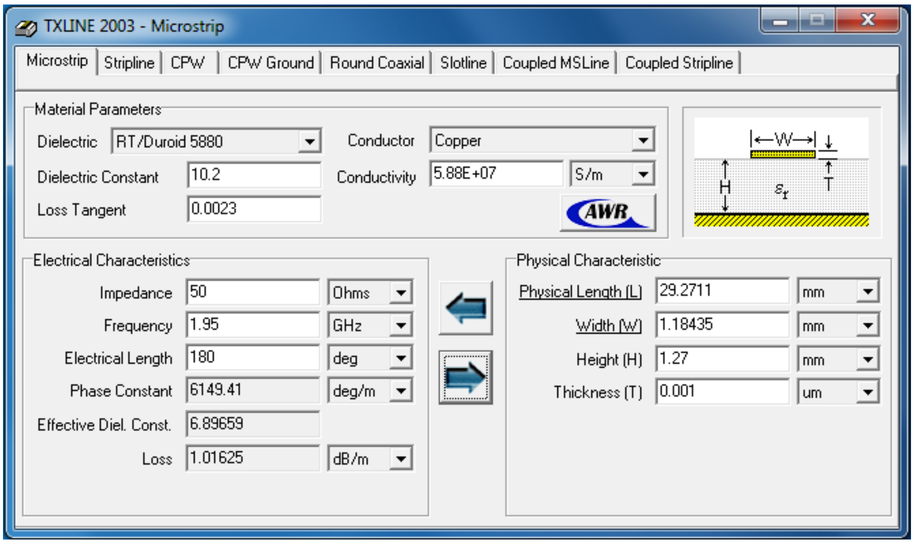

Figure 4-24: TXLINE tool for calculating length and width of the microstrip line of a dielectric constant 10.2 at 1.95 GHz

4.6.1 External coupling

The input/output coupled-feeds sometimes have a small coupling gap between input and output ports, which is difficult to address in the fabricating process. Another alternative method of input/output coupling by using tapped-feed is introduced to transfer the signal from input to resonator directly. The input and output feeds can be introduced by placing a tapped-line as shown in Figure 4-25.

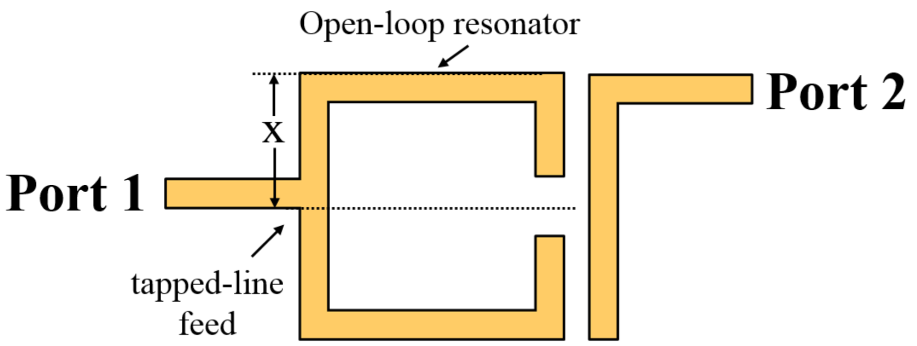

Figure 4-25: Microstrip resonator with tapped-feed for extracted external quality factor

The external loaded Q of the resonator is coupled to the input/output port by a tapped-feed, as shown in Figure 4-25. The Q_e values can be extracted by changing tapped-feed position (x) and open-loop resonator. The calculation for extracting the external quality factor (Q_e) can be obtained as.

$$Q_e = f_0/\Delta f_{3dB} \tag{4.34}$$

The external coupling is found by measuring at the 3 dB bandwidth of the resonant curve of the S_{21} magnitude fallen to 0.707 (-3dB) of maximum value as shown in figure 4-26.

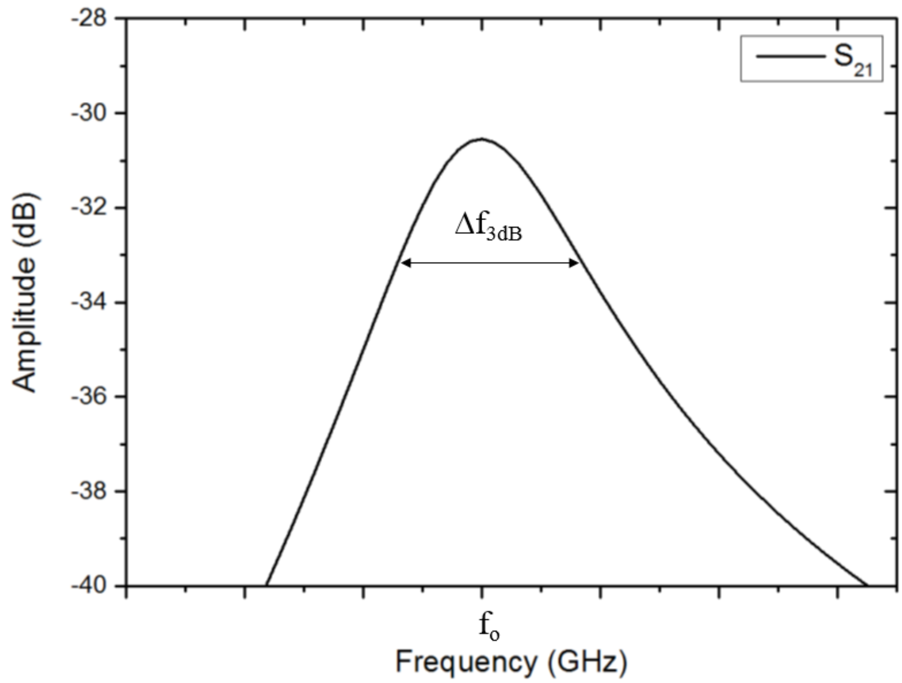

Figure 4-26: Response of S_{21} of the microstrip with tapped-feed

Tapped-feed design methodology uses the same methodology as in coupling-feed structure because they have the same external Q-factor (Q_e) values but different feeder structure. The relationship between external Q-factor and tapped-feed position (x) is shown in Figure 4-27. The external Q-factor at the centre frequency of 1.95 GHz with Q_e= 25.9 is equal to 2.1 mm and that of 2.14 GHz with Q_e= 28.44 is equal to1.75 mm, respectively.

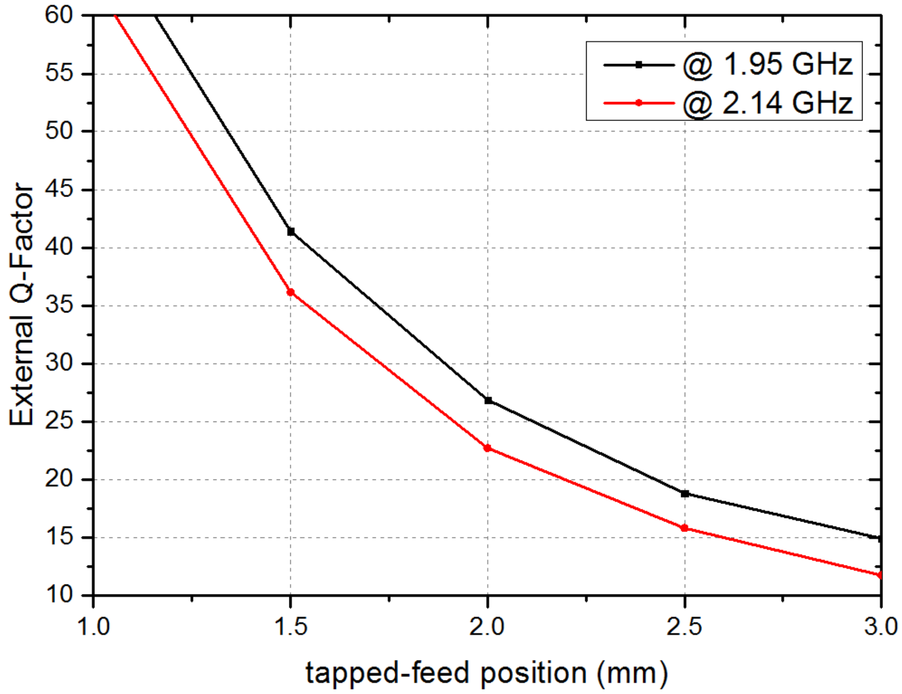

Figure 4-27: External quality factor Q_e versus the distance of the coupling line to the resonator

4.6.2 Inter-resonator coupling

The inter resonator coupling calculation of tapped-feed uses the same consideration as in coupling-feed structure. By varying the space between the two resonators, the coupling coefficient is dependent on the spacing between them [52]. It can then be calculated by

$$K = \pm \frac{f_{p2}^2 - f_{p1}^2}{f_{p2}^2 + f_{p1}^2} \tag{4.35}$$

Where f_{p1} and f_{p2} are the lower and higher spilt resonant frequencies of a pair of coupled resonators. The coupling coefficients (K_{ij}) can be extracted from the spacing between adjacent resonators, as shown in Figure 4-28. The frequency response of a decoupled resonator structure for extracting the coupling coefficient can be represented in Figure 4-29.The relationship between coupling coefficients and spacing of two resonators is represented in Figure 4-30. The coupling coefficients between two resonators at 1.95 GHz, K_{12}=0.0426, and at 2.14 GHz, K_{12}=0.0387, are 0.18 and 0.29 mm, respectively.

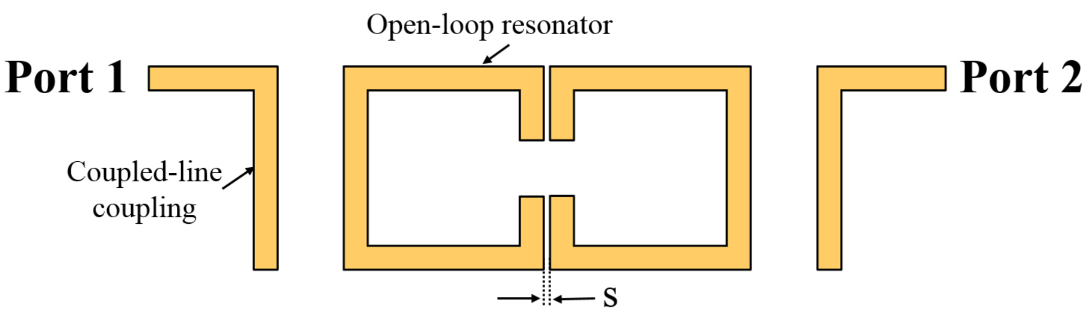

Figure 4-28: Two microstrip open-loop resonators for extracted coupling coefficient

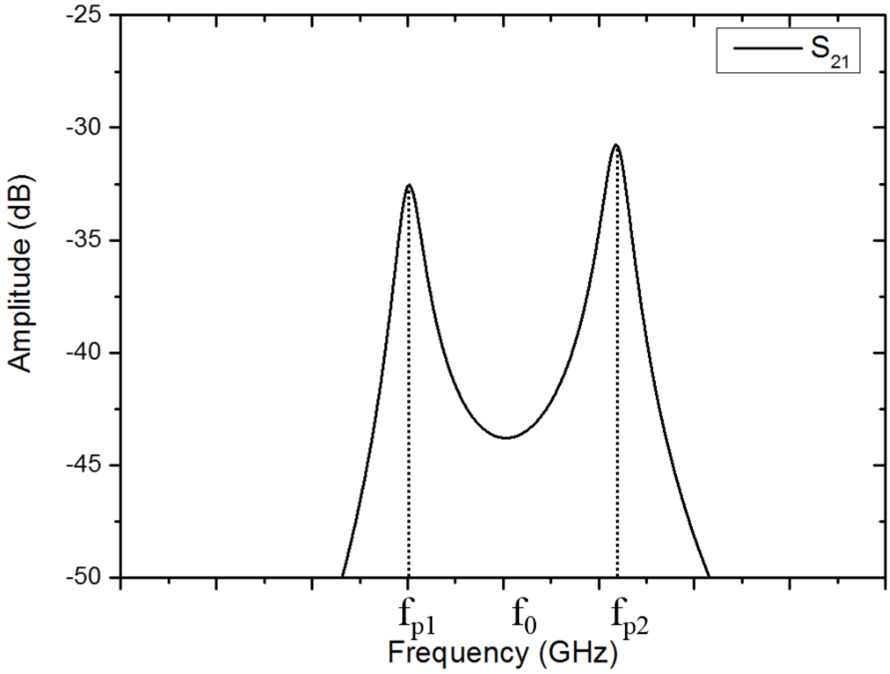

Figure 4-29: A typical frequency response of a decoupled resonator structure for extracting the coupling coefficient

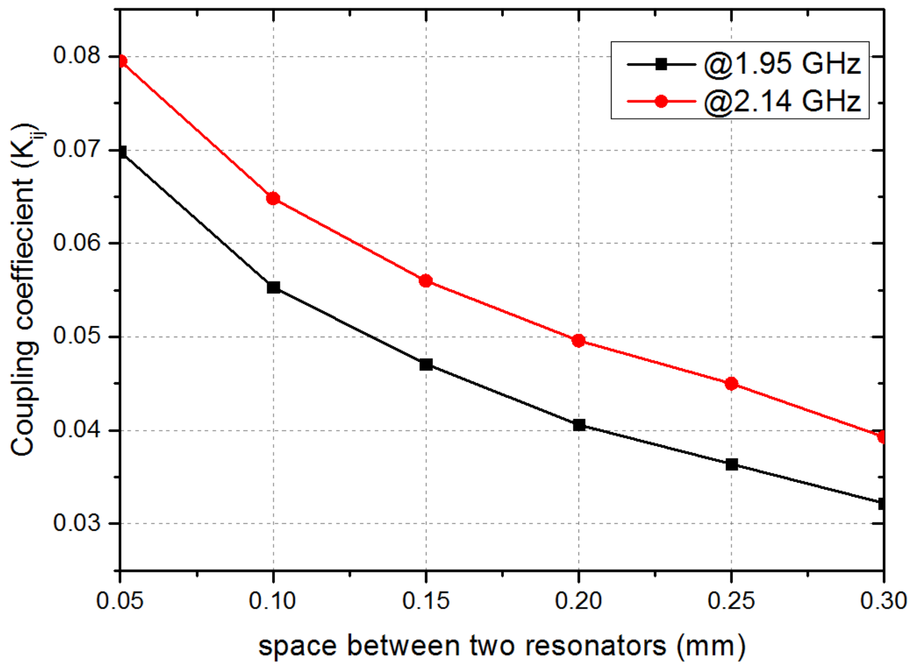

Figure 4-30: The coupling coefficient K versus the spacing between two resonators (s)

4.6.3 Physical simulation of the microstrip filter with tapped-feed

The simulation of bandpass filters can be achieved using a microstrip open-loop resonator with tapped-feed. The input/output feeders are connected directly to the open–loop resonators. The dimensions of the microstrip loop-resonator are listed in Table 4-7. The geometry of the proposed filters can be achieved as shown in Figure 4-31.

Table 4-7: Simulated dimensions of the microstrip open-loop resonator filter with tapped-feed

Dimensions	R_X=1.95 GHz	T_X=2.14 GHz
Microstrip width (w)	1mm	1mm
Space between two resonators (s)	0.18 mm	0.29 mm
Tapped-line feed (x)	2.13 mm	1.75 mm
Resonator length (a)	7.4 mm	7.4 mm
Open-loop length (b)	2.48 mm	1.119 mm
Feed length (f)	5 mm	5 mm

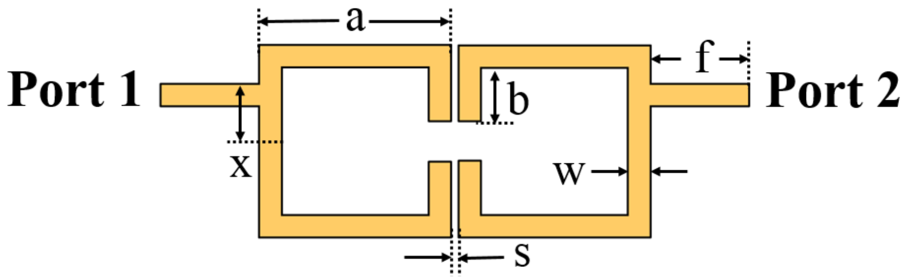

Figure 4-31: Second-order microstrip open-loop resonator filter with tapped-feed

The simulated response of the second-order microstrip filter with tapped-feed is portrayed in Figure 4-32. The bandwidth is 2.6% (50 MHz at 1.95 GHz). The passband IL is less than 1.22 dB and the RL is better than 20.42 dB in the passband, which agree well with the calculation

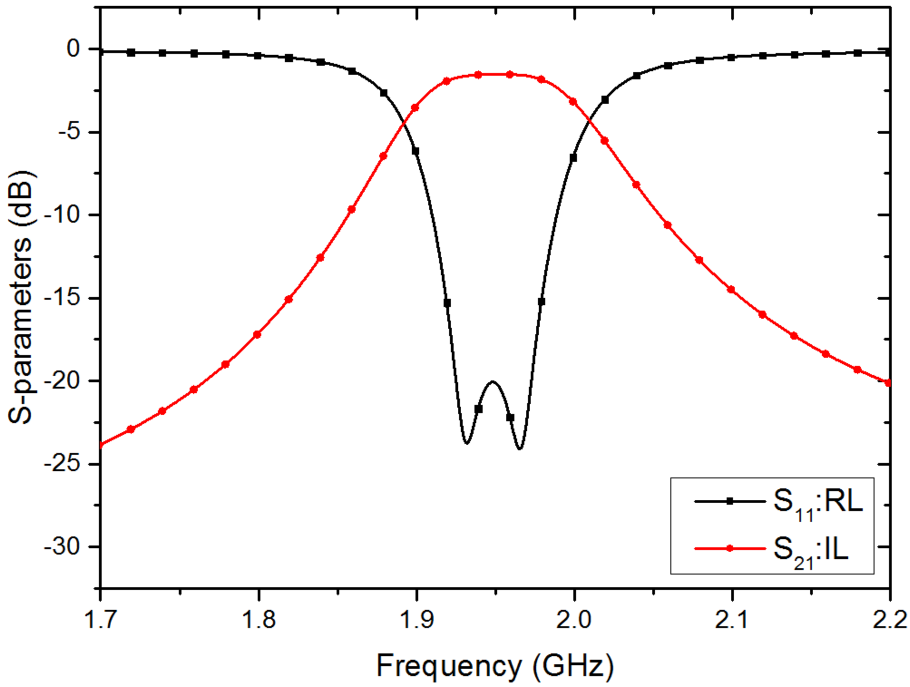

Figure 4-32: The microstrip filter with tapped-feed simulated at 1.95 GHz

The simulated response of the microstrip open-loop resonator with tapped-feed designed at the centre frequency of 2.14 GHz is plotted in Figure 4-33. The fractional bandwidth is 2.3% (50 MHz at 2.14 GHz). The passband IL is less than 1.19 dB and the RL is better than 20 dB in the passband.

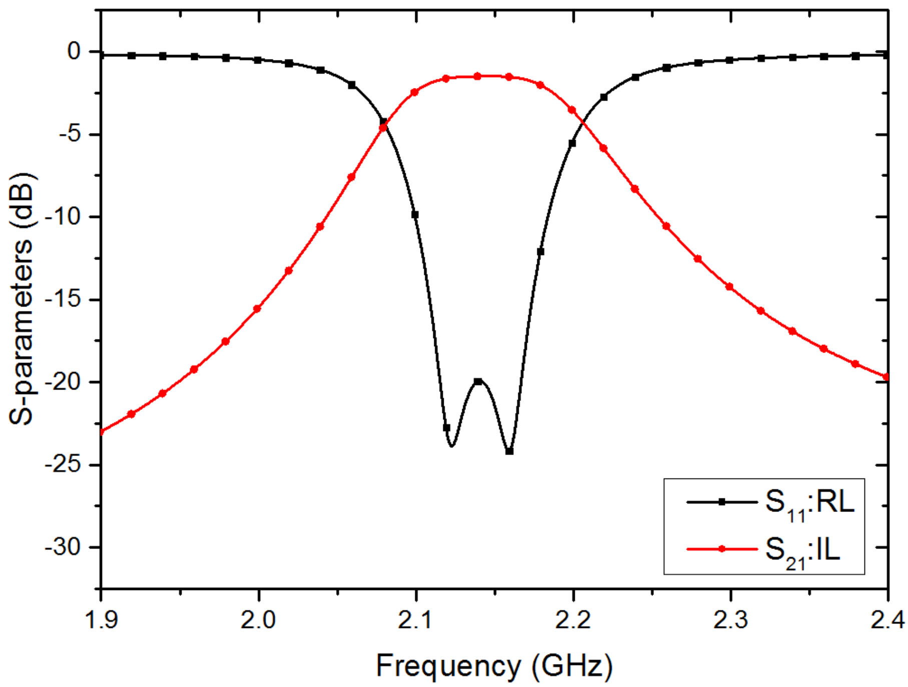

Figure 4-33: The microstrip filter with tapped-feed simulated at 2.14 GHz

4.6.4 Second-order microstrip resonator diplexer with tapped-feed

The diplexer design is based on the design of the two bandpass filters independently: one of them meeting the desired frequency band in the Rx band at 1.95 GHz and the other desired frequency band in the Tx band at 2.14 GHz. Then, the T-junction is used to connect the two independent bandpass filters together. The dimensions of the microstrip open-loop resonator diplexer are shown in Table 4-8. The geometry of the proposed diplexer is designed at 1.95 and 2.14 GHz, as shown in Figure 4-34.

Table 4-8: Simulated dimensions of the three-port diplexer with tapped-feeds

Dimensions	Rx=1.95 GHz	Tx=2.14 GHz
Microstrip width (w)	1mm	1mm
Space between two resonators (s)	0.18 mm	0.29 mm
Tapped-line feed (x)	2.13 mm	1.75 mm
Resonator length (a)	7.4 mm	7.4 mm
Open-loop length (b)	2.48 mm	1.119 mm
Feed length (ft)	14 mm	14 mm
Tap length (t)	14.8 mm	

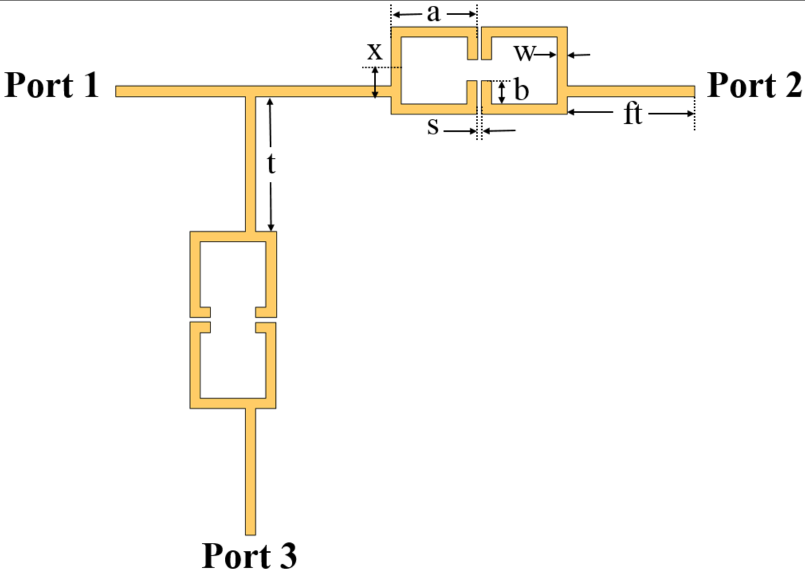

Figure 4-34: Geometry of the microstrip open-loop diplexer with tapped-feed

The simulated response of the microstrip diplexer is portrayed in Figure 4-33. The passband IL in the Rx band is less than 1.429 dB and, in the Tx band, 1.412 dB. The RLs in both channels are better than 18.9 dB in the passband. The simulated isolation between Rx and Tx bands is better than 22.78 dB in transmit and receive bands, as shown in Figure 4-36. Figure 4-37 shows the wide-band simulation of the microstrip three-port diplexer with tapped-feed. It can also be seen that the simulated wideband has a spurious response at 3.32 GHz and 4.6 GHz.

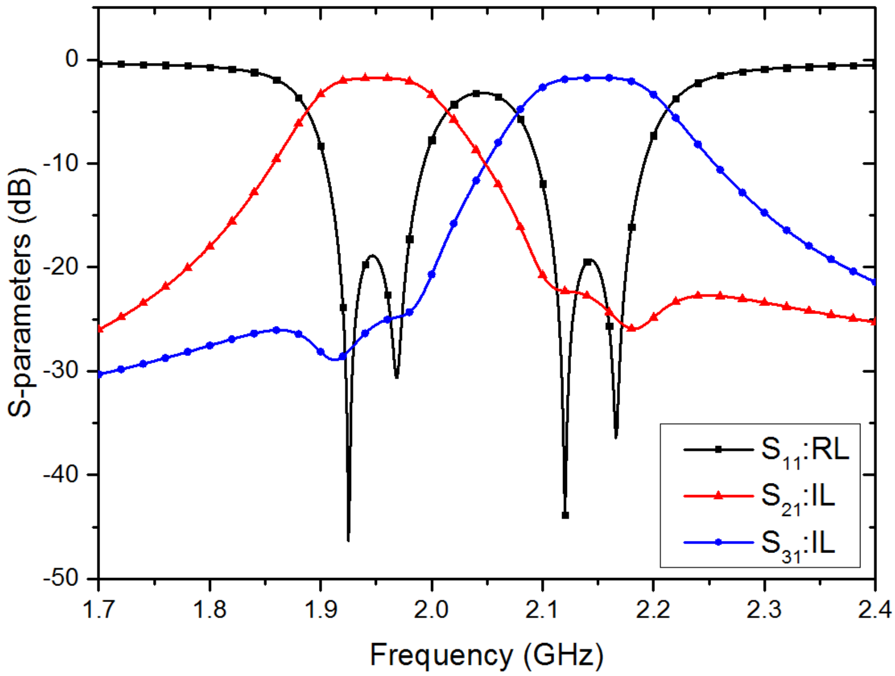

Figure 4-35: Simulated response of the microstrip open-loop diplexer with tapped-feed design at 1.95 GHz and 2.14 GHz

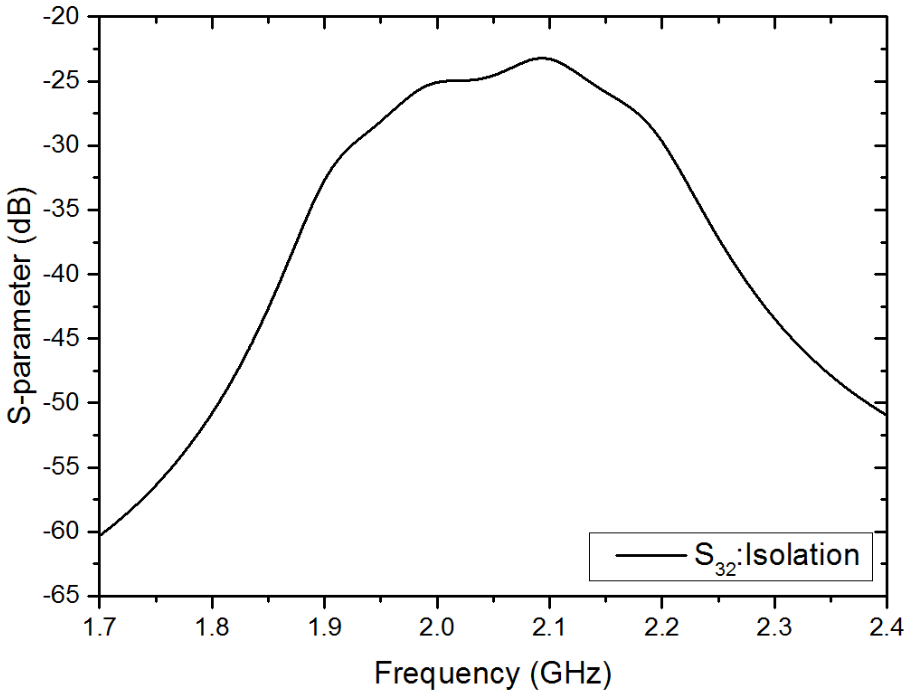

Figure 4-36: Simulated response of signal isolation of the diplexer

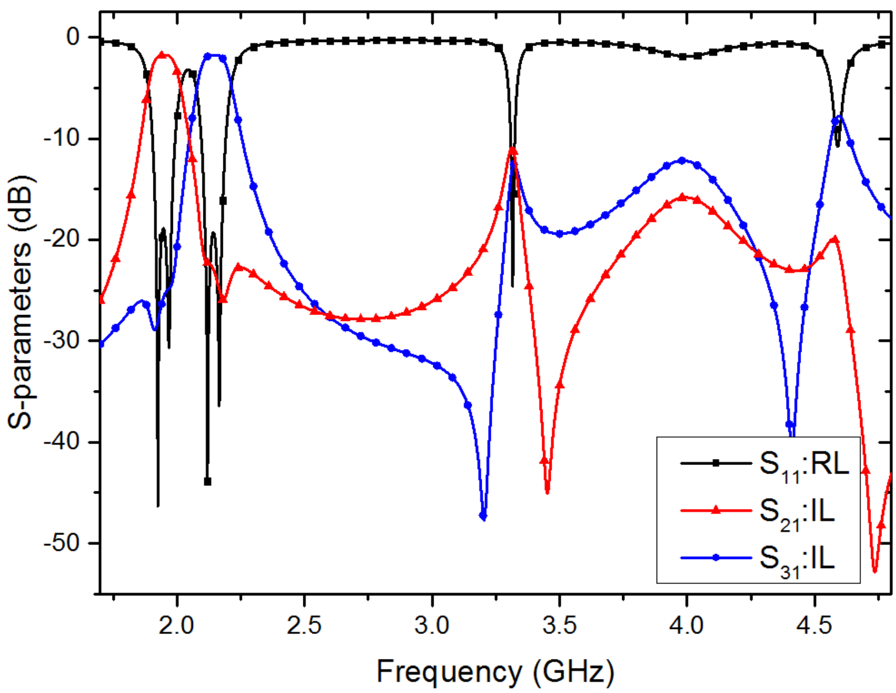

Figure 4-37: Wide-band response of the second-order microstrip diplexer

4.6.5 Second-order microstrip four-port diplexer with tapped-feed

The four-port diplexer for high Tx/Rx isolation with relatively low-order filter topology is presented here. The design technique is based on two back-to-back second-degree microstrip-open loop diplexers with tapped-feeders, which are combined to form a four-port diplexer. The delayed-line is used to tune the phase between ports 2 and 4 to achieve a 180° phase shift. The geometry of the four-port diplexer is shown in Figure 4-38. The dimensions of the microstrip open-loop diplexer are listed in Table 4-9.

Table 4-9: Simulated dimensions of the four-port diplexer with tapped-feeds

Dimensions	**R_X=1.95 GHz**	**T_X=2.14 GHz**
Microstrip width (w)	1mm	1mm
Space between two resonators (s)	0.18 mm	0.29 mm
Tapped-line feed (x)	2.13 mm	1.75 mm
Resonator length (a)	7.4 mm	7.4 mm
Open-loop length (b)	2.48 mm	1.119 mm
Feed length (ft)	14 mm	14 mm
Tap length (t)	14.8 mm	
Microstrip line m)	3 mm	
Microstrip line (k)	13.75 mm	
Microstrip line (n)	6.8 mm	

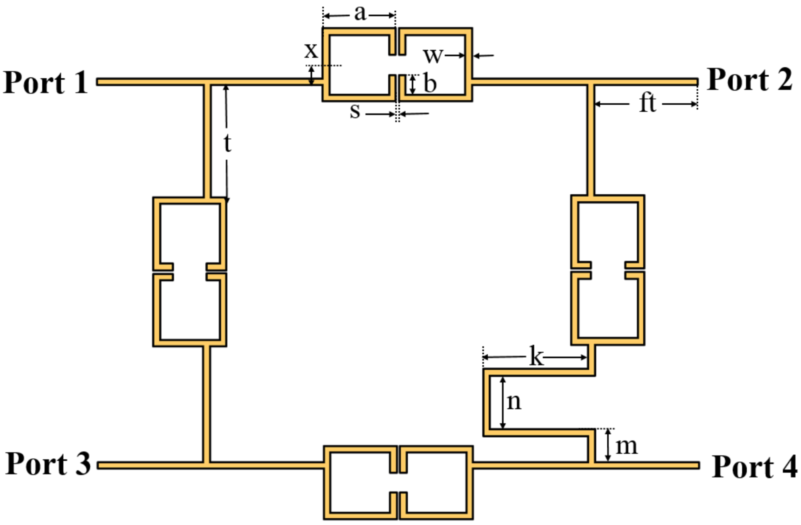

Figure 4-38: Second-order four-port diplexer with tapped-feeds

The diplexer simulated response is portrayed in Figure 4-39. The passband IL in the Rx band is less than 1.46 dB and, in the Tx band, 1.45 dB. The RL in both channels is better than 16.43 dB in the passband. The simulated isolation between Rx and Tx bands is better than 52.25dB in transmit and receive bands, as shown in Figure 4-40.

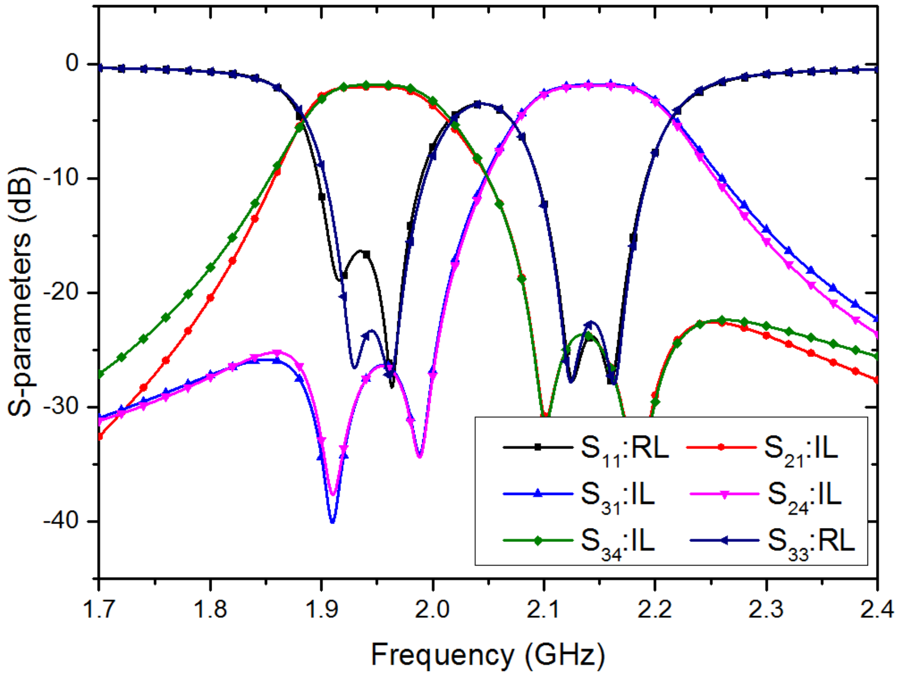

Figure 4-39: Simulated results of the microstrip four-port diplexer with tapped-feed

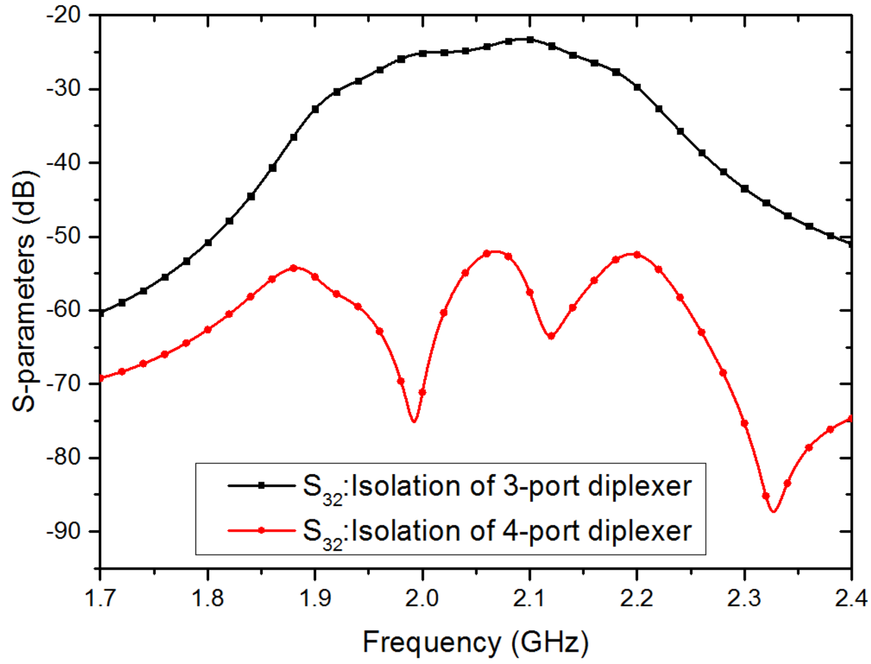

Figure 4-40: Comparison of simulated results of isolation (S_{32}) between three-port diplexer and four-port diplexer

The phase responses of S_{21} and S_{34} have the same phase but the phases of S_{31} and S_{24} are 80.52° and -99.4°, resulting in a phase difference of 179.92°, as plotted in Figure 4-41. Figure 4-42 shows the wide-band simulation of this second-order diplexer. It can also be seen that the simulated wideband has spurious response at 3.95 and 4.33 GHz.

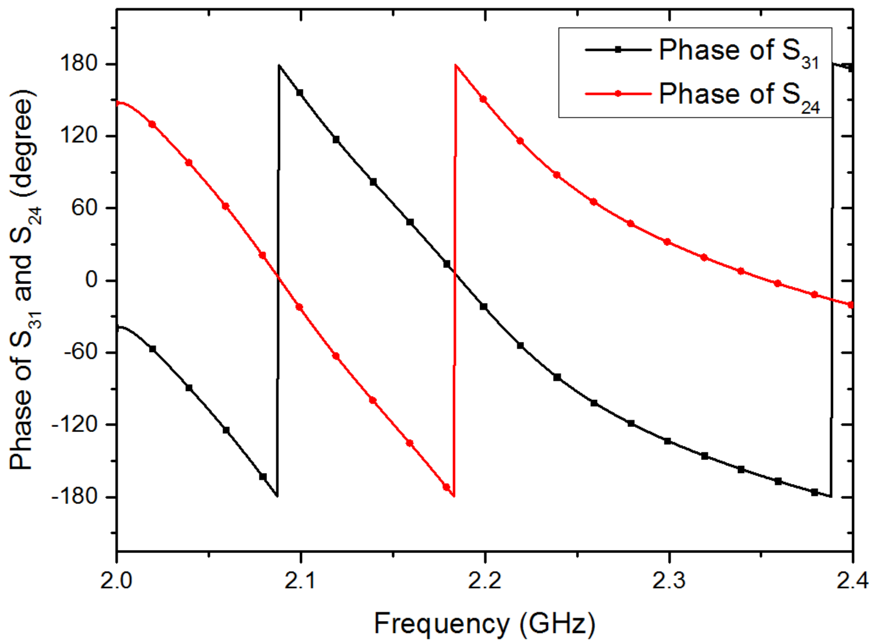

Figure 4-41: Simulated phase responses of S_{31} and S_{24} with 179.92° phase difference at 2.14 GHz

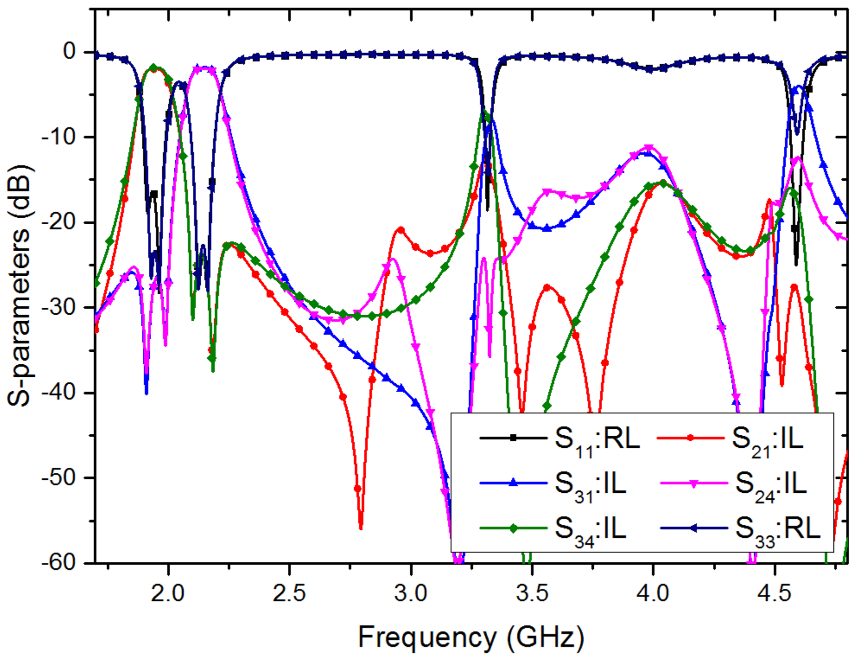

Figure 4-42: Wide-band response of the microstrip four-port diplexer

4.7 Summary

This chapter began by presenting a second-order capacitively coupled bandpass filter as an example of Chebyshev response. Then, the half-wavelength microstrip resonator and Q-factor were determined to calculate the insertion loss of filters. The second-order three-port diplexer using a microstrip open-loop resonator with coupled-feed and tapped-feed are simulated and compared to four-port diplexer structure. The second-order four-port diplexer using a microstrip open-loop resonator with coupled-feed was presented as a low Q-factor resonator. The delayed-line was successfully used to tune the phase between ports 2 and 4 to achieve a 180° phase shift. Finally, another alternative solution of a microstrip open-loop resonator using a tapped-feed was designed as having no coupled line between the input and the microstrip open-loop resonator. The next chapter is introduced the four-port diplexer with high Q factors which is an alternative technology to reduce overall signal losses and increase power handling with the same or better isolation compared with the microstrip technology is combline coaxial resonator structures.

Chapter 5
Modelling and Development of a High-Q Four-port Diplexer

5.1 Introduction

As the diplexer designs based on the microstrip structure can achieve low cost, small filter size and ease of integration but provide low power handling and high signal losses due to dielectric and ohmic losses. Therefore, the diplexer design with high Q factors by using combline resonator can be presented in this chapter. An equivalent circuit of a second-order combline filter with the introduction of input transformers is presented in details. Then, example prototypes with high Q-factors developed by using a combline structure are proposed as a four-port diplexer. Four-port diplexers with the same Q-factors and dissimilar Q-factors are successfully designed for high Tx/Rx signal isolation.

5.2 Lumped-element combline filter design

In this section, the design of the second-order Chebyshev filter is presented. Chebyshev filter response has better roll off but it introduces some ripples between two values in the pass band up to its cut off frequency and then roll off quickly in stop band. The specifications of the required filters are shown in Table 5-1

Table 5-1: Specifications of the combline bandpass filter design

Centre frequency (f_0)	R_X=1.73 GHz and T_X=2.13 GHz
Passband bandwidth, '(ΔF)'	50 MHz (FBW=2.89% and 2.35%)
Stopband insertion loss 'L_A'	>40 dB at $f_0 = \pm 1000\ MHz$
Return loss, 'RL'	> 20 dB
Insertion loss, 'IL'	< 0.5 dB
System Impedance, 'Z_0'	50 Ω

Firstly, the order of the filter can be calculated in [3].

$$N \geq \frac{L_A + L_R + 6}{20\ log_{10}[S + (S^2 - 1)^{1/2}]} \tag{5.1}$$

Where N is the order of the filter

When

$$L_A=40 \text{ and } L_R=20 \qquad (5.2)$$

Where L_A is the stopband insertion loss

R_L is the return loss

S is the selectivity and S is the ratio of stopband to passband bandwidth. Hence

$$S = \frac{Stopband\ insetion\ loss}{\text{Passband bandwidth}} = \frac{2000}{50} = 40 \qquad (5.3)$$

$$N \geq =1.734 \qquad (5.4)$$

Therefore, the order of the filter required to meet the specification is second order.

The ripple level ε is

$$\varepsilon = (10^{L_R/10} - 1)^{-1/2} \qquad (5.5)$$

$$=0.1005$$

Hence

$$\eta = \sinh[\frac{1}{N} sinh^{-1}(1/\varepsilon) \qquad (5.6)$$

$$=2.1213$$

And the shunt capacitive element value of the capacitive element Chebyshev lowpass prototype is

$$C_r = \frac{2}{\eta}\sin[\frac{(2r-1)\pi}{2N}] \qquad (5.7)$$

Where r=1,…, N

$$C_1 = C_2 = 0.6667$$

The element value of the normalised inverter coupled Chebyshev lowpass prototype is

$$K_{r,r+1} = \frac{[\eta^2 + sin^2(r\pi/N)]^{1/2}}{\eta} \qquad (5.8)$$

Where r=1,…, N-1

Therefore, the inverter value is

$$K_{12} = 1.1055$$

The normalised Chebyshev inverter coupled lowpass prototype is represented in Figure. 5-1.

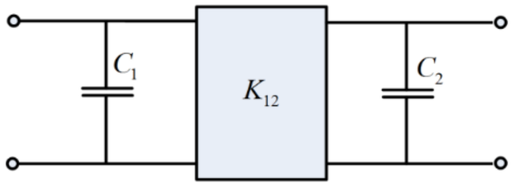

Figure 5-1: Equivalent circuit of impedance inverter

At the centre frequency of 1.73 GHz and 2.13 GHz and Z=50 ohm

$$\omega = 2\pi f \tag{5.9}$$

at 1.73 GHz, ω = 10.87x10^9 and at 2.13 GHz, ω = 13.38x10^9

and $$\Delta\omega = 2\pi * \Delta f \tag{5.10}$$

at 1.73 GHz, $\Delta\omega$ =3.1416 x10^8 and at 2.13 GHz, $\Delta\omega$ =3.1416 x10^8

Choose θ_0=50°, i.e. 0.8726 radians, then determine the α

$$\alpha = \frac{2\omega_0 \tan(\theta_0)}{\Delta\omega\{\tan(\theta_0)+\theta_0[1+tan^2(\theta_0)]\}} \tag{5.11}$$

at 1.73 GHz, α =3.1416 x10^8 and at 2.13 GHz, α =3.1416 x10^8

From

$$\beta = \frac{1}{\omega_0 \tan(\theta_0)} = \frac{C_{Lr}}{Y_{rr}} \tag{5.12}$$

By choosing Y_{rr}=1= $\frac{C_r}{\beta}$, then $C_r = \beta$

at 1.73 GHz, β =7.7195 x10^{-11} and at 2.13 GHz, β =6.2698 x10^{-11}

And from

$$n_r = [\frac{\alpha C_r \tan(\theta_0)}{Y_{rr}}]^{1/2} \tag{5.13}$$

Where r=1,…, N

at 1.73 GHz, n_1=n_2 =4.4533 and at 2.13 GHz, n_1=n_2 =4.9414

From

$$Y_{r,r+1} = \frac{K_{r,r+1}\tan(\theta_0)}{n_r n_{r+1}} \tag{5.13}$$

Where r=1,…, N-1

at 1.73 GHz, Y_{12} =0.0664 and at 2.13 GHz, Y_{12} =0.054

From

$$Y_1 = Y_N = Y_{11} - Y_{12} + \frac{1}{n_1^2} - \frac{1}{n_1 \cos(\theta_0)} \qquad (5.14)$$

Where r=1 and N

at 1.73 GHz, Y_1=Y_2 =0.6346 and at 2.13 GHz, Y_1=Y_2 =0.6722

From

$$Y_0 = Y_{N+1} = 1 - \frac{1}{n_1 \cos(\theta_0)} \qquad (5.15)$$

at 1.73 GHz, Y_0=Y_3 =0.6507 and at 2.13 GHz, Y_0=Y_3 =0.6852

From

$$Y_{01} = \frac{1}{n_1 \cos(\theta_0)} \qquad (5.16)$$

at 1.73 GHz, Y_{01} =0.3493 and at 2.13 GHz, Y_{01}=0.3148

The element values of the second-order combline diplexer are shown in Table 5-2.

To convert from an admittance to an impedance level of 50 ohm, we simply scale by Z=50/Y.

Table 5-2: Element values of the second-order combline filters at 1.73 and 2.13 GHz

Elements	Tx=1.73 GHz	Rx=2.13 GHz
Z_0	76.8451 Ω	72.975 Ω
Z_1	78.7837 Ω	74.3869 Ω
Z_{01}	143.127 Ω	158.8139 Ω
Z_{12}	752.6218 Ω	926.6383 Ω
C	1.5439 pF	1.254 pF

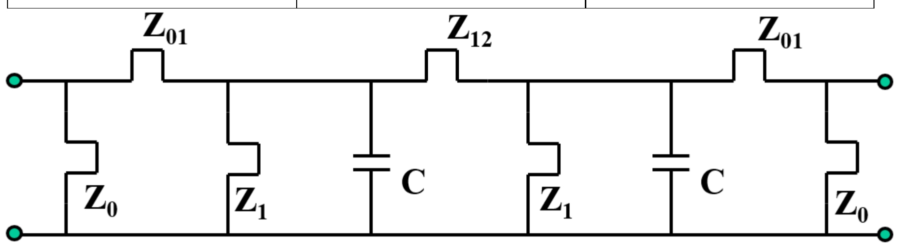

Figure 5-2: Equivalent circuit of the second-order combline filter with the introduction of the input transformer

The simulated response of the combline filter at 1.73 GHz is portrayed in Figure. 5-3. The 20-dB bandwidth is 50 MHz. The passband IL in the Rx band is less than 0.12 dB. The RL is better than 20 dB in the passband. A Q-factor of resonators is selected to be 1800.

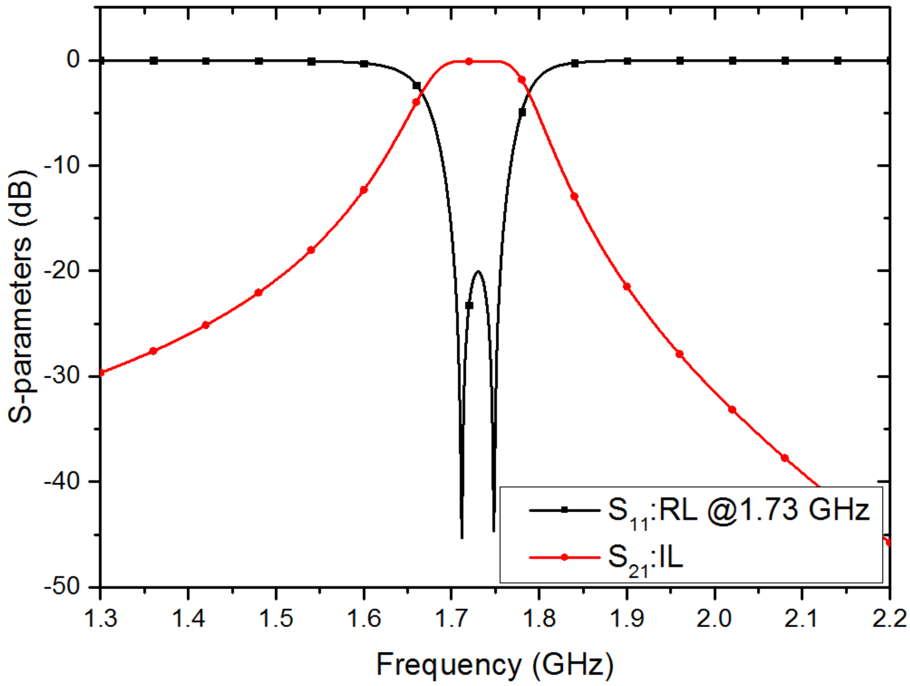

Figure 5-3: Simulated response of the combline filter at 1.73 GHz

The combline filter designed in Tx at a centre frequency of 2.13 GHz with 50 MHz bandwidth at 2.13 GHz simulated response by AWR Microwave Office is portrayed in Figure 5-4. The 20-dB bandwidth is 50 MHz. The passband IL in the Tx band is less than 0.13 dB. The RL is better than 20 dB in the passband.

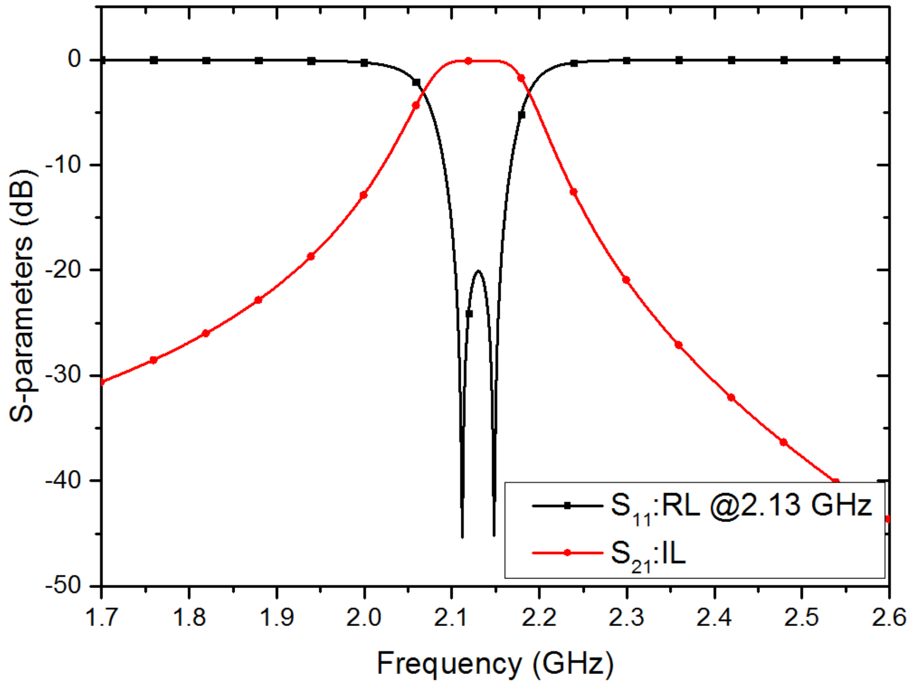

Figure 5-4: Simulated response of the combline filter at 2.13 GHz.

5.3 Combline resonator filter with input transformer

In this section, the design of the second-order Chebyshev combline resonator filter is presented. The specifications of the required filters are shown below:

Table 5-3: Specifications of the combline diplexer design

Centre frequency (f_0)	Rx=1.73 GHz and Tx=2.13 GHz
Passband bandwidth, '(ΔF)'	50 MHz (FBW=2.89%, 2.35%)
Stopband insertion loss	>40 dB
Return loss, 'RL'	> 20 dB
Insertion loss, 'IL'	< 0.5 dB
System impedance, 'Z_0'	50 Ω

The doubly loaded resonator normalised lowpass prototype filter element values (g_i) can be calculated as [48]

$$g_0 = 1$$

$$\beta = \ln\left(\coth\left(\frac{L}{17.37}\right)\right)$$

$$\gamma = \sinh\left(\frac{\beta}{2n}\right)$$

$$a_k = \sin\left[\frac{(2k-1)\pi}{2n}\right], \quad k = 1, 2, ..., n$$

$$b_k = \gamma^2 + \sin^2\left(\frac{k\pi}{n}\right), \quad k = 1, 2, ..., n$$

$$g_1 = \frac{2a_1}{\gamma}$$

$$g_k = \frac{4a_{k-1}a_k}{b_{k-1}g_{k-1}}, \quad k = 2, 3, ..., n$$

$$g_{n+1} = \begin{cases} 1 & n \text{ odd} \\ \coth^2\left(\frac{\beta}{4}\right) & n \text{ even} \end{cases} \tag{5.17}$$

Then, the element values of the second-order Chebyshev filter operating at the centre frequency of 1.73 GHz and 2.13 GHz are given as

g_0=1, g_1= 0.6682, g_2= 0.5462, g_3= 1.2222

The external values can be calculated by

$$Q_e = \frac{g_0 g_1}{FBW} \tag{5.18}$$

At 1.73 GHz, Qe= 23.12

At 2.13 GHz, Qe= 28.47

The coupling coefficient can be calculated by

$$K_{i,i+1} = \frac{FBW}{\sqrt{g_1 g_2}} \qquad \text{for i=1 to n-1} \tag{5.19}$$

At 1.73 GHz, K_{12}=0.0478

At 2.13 GHz, K_{12}=0.0389

5.4 Second-order combline resonator filter with the same Q-factors

To design a combline resonator filter, a basic understanding of the combline resonator structure is necessary. Practically, the combline resonator can be achieved by using a HFSS simulator. HFSS is a tool that has a high-performance full-wave electromagnetic (EM) field simulator for arbitrary 3D volumetric passive devices by using the Finite Element Method (FEM). HFSS is an interactive simulation system to solve any arbitrary 3D geometry, especially complex curves and shapes. Ansoft HFSS can be used to calculate parameters such as S-parameters, resonant frequency and field patterns. By using this simulator, three solution types can be achieved: driven mode, driven terminal and Eigen mode.

Firstly, in driven mode, the external sources of energy at a physical access port of simulated geometry are calculated by using the S-parameters mode. It can also simulate the S-parameters in terms of the incident and reflected losses. Secondly, the driven terminal is used to calculate the S-parameters of transmission line ports. Finally, the Eigen mode is defined as short-circuited planes without any sources and this mode is used to calculate the resonant frequencies, Q factor of any 3D structure and field patterns [54].

The resonant frequency for the fundamental mode of the combline resonator is determined by the HFSS program. In this case, the metallic rod resonator is placed in the centre of a conductivity enclosure, b=14.4 mm and 26.2 mm height. The diameter of resonator (a) is 7.6 mm and the height of the metallic bar is 24.2 mm.

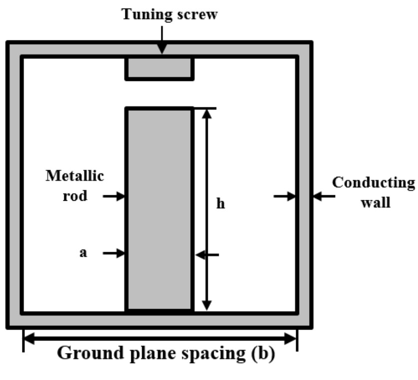

Figure 5-5: Combline resonator by using metallic rod

From HFSS software, it can be seen that the first mode is at Rx frequency (1.73 GHz with Q value at 1800) and the second mode is at 6.041 GHz with Q value at

3004.96. In Tx frequency, the first mode is at 2.13 GHz with Q value at 2015.68 and the second mode is at 6.65 GHz with Q value at 3300.3. The Eigen mode resonances and Q-factors data are listed in Table 5-4.

Table 5-4: Eigen modes and Q factors of metallic combline resonator

Eigenmode	(Rx) Frequency (GHz)	Q-factor	Eigenmode	(Tx) Frequency (GHz)	Q-factor
Mode 1	1.73409	1810	Mode 1	2.1326	2015
Mode 2	6.0417	3004	Mode 2	6.65807	3300
Mode 3	9.49759	4413	Mode 3	9.42865	4328

The characteristic impedance of the combline line can be calculated as [3].

$$Z_0 = \frac{60}{\sqrt{\varepsilon_r}} log_e\left(\frac{b}{a}\right) \tag{5.20}$$

Where $\varepsilon_r = 1$, the Z_0 is 38.4 Ω.

From [3], the ground plane spacing (b) in centimetres and frequency in gigahertz for the characteristic impedance Z_0=38.4 Ω and the Q-factor at 1.73 GHz and 2.13 GHz can be calculated as

$$\frac{Q}{b\sqrt{f}} = 1000 \tag{5.21}$$

Hence at 1.73 GHz, Q =1894 and at 2.13 GHz, Q=2101

In addition, the electric and magnetic field patterns of the combline resonator simulated by HFSS are shown in Figure 5-6 and Figure 5-7, respectively. The combline resonator have high voltages or strong electric fields near the top of resonator and high current density or strong magnetic fields near the bottom [55].

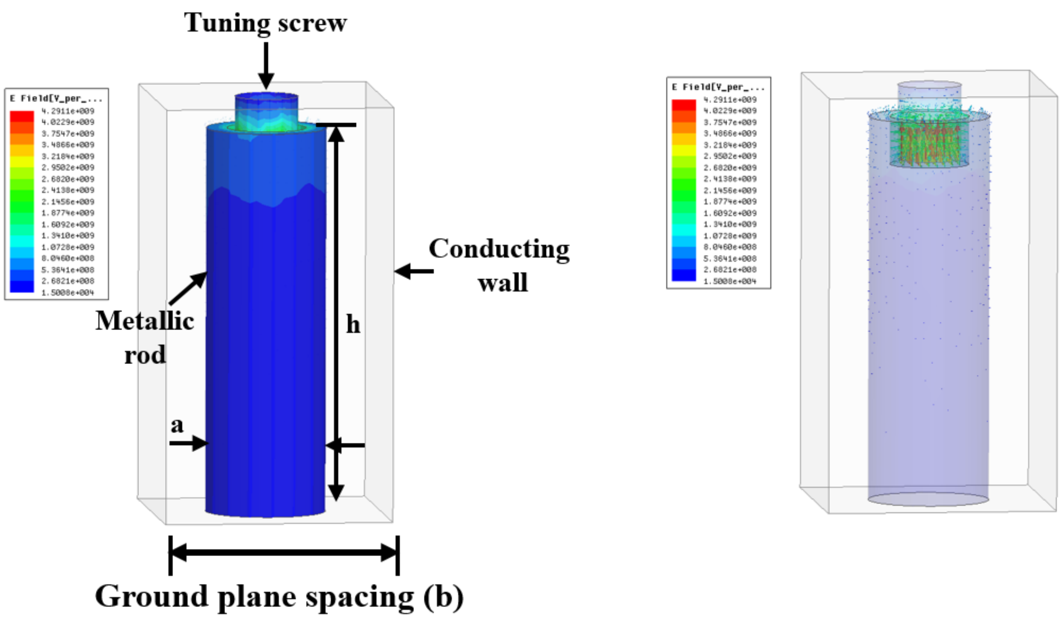

Figure 5-6: The magnitude and vector of E-field distribution of the combline resonator

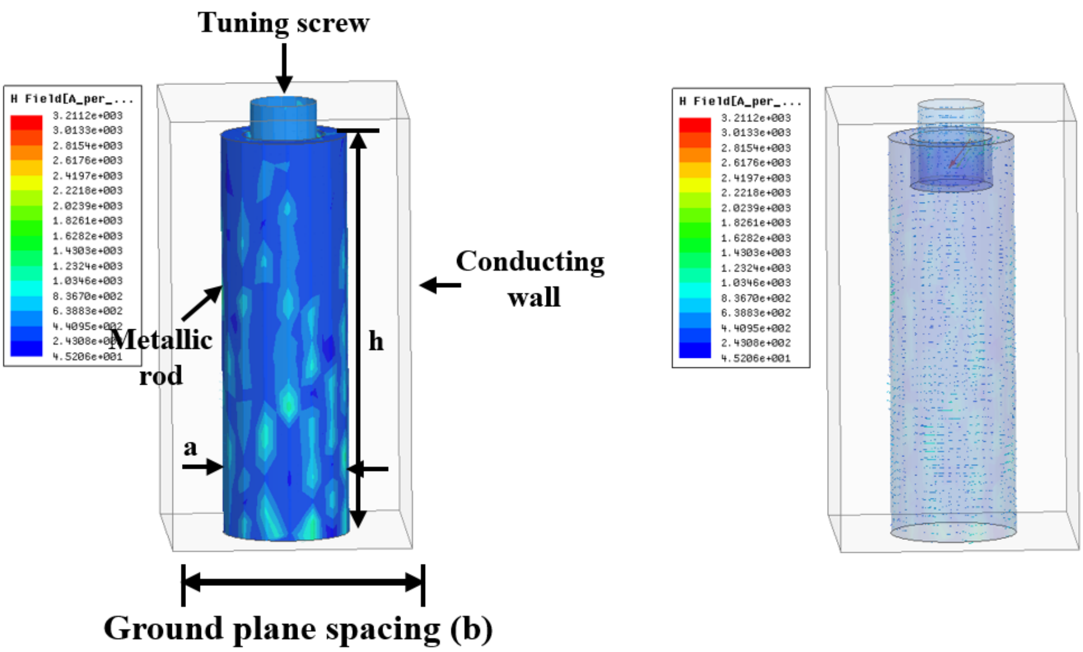

Figure 5-7: The magnitude and vector of H-field distribution of the combline resonator

5.4.1 External coupling

First of all, the external coupling is used to couple the filter with other devices in the system, which is expressed as Q values or it is called external loaded Q. The input transformer of the combline resonator is shown in Figure 5-8. The input transformer (r1) is 7.2 mm and the combline resonator (r2) is 7.6 mm. The calculation of extracting external quality factor (Q_e) can be obtained as expressed in [55].

$$Q_e = f_0/\Delta f_{3dB} \tag{5.22}$$

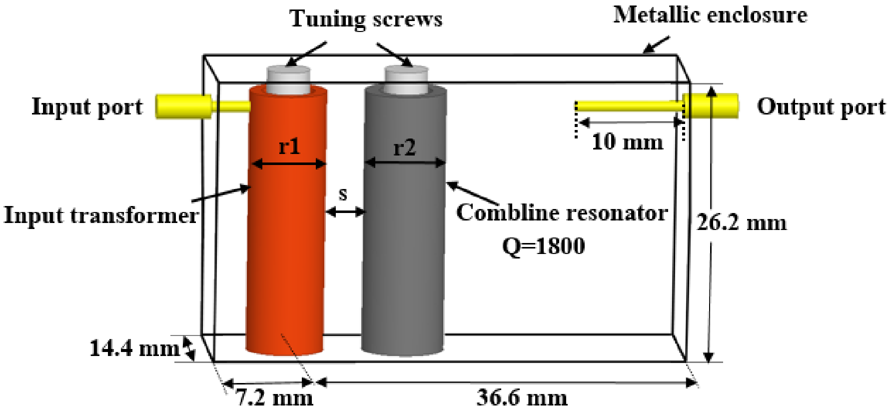

Figure 5-8: Combline resonator for extracted external quality factor

The external coupling is found by measuring at the 3 dB bandwidth of the resonant curve of the S_{21} magnitude fallen to 0.707 (-3dB) of maximum value, as shown in Figure 5-9.

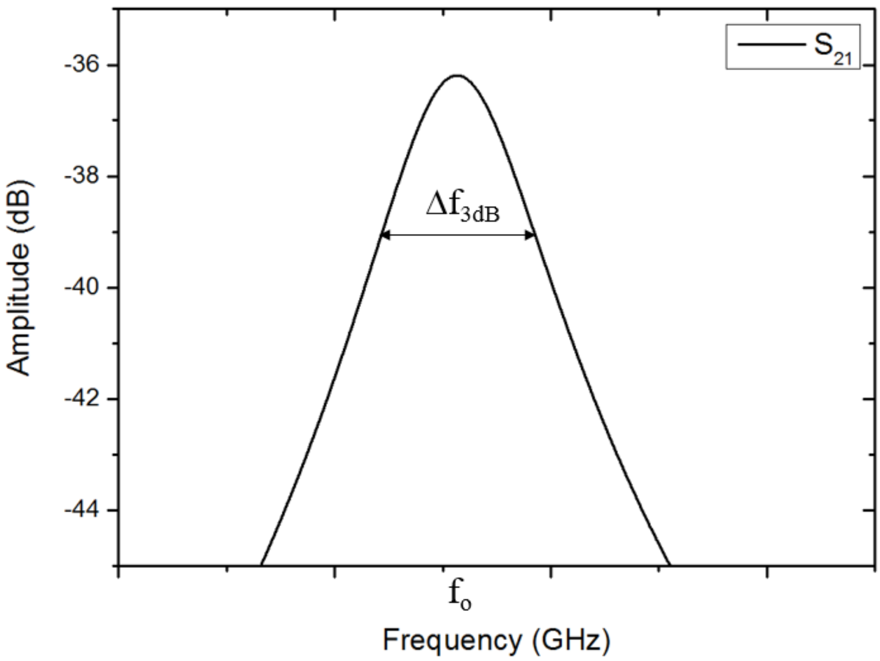

Figure 5-9: Response of S_{21} for extracted external quality factor

Figure 5-10 shows the external quality factor of the combline resonator which is extracted from spacing between the input transformer and the combline resonator. The distance (s) of the input transformer to the combline resonator operating at the centre frequency of 1.73 GHz with Q_e= 23.12 is 2.15 mm and that of 2.13 GHz with Q_e= 28.47 is 2.45 mm, respectively.

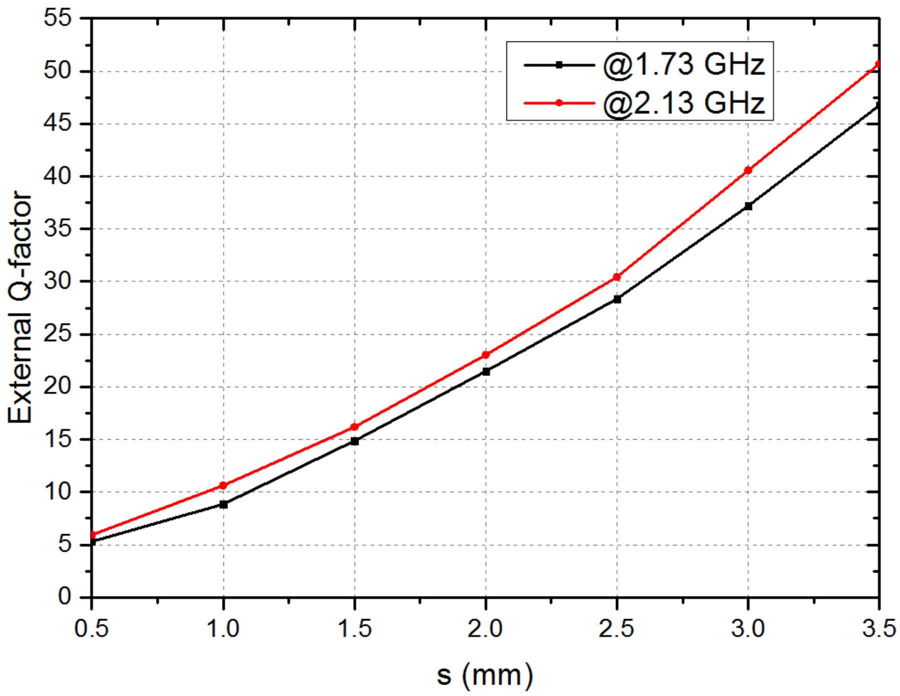

Figure 5-10: External quality factor Q_e versus the distance of the input transformer to the resonator

5.4.2 Positive inter-resonator coupling

The coupling coefficients between adjacent resonators are shown in Figure 5-11. By varying the space between two resonators, the coupling coefficient is dependent on the spacing between them. It can then be calculated by

$$K = \pm \frac{f_{p2}^2 - f_{p1}^2}{f_{p2}^2 + f_{p1}^2} \tag{5.23}$$

Where f_{p1} and f_{p2} are the lower and higher spilt resonant frequencies of a pair of coupled resonators. The response of the decoupled resonator structure for extracting the coupling coefficient can be plotted as shown in Figure 5-12 and the coupling coefficients values between two resonators are as shown in Figure 5-13. By using equation (5.23), the coupling coefficients between two resonators at 1.73 GHz, K_{12}=0.0478 and at 2.13 GHz, K_{12}=0.0389 are equal to 9.25 mm and 9.00 mm, respectively.

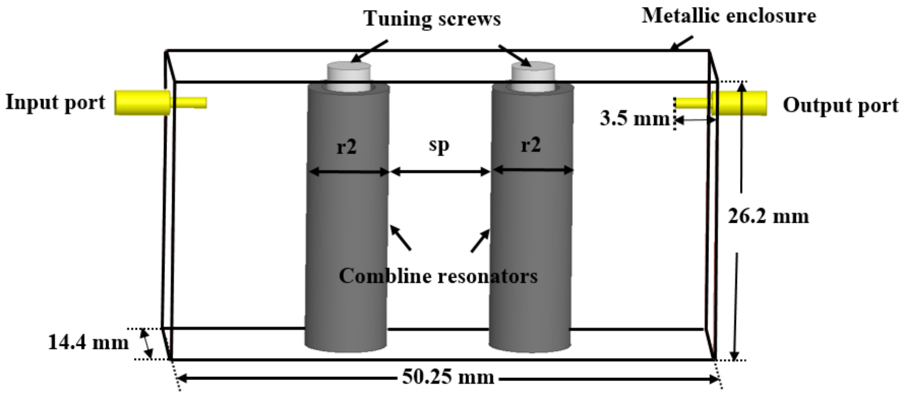

Figure 5-11: Two combline resonators for extracted coupling coefficient

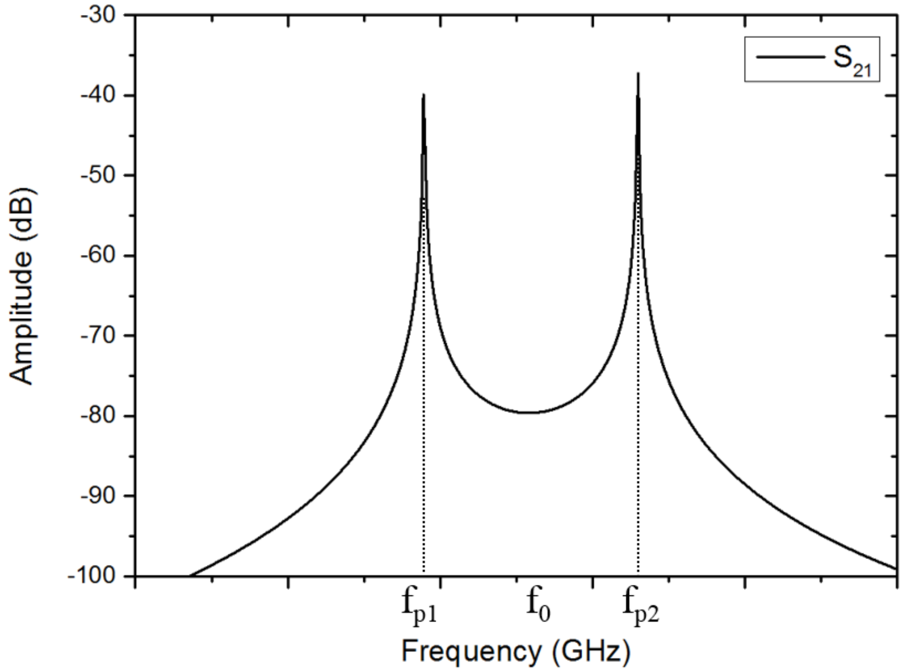

Figure 5-12: A typical frequency response of the decoupled resonator structure for extracting the coupling coefficient

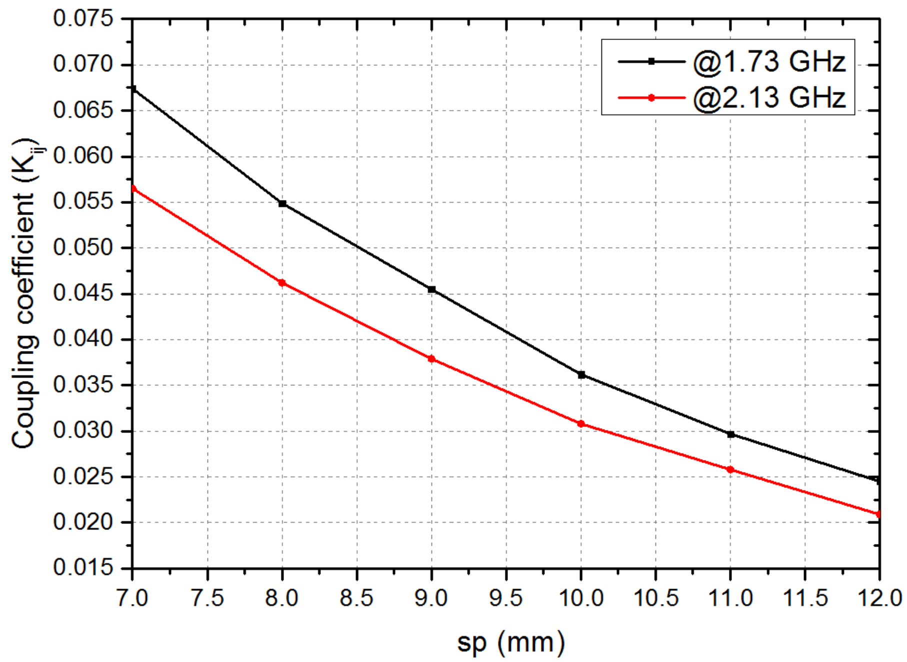

Figure 5-13: The coupling coefficient K versus the spacing between two resonators (sp)

5.4.3 Negative inter-resonator coupling

The negative coupling structure can be achieved by an opening in the upper part of the wall by which the electric fields will couple. To increase the capacitive coupling, an inversed U-shape metallic wire is suspended in the iris between the resonators, as shown in Figure 5-14. In practice, the metallic wire is supported by Teflon with dielectric constant 2.1 or any other dielectric materials, which have a dielectric property close to air. The relationship between coupling coefficients and spacing of two resonators is as represented in Figure 5-15. The coupling coefficient between two resonators at 2.13 GHz, K_{12}=0.0389, is 7.94 mm.

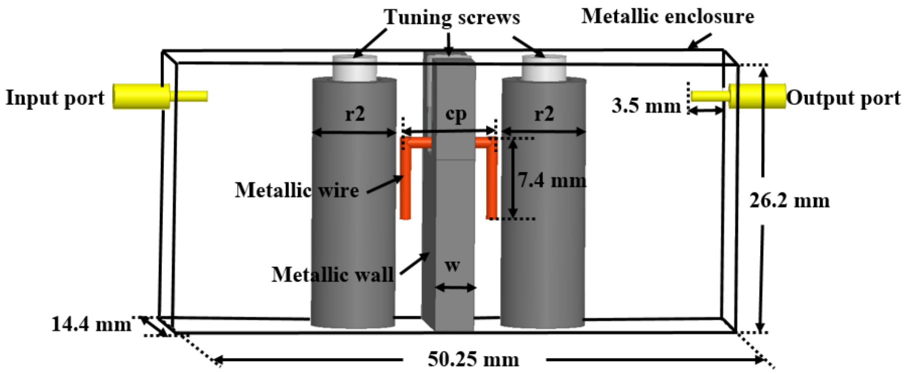

Figure 5-14: Two combline resonators for extracted coupling coefficient

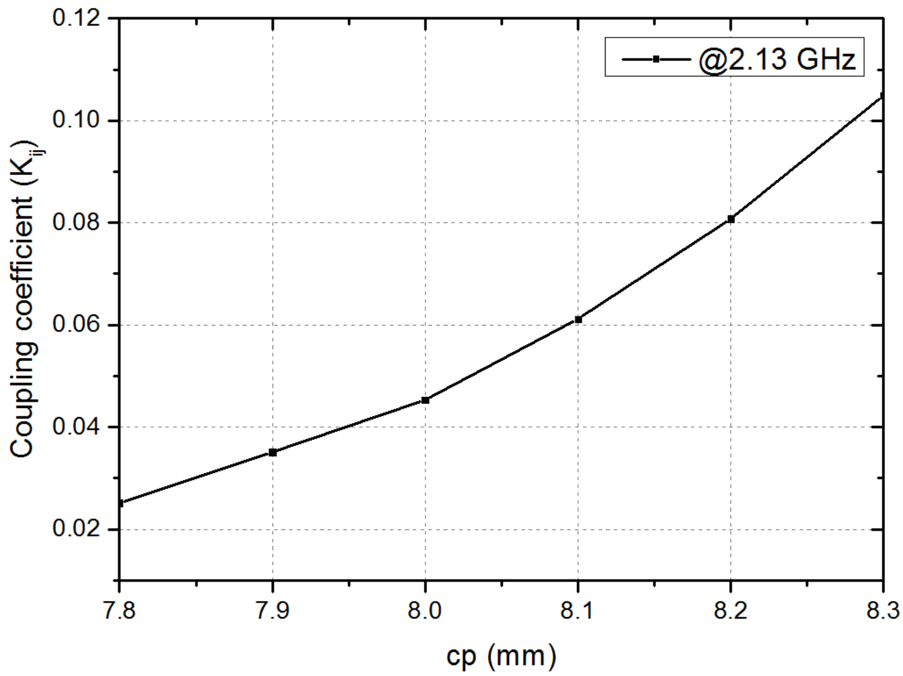

Figure 5-15: The coupling coefficient K versus the length of metallic wire

5.4.4 Physical simulation of the combline resonator filter

The simulation of bandpass filters can be achieved using a second-order combline resonator. The dimensions of the second-order combline resonator are shown in Table 5-5. The geometry of the positive coupling combline filter can be achieved as shown in Figure 5-16 and the negative coupling structure is shown in Figure 5-17.

Table 5-5: Simulated dimensions of the combline resonator filter

Dimensions	**R_X=1.73 GHz (Positive coupling)**	**T_X=2.13 GHz (Positive coupling)**	**T_X=2.13 GHz (Negative coupling)**
Input transformer diameter (r1)	7.20 mm	7.20 mm	7.20 mm
Combline diameter (r2)	7.60 mm	7.60 mm	7.60 mm
Distance between wall and input transformer (s1)	7.20 mm	7.20 mm	7.20 mm
Distance between input transformer and resonator (s2)	9.55 mm	9.60 mm	9.60 mm
Distance between resonator and resonator (s3)	17.10 mm	17.00 mm	17.00 mm

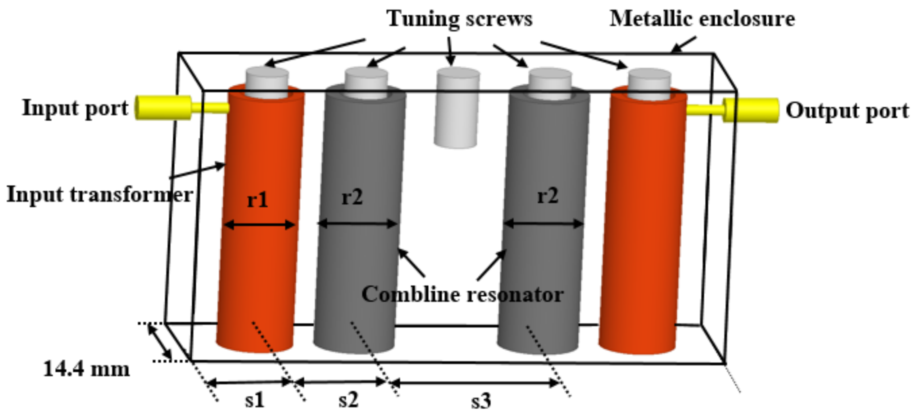

Figure 5-16: Geometrical structure of the positive coupling combline resonator filter

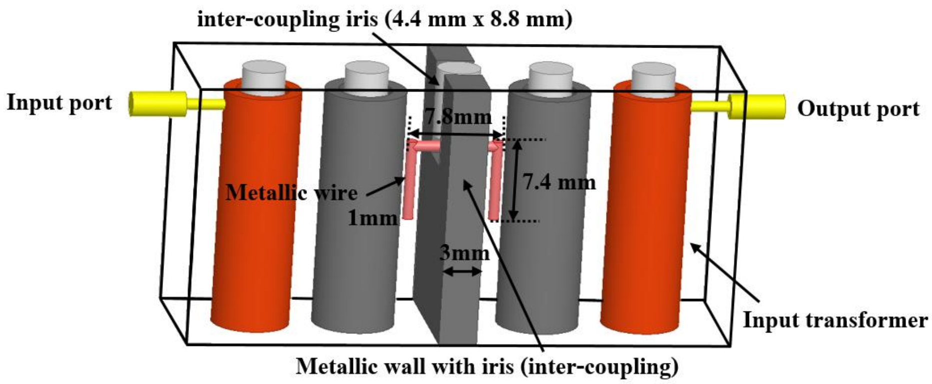

Figure 5-17: Geometrical structure of the negative coupling combline resonator filter

The simulated response of the second-order combline filter at the Rx band is portrayed in Figure 5-18. The fractional bandwidth is 2.89% (50 MHz at 1.73 GHz). The passband IL is less than 0.035 dB and the RL is better than 20.92 dB in the passband.

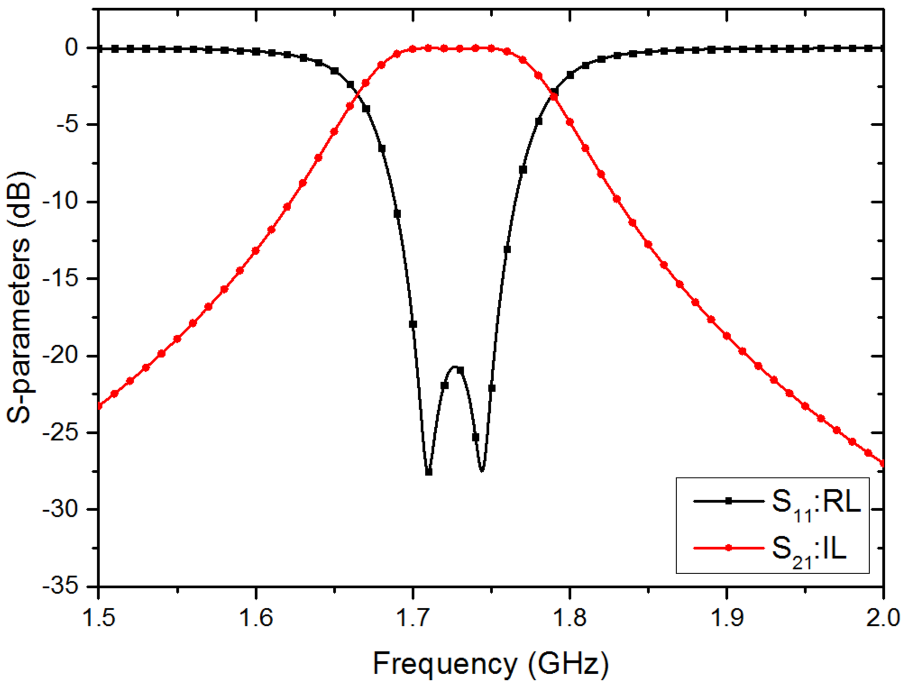

Figure 5-18: Simulated response of the second-order combline filter at 1.73 GHz

A comparison of IL and RL between positive and negative combline structures is shown in Figure 5-19. The fractional bandwidth is 2.35% (50 MHz at 2.13 GHz). The passband ILs are less than 0.014 dB and the RLs are better than 24.57 dB in the passband. A comparison of phases between positive and negative designs has out of phase as displayed in Figure 5-20. It is evident that the phase difference between positive and negatively coupled designs is 177.4°, which is only a 2.6° phase error from the mathematical model. However, the phase error of combline filters can be varied due to fabrication accuracy, but can be compensated by tuning screws.

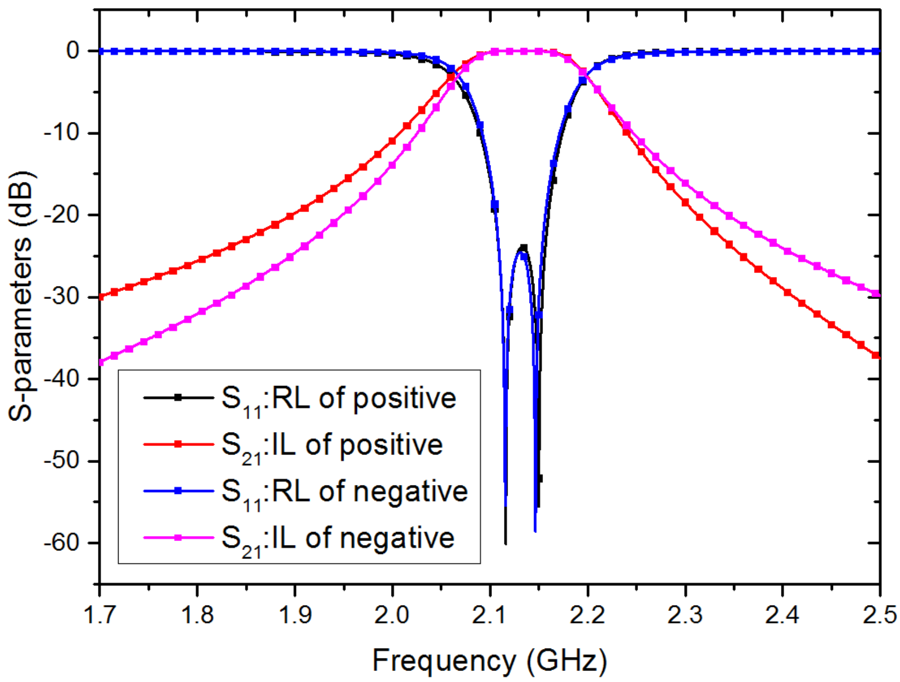

Figure 5-19: Simulated responses of the positive and negatively coupled filters simulated by HFSS program at 2.13 GHz

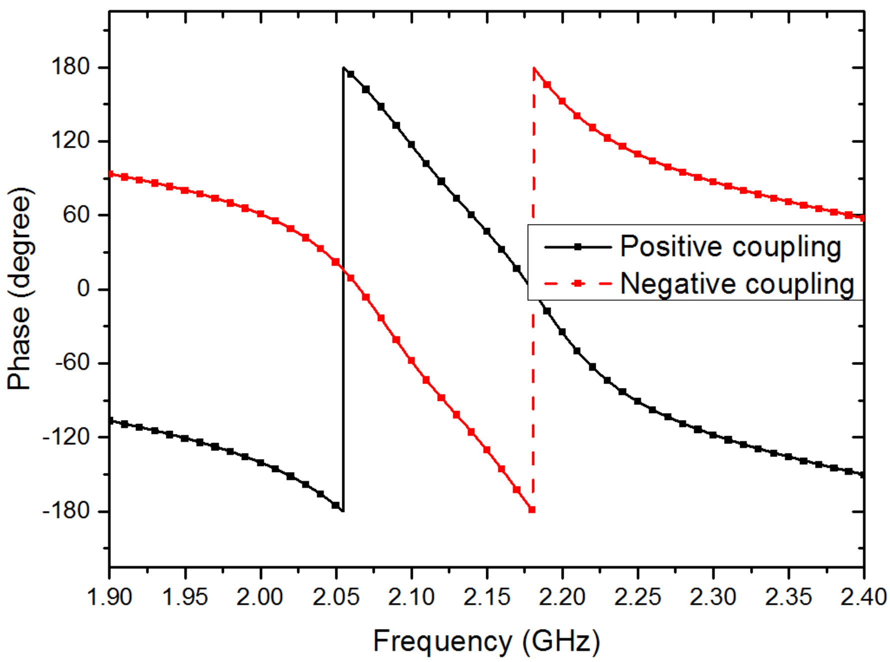

Figure 5-20: Simulated responses of comparison of the phase between the positive and negatively coupled filters at 2.13 GHz

5.4.5 Second-order combline three-port diplexer

To design a conventional diplexer, all diplexer structures are based on the three-port diplexer. However, the main drawback of this design technique is that the degree of the filters increases linearly when higher signal isolation is required. If the degree of filters increases, the size and losses of filters also increase. Moreover, high order filters increase the complicated structure because many coupling components have to consider such as external coupling and inter resonator coupling. The conventional diplexer design is based on the design of the two bandpass filters independently: one of them meeting the desired frequency band in the Rx band at 1.73 GHz and the other desired frequency band in the Tx band at 2.13 GHz. Then, the input transformer is used to couple the two independent bandpass filters together. The dimensions of the second-order combline resonator diplexer are shown in Table 5-6. The optimised geometry of the diplexer is designed at 1.73 and 2.13 GHz, as shown in Figure 5-21.

Table 5-6: Simulated dimensions of the second-order combline resonator diplexer

Dimensions	**Rx=1.73 GHz**	**Tx=2.13 GHz**
Input transformer diameter (r1)	7.20 mm	7.20 mm
Combline diameter (r2)	7.60 mm	7.60 mm
Distance between wall and input transformer (s1)	7.20 mm	7.20 mm
Distance between input transformer and resonator	s2=9.45 mm	s4=8.9 mm
Distance between resonator and resonator	s3=17.10 mm	s5=17.00 mm

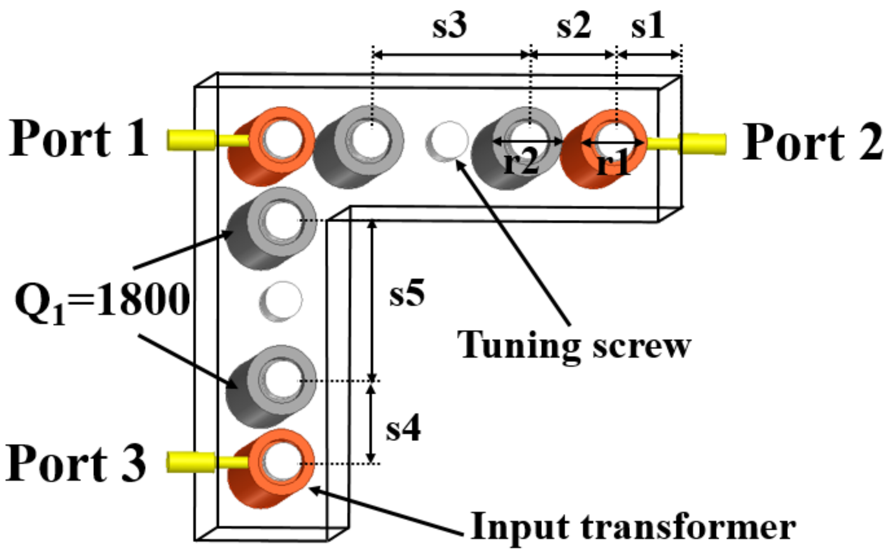

Figure 5-21: Geometrical structure of the second-order combline diplexer

The simulated response of the combline diplexer is portrayed in Figure 5-22. The passband IL in the Rx band is less than 0.04 dB and, in the Tx band, 0.03 dB. The RL in both channels is better than 17.9 dB in the passband. The simulated isolation between Rx and Tx bands is better than 26.3 dB in transmit and receive bands, as shown in Figure 5-23. Figure 5-24 shows the wide-band simulation of the second-order combline diplexer. It can also be seen that the simulated wideband has a spurious response at 6.25 GHz.

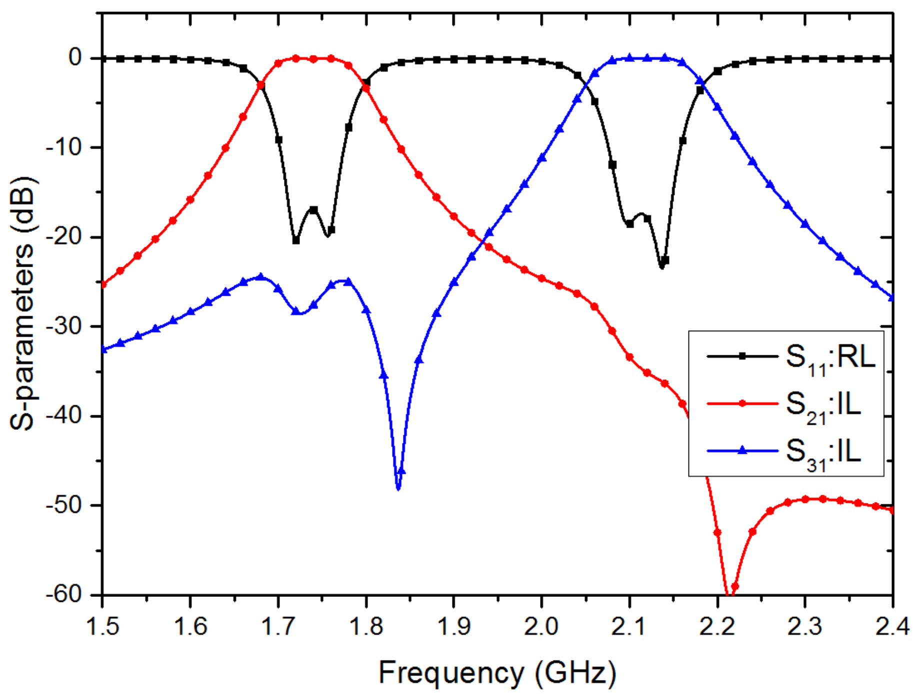

Figure 5-22: Simulated response of the second-order three-port diplexer simulated by HFSS program at 1.73 GHz and 2.13 GHz

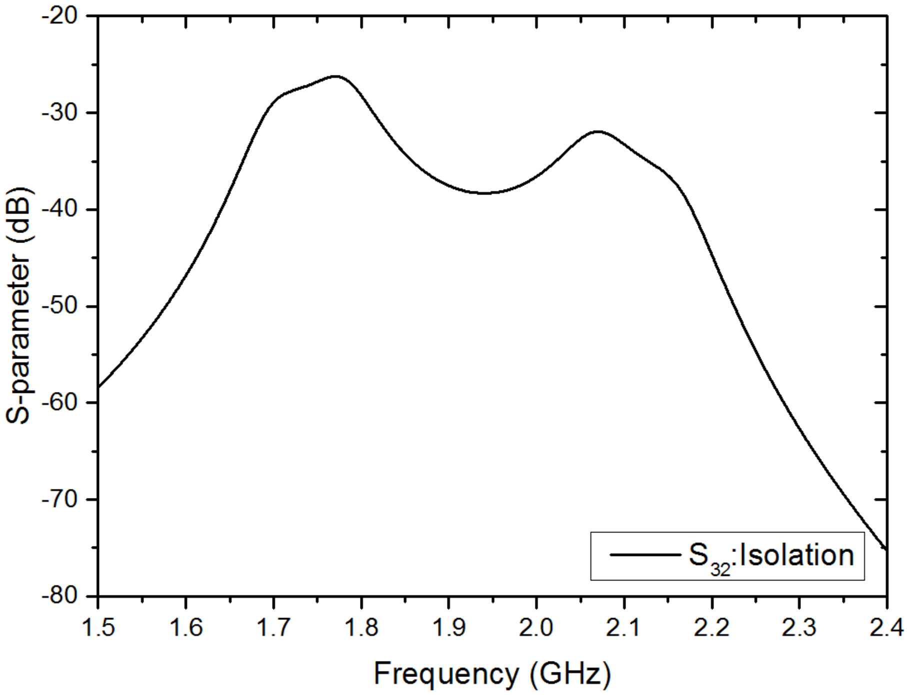

Figure 5-23: Simulation of signal isolation of the three-port diplexer

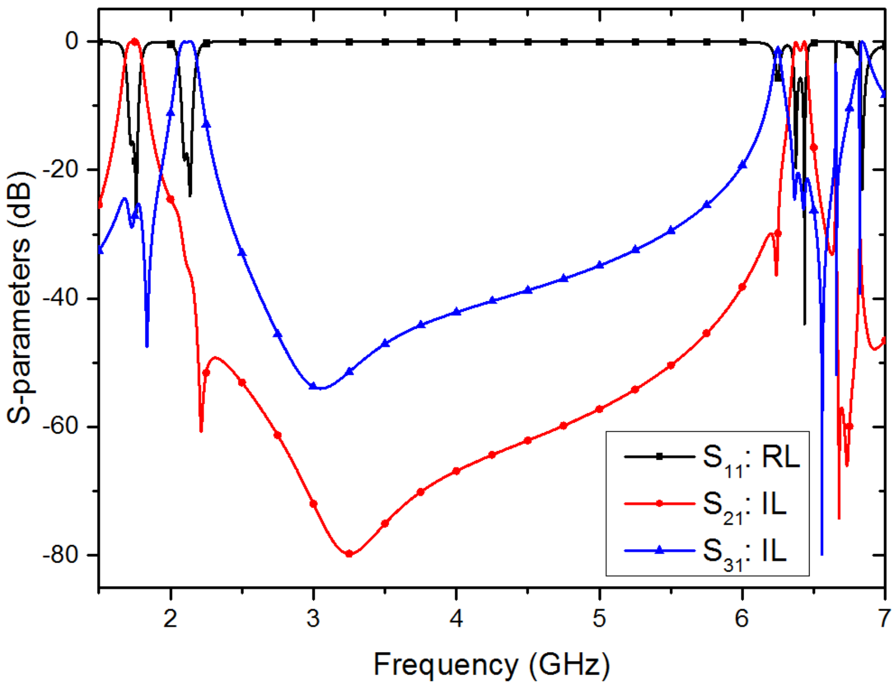

Figure 5-24: Wide-band response of the second-order combline diplexer

5.4.6 Second-order four-port diplexer with similar Q-factors

A combination of four filters is used to complete the four-port diplexer design. The 3D geometrical structure of the four-port diplexer with all filters designed with equal Q-factors (Q_1=Q_2=1800) is shown in Figure 5-25. The optimised parameters for the four-port diplexer with equal Q-factors are listed in Table 5-7.

Table 5-7: Simulated dimensions of the combline diplexer

Dimensions	**Values**
Cavity width (a)	50.6 mm
Cavity length (b)	48.8 mm
Cavity height (h)	24.2 mm
Tuning screw (t)	4 mm
Input transformer diameter (r1)	7.20 mm
Combline diameter (r2)	7.60 mm
Wall thickness (w)	3 mm
Iris of the wall (g)	4.4 mm
Height of the iris (z)	8.7 mm
Distance between wall and input transformer (s1)	7.20 mm
Distance between input transformer and resonator (s2)	9.55 mm
Distance between resonator and resonator (s3)	17.10 mm
Distance between input transformer and resonator (s4)	8.6 mm
Distance between resonator and resonator (s5)	17.2 mm

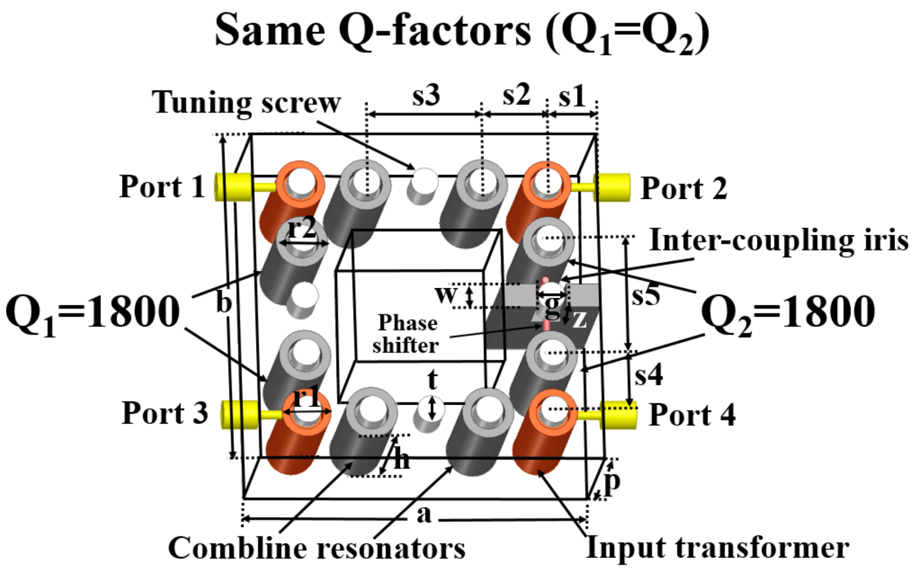

Figure 5-25: Geometrical structure of the second-order four-port diplexer with equal Q-factors

The simulated S-parameters of the four-port diplexer with the same Q-factors in all branches are shown in Figure 5-26. The passband IL in the Rx band is less than 0.06 dB and, in the Tx band, 0.05 dB, respectively. The RL in both channels is better than 22.8 dB in the passband. Figure 5-27 represents the comparison of simulated Tx/Rx isolation of a conventional three-port diplexer and the four-port diplexer with the same Q-factors (Q=1800). At the centre frequency of 1.73 GHz and 2.13 GHz for Rx and Tx modules, the simulated Tx/Rx isolation of the conventional three-port diplexer is 26.3 dB and it is 37.08 dB for the four-port diplexer. Figure 5-28 depicts the simulated phase response of Tx filter branches, S_{31} and S_{24}, at the centre frequency of 2.13 GHz. From the simulation results, the phases of S_{31} and S_{24} are 122.34° and -56.01°, respectively. Therefore, the phase difference between the Tx and Rx branches is 178.36°, which is only a 1.64° error compared to the analytical model. Figure 5-29 shows the wide-band simulation of the four-port diplexer with the same Q-factor. It can also be seen that the simulated wideband has a spurious response at 6.125 GHz.

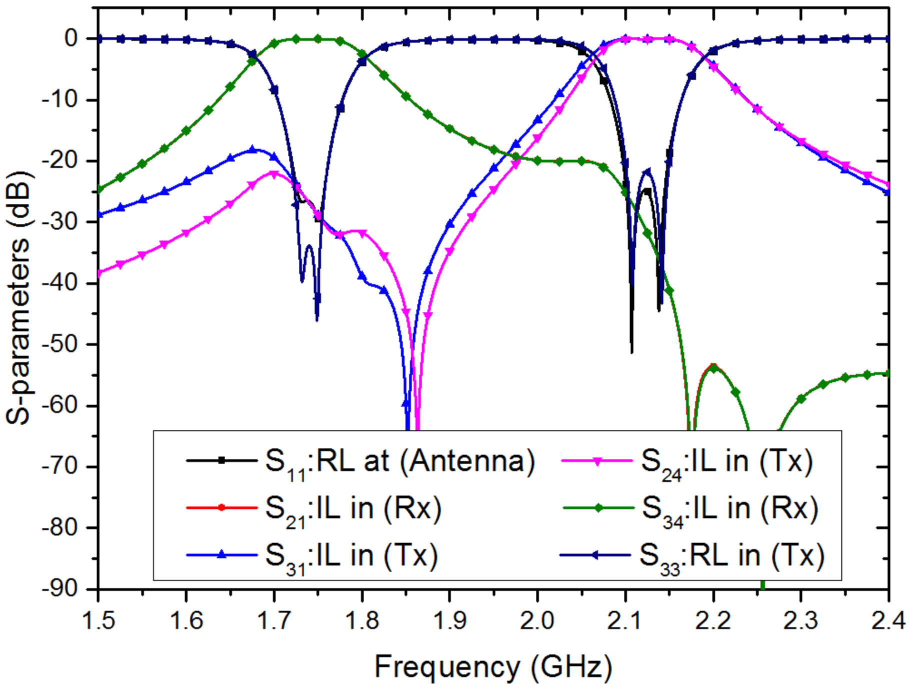

Figure 5-26: Simulation results of S-parameters of the four-port diplexer with the same Q-factors at Rx=1.73 GHz, Tx= 2.13 GHz

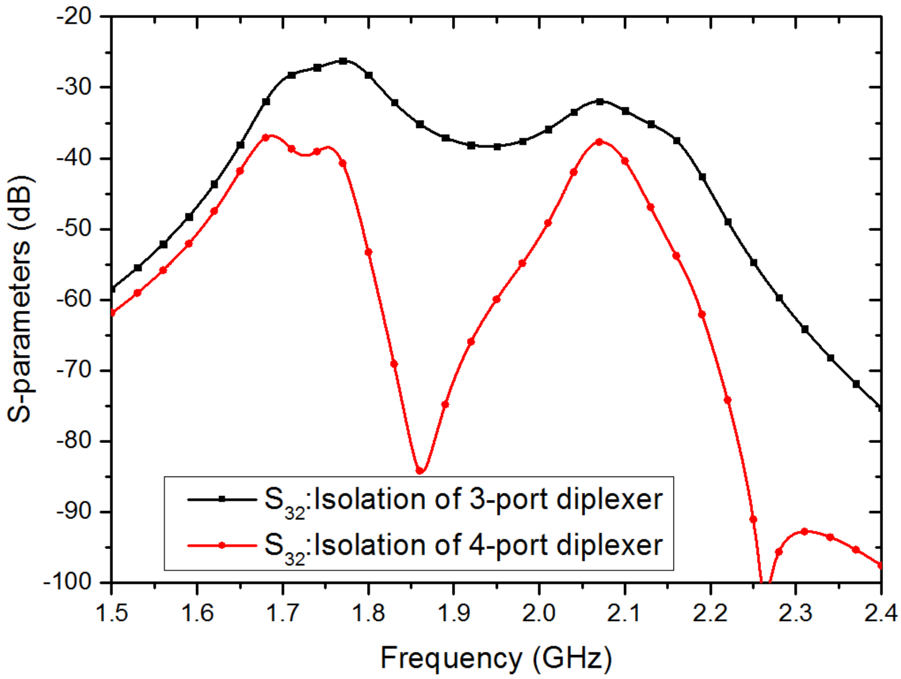

Figure 5-27: Simulation results of signal isolation, S_{32}, of the four-port diplexer with similar Q-factors and the three-port diplexer

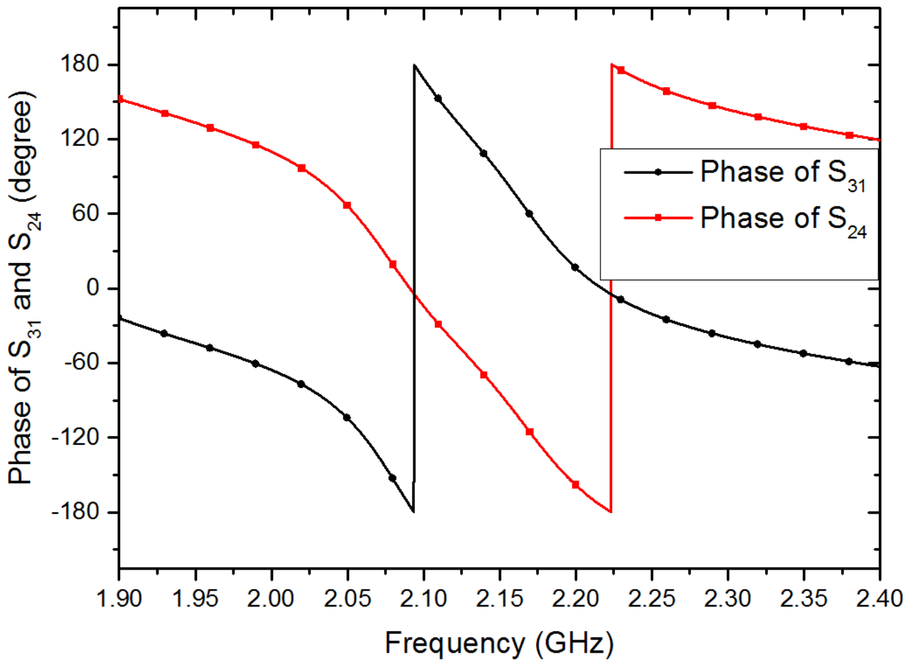

Figure 5-28: Simulation results of phase of S_{31} and S_{24} at 2.13 GHz

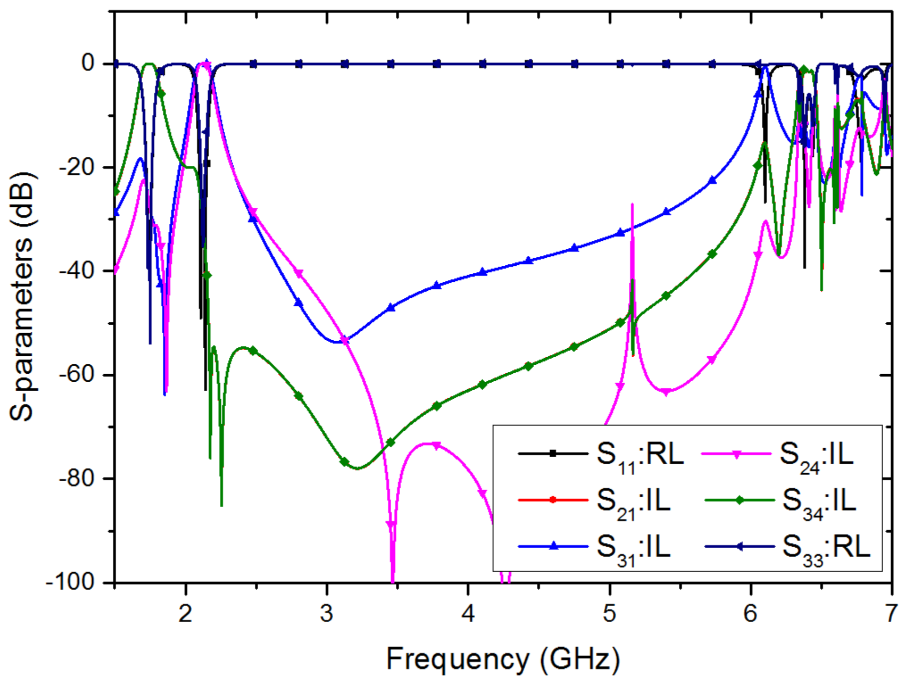

Figure 5-29: Simulations of wide-band response of the four-port diplexer with the same Q-factors

5.4.7 Fabrication and Measurement results

The fabricated prototype of the four-port diplexer with all filters designed with equal Q-factors is shown in Figure 5-30 The prototype is fabricated by using a computer numerically controlled (CNC) machine and aluminium and copper are used as structural materials. Tuning screws are implemented between each resonator to compensate for manufacturing errors as well as to optimise the resonant frequencies and inter-resonator couplings.

The measured S-parameters of the four-port diplexer with the same Q-factors in all branches are shown in Figure 5-31 The passband IL in the Rx band is less than 0.46 dB and, in the Tx band, 0.48 dB, respectively. The RL in both channels is better than 20 dB in the passband. Figure 5-32 represents the comparison of measured Tx/Rx isolation of a conventional three-port diplexer and the four-port diplexer with the same Q-factor (Q=1800). At the centre frequency of 1.73 GHz and 2.13 GHz for Rx and Tx modules, the measured Tx/Rx isolation of the conventional three-port diplexer is 26.28 dB and it is 35.15 dB for the four-port diplexer. Figure 5-33 depicts the measured phase response of Tx filter branches, S_{31} and S_{24}, at the centre frequency of 2.13 GHz. From the measured results, the phases of S_{31} and S_{24} are 15.05° and -162.6°, respectively. Therefore, the phase difference between the Tx and Rx branches is 177.65°, which is only a 2.35° error compared to the analytical model.

To compare the measured and simulated S-parameters of four-port diplexer with the same Q-factors, the measured passband ILs of both Tx and Rx bands are less than 0.46 and 0.48 dB and they are 0.06 dB and 0.05 dB for the simulated results. The degraded performance of fabricated four-port diplexer is mainly due to material losses because four-port diplexer is simulated by using perfect conductor for prototype structure. In practice, the prototype of four-port diplexer is fabricated by using aluminium and copper. Another loss is the leakage at input and output terminals. A good soldering of input/output pins to combline resonator can bring measurements well in agreement to the simulated response. At the center frequency of 1.73 and 2.13 GHz for Rx and Tx module, the measured Tx/Rx signal isolation of four-port diplexer is 35.15 dB and it is 37.08 dB for simulated four-port structure. It can be explained that the Tx/Rx signal isolation of four-port diplexer depends on the different phase between port 2 and 4. To achieve the filter design with 180° phase shift, the positive coupled and negative coupled combline are required. The positive coupling can be implemented by using conventional combline resonator filter while the negative coupling can be designed with an opening in the upper part of the wall (iris/window), by which the electric field coupling is strongest. To increase the efficiency of the negative coupling, an inversed U-shape metallic wire is suspended above the iris between the resonators. In practice, the metallic wire is supported by Teflon with a dielectric constant 2.1 or any other dielectric materials, which have a dielectric property close to air. Therefore, the fabrication errors from negative coupled structure can degrade the performance of Tx/Rx signal isolation.

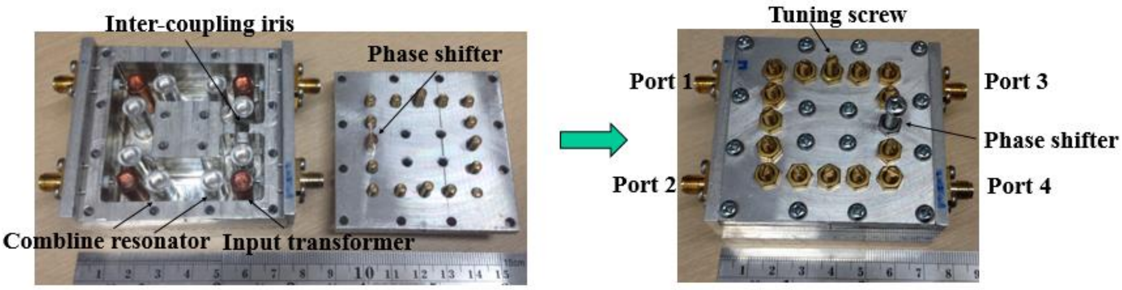

Figure 5-30: Photographs of the four-port diplexer with the same Q-factors

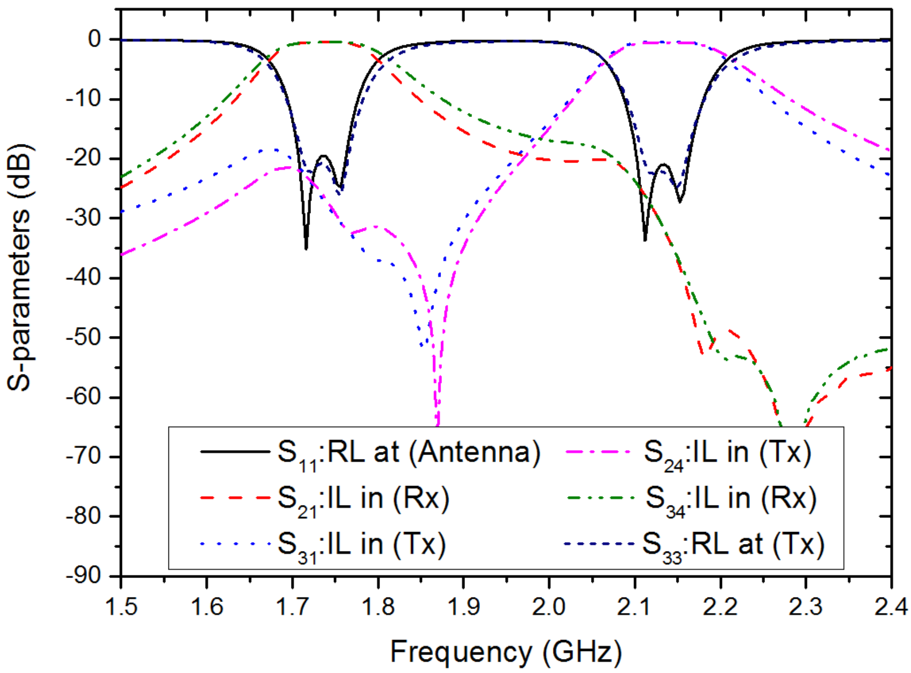

Figure 5-31: Measurement results of S-parameters of the four-port diplexer with similar Q-factors where Q1=Q2=1800 at Tx=2.13 GHz, Tx=1.73 GHz

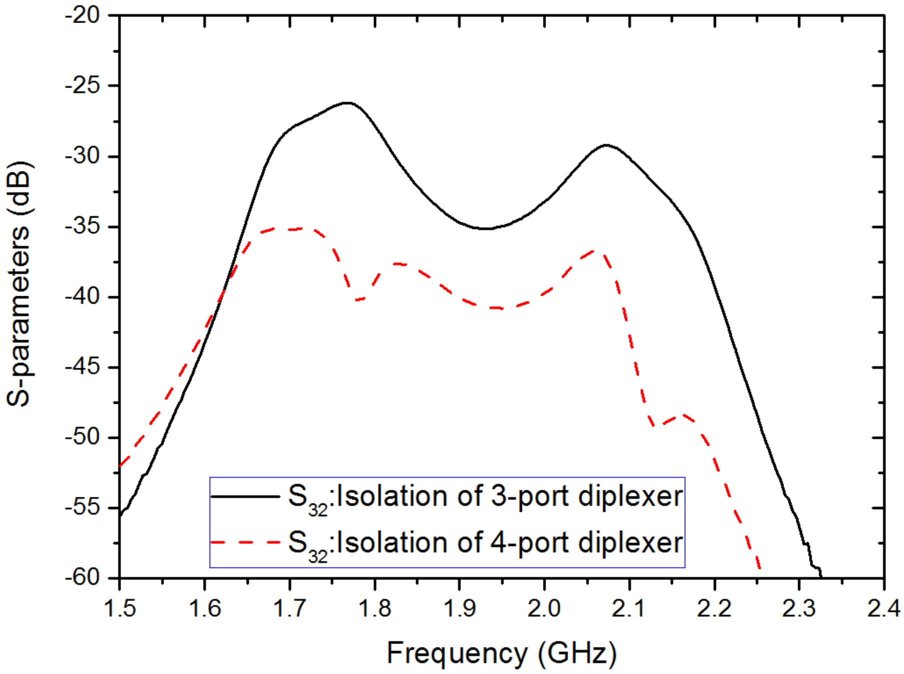

Figure 5-32: Measurement results of signal isolation, S_{32}, of the four-port diplexer with similar Q_1-factors (35.15 dB) and the three-port diplexer (26.28 dB)

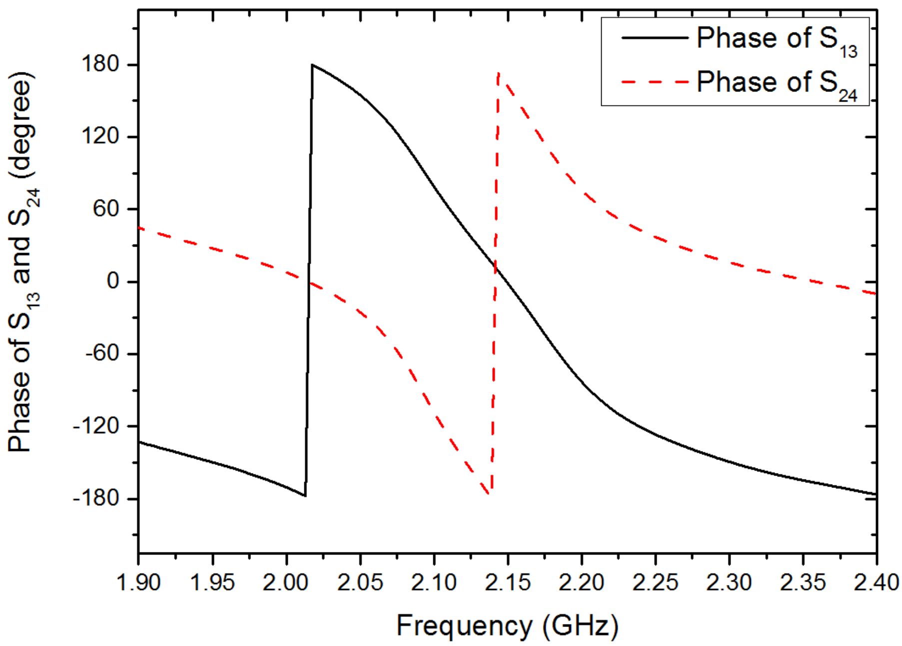

Figure 5-33: Measurement results of phases of S_{13} and S_{24} with 177.65° phase difference at 2.13 GHz

5.5 Second order combline resonator filter with the different Q-factors

The resonant frequency for the fundamental mode of the combline resonator is successfully determined by the HFSS program. In this case, the resonator is placed in the centre of a conductivity enclosure, b=22.4 mm and 26.2 mm height. The diameter of resonator (a) is 12 mm and the height of the metallic bar is 24.2 mm. The combline resonator by using metallic rod is shown in Figure 5-34.

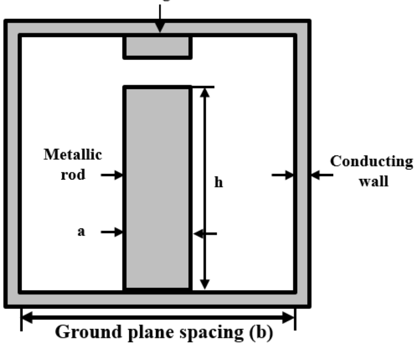

Figure 5-34: Combline resonator by using metallic rod

From HFSS software, it can be seen that the first mode is at Rx frequency (1.73 GHz with Q value at 3684) and the second mode is at 6.27 GHz with Q value at 5606. In Tx frequency, the first mode is at 2.13 GHz with Q value at 3883 and the second mode is at 7.23 GHz with Q value at 5899. The Eigen mode resonances and Q-factor data are shown in Table 5-8..

Table 5-8: Eigen modes and Q factors of metallic combline resonator

Eigenmode	(Rx) Frequency (GHz)	Q-factor	Eigenmode	(Tx) Frequency (GHz)	Q-factor
Mode 1	1.73078	3684	Mode 1	2.13769	3883
Mode 2	6.2403	5606	Mode 2	7.22797	5889
Mode 3	6.78825	5725	Mode 3	7.24039	5362

In addition, the electric and magnetic field patterns of the combline resonator simulated by HFSS are shown in Figure 5-35 and Figure 5-36. The combline resonator has high voltages or strong electric fields near its top and high current density or strong magnetic fields near the bottom [55].

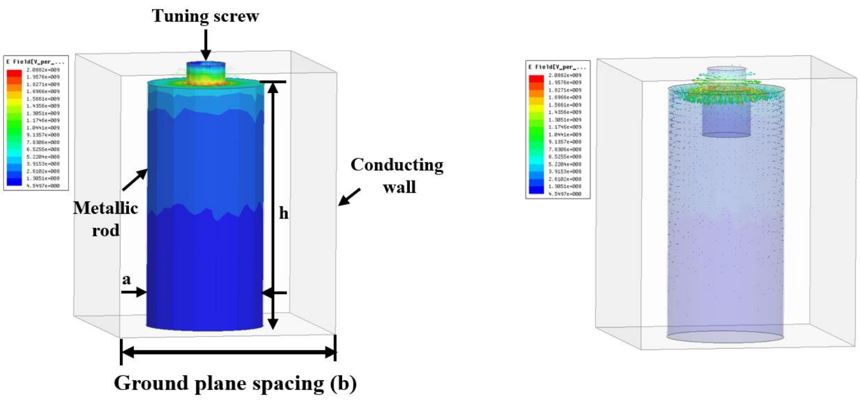

Figure 5-35: The magnitude and vector of E-field distribution of the combline resonator

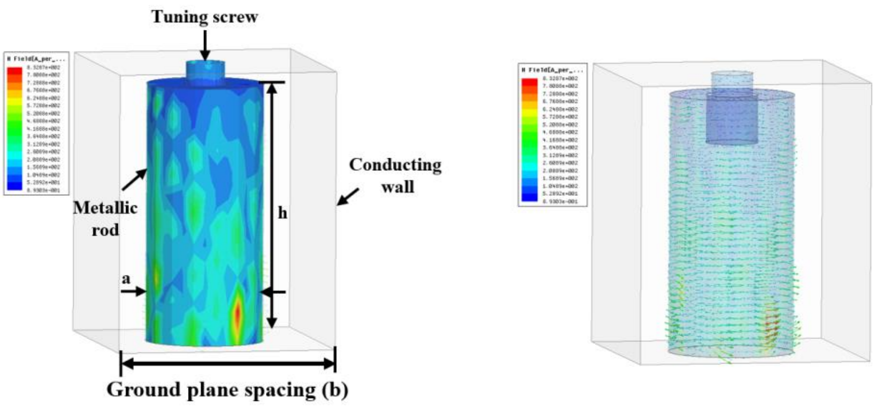

Figure 5-36: The magnitude and vector of E-field distribution of the combline resonator

5.5.1 External coupling

The external coupling is extracted as follows. The input transformer of the combline resonator is shown in Figure 5-37. The input transformer (r1) is 7.2 mm and the combline resonator (r2) is 12 mm.

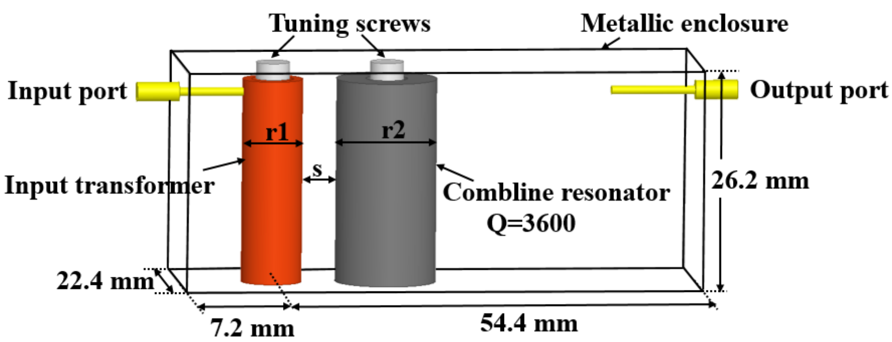

Figure 5-37: Combline resonator for extracted external quality factor

Figure 5-38 shows the external quality factor of the combline resonator which is extracted from spacing between the input transformer and combline resonator.

The distance (s) between the input transformer and combline resonator operating at the centre frequency of 1.73 GHz with Q_e= 23.12 is 2.05 mm and that of 2.13 GHz with Q_e= 28.47 is 2.15 mm, respectively.

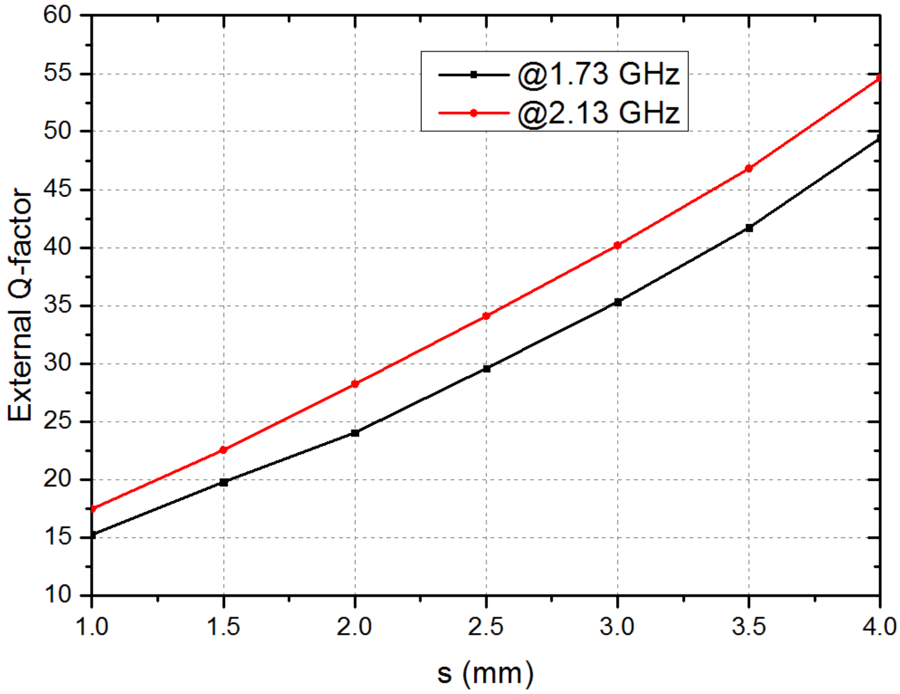

Figure 5-38: External quality factor Q_e versus the distance of input transformer to the resonator

5.5.2 Inter-resonator positive coupling

The geometric structure of the coupling coefficient between adjacent resonators can be shown as in Figure 5-39. By varying the space between the two resonators, the coupling coefficient is dependent on the spacing between them. The coupling coefficient values between the two resonators are shown in Figure 5-40. By using equation (5.23), the coupling coefficients between two resonators at 1.73 GHz, K_{12}=0.0478 and at 2.13 GHz, K_{12}=0.0389 are equal to 14.15 mm and 15.1 mm, respectively.

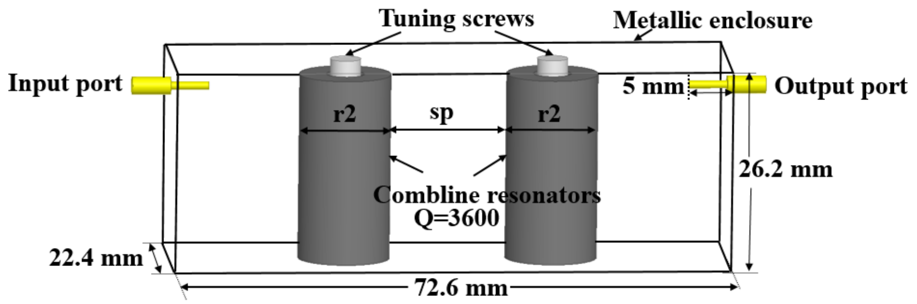

Figure 5-39: Two combline resonators for extracted coupling coefficient

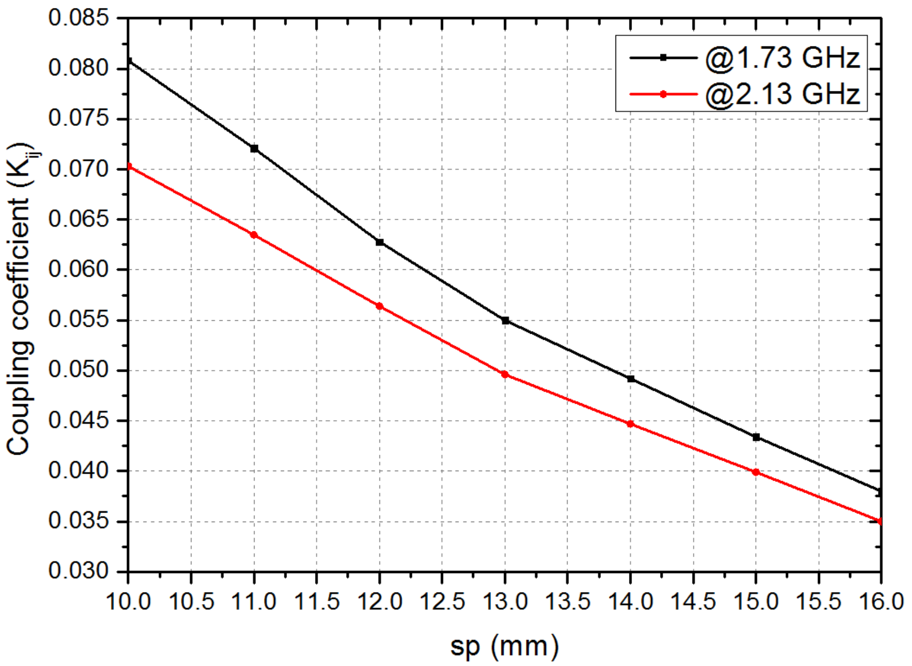

Figure 5-40: The coupling coefficient K versus the spacing between two resonators (sp)

5.5.3 Inter-resonator negative coupling

Negative coupling can be achieved by an opening in the upper part of the wall by which the electric fields will couple between resonators. To increase the capacitive coupling, an inversed U-shape metallic wire is suspended in the iris between the resonators, as shown in Figure 5-41. The coupling coefficient is extracted by metallic wire length (cp), as shown in Figure 5-42. From Figure 5-42, the coupling coefficient between two resonators at 2.13 GHz, K_{12}=0.0389, is equal to 13.2 mm.

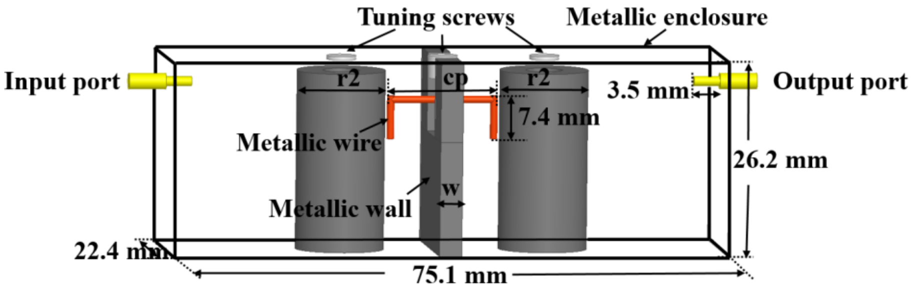

Figure 5-41: Two combline resonators for extracted coupling coefficient

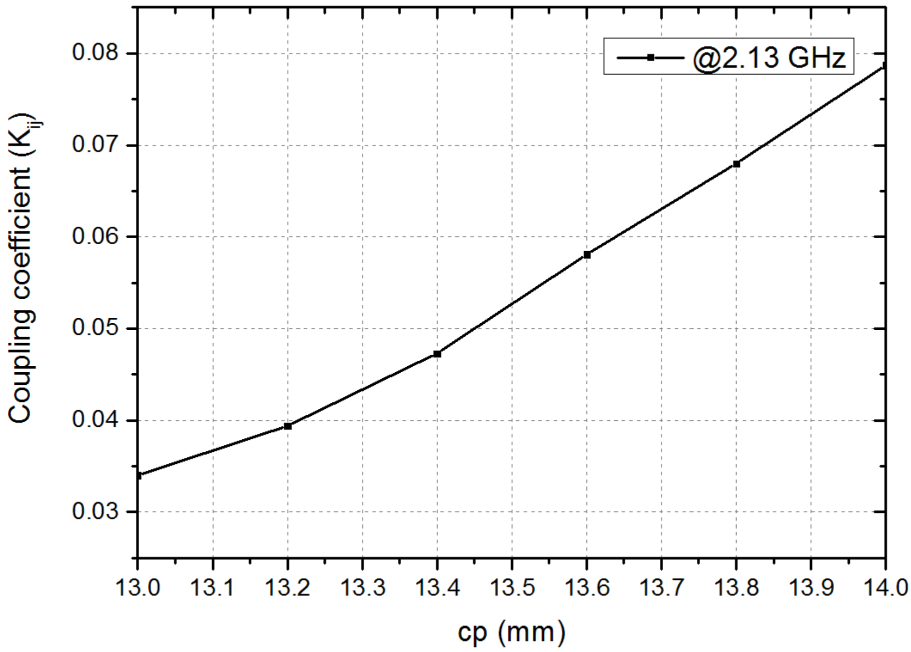

Figure 5-42: The coupling coefficient K versus the length of metallic wire (cp)

5.5.4 Physical simulation of the combline resonator filter

The simulation of bandpass filters with Q=3600 can be achieved using a second-order combline resonator. The dimensions of the second-order combline resonator are listed in Table 5-9. The geometry of the positive coupling filters can be achieved as shown in Figure 5-43 and that for the negative coupling filter is shown in Figure 5-44.

Table 5-9: Simulated dimensions of the combline resonator filter

Dimensions	**R_X=1.73 GHz** **(Positive coupling)**	**T_X=2.13 GHz** **(Positive coupling)**	**T_X=2.13 GHz** **(Negative coupling)**
Input transformer diameter (r1)	7.20 mm	7.20 mm	7.20 mm
Combline diameter (r2)	12.00 mm	12.00 mm	12.00 mm
Distance between wall and input transformer (s1)	7.20 mm	7.20 mm	7.20 mm
Distance between input transformer and resonator (s2)	11.75 mm	12.05 mm	12.05 mm
Distance between resonator and resonator (s3)	26.15 mm	27.10 mm	27.10 mm

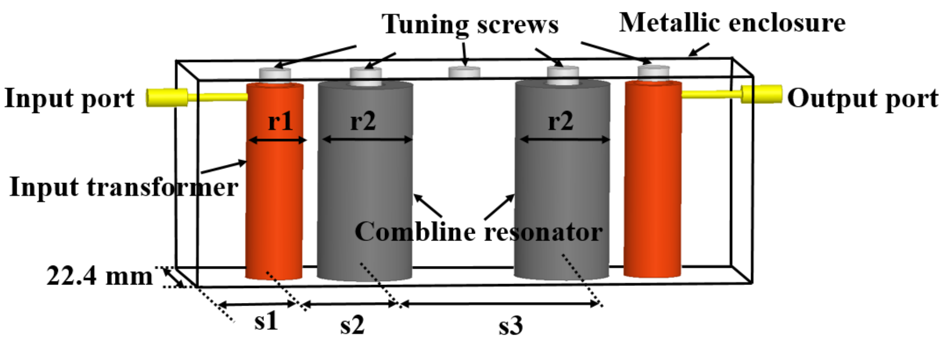

Figure 5-43: Geometrical structure of the positive coupling combline resonator filter

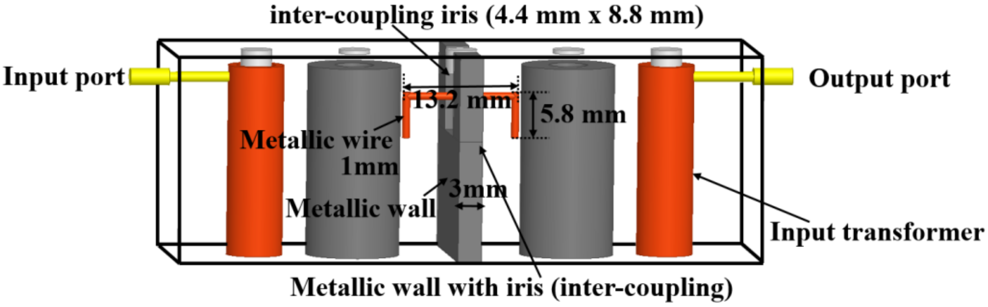

Figure 5-44: Geometrical structure of the negative coupling combline resonator filter

The simulated response of the second-order combline filter of the Rx band is portrayed in Figure 5-45. The fractional bandwidth is 2.89% (50 MHz at 1.73 GHz). The passband IL is less than 0.036 dB and the RL is better than 20.8 dB in the passband.

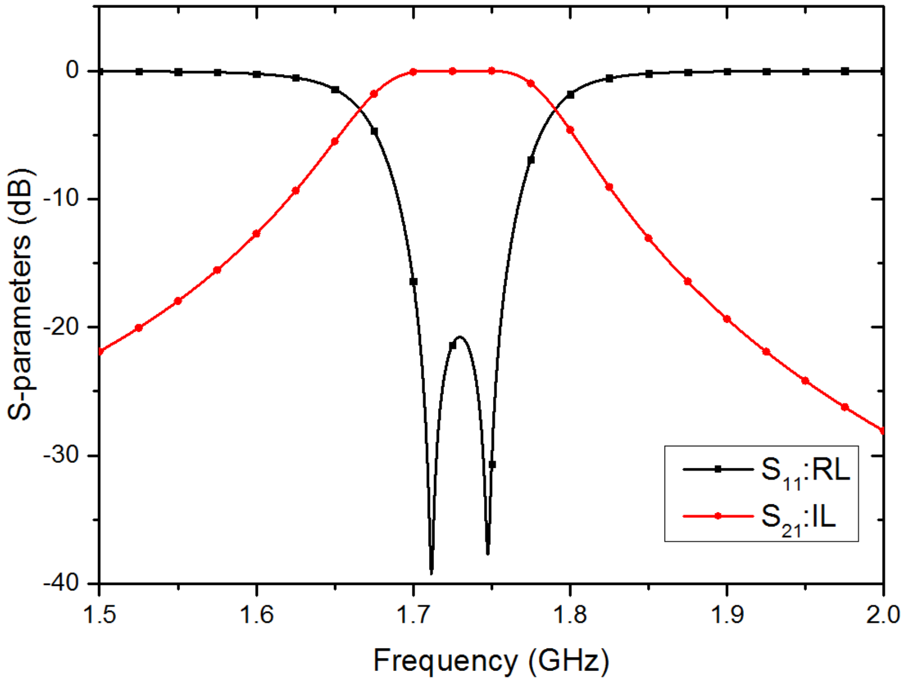

Figure 5-45: Simulated response of the combline filter at 1.73 GHz

A comparison of IL and RL responses between positive and negative combline structure is shown in Figure 5-46. The passband ILs are less than 0.01 dB and the RLs are better than 26 dB in the passband at the centre frequency of 2.13 GHz. A comparison of phases between the positive and negative designs shows that they have different phases. Figure 5-47 depicts the simulated phase response of the positive and negative coupling filters at the centre frequency of 2.13 GHz. From the simulation results, the phases of the positive and negative filters are 61.9° and -115.8°, respectively. Therefore, the phase difference between the Tx and Rx branches is 177.7°, which is only a 2.3° error compared to the analytical model.

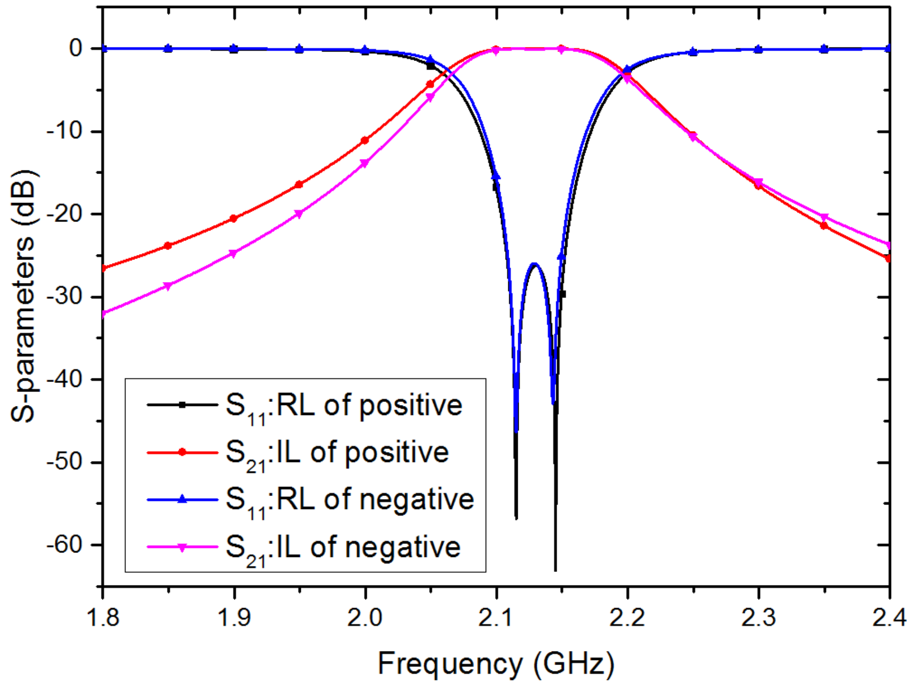

Figure 5-46: Simulated responses of the positive and negatively coupled filters at 2.13 GHz

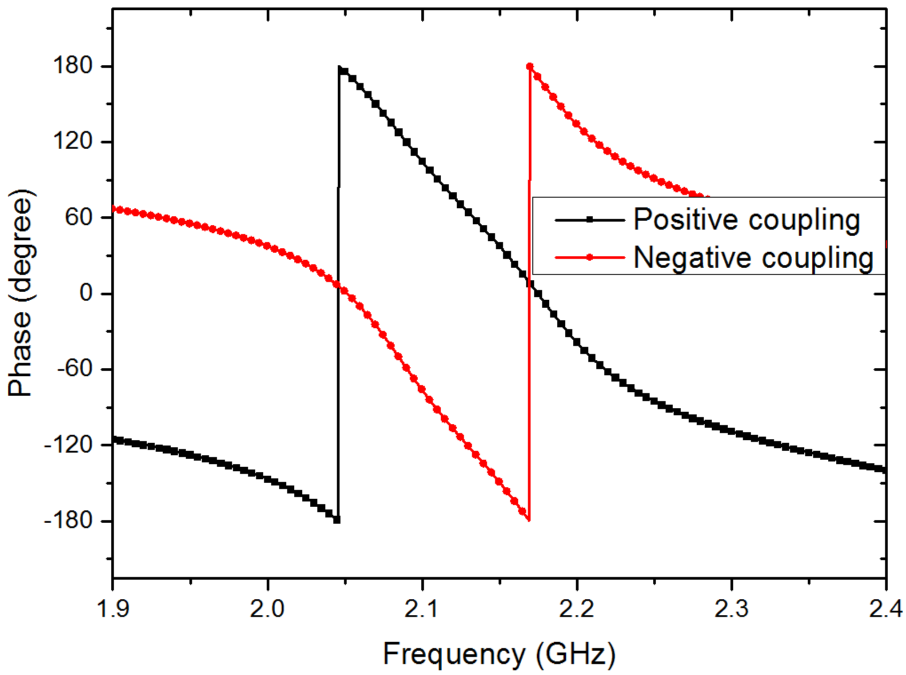

Figure 5-47: Simulated responses comparing the phases between the positive and negatively coupled filters at 2.13 GHz

5.5.5 Second-order four-port diplexer with dissimilar Q-factors

A combination of four filters is used to complete the four-port diplexer design. The 3D geometrical structure of the four-port diplexer with different Q-factors (Q_1=1800, Q_2=3600) is shown in Figure 5-48. The optimised parameters for this diplexer are listed in Table 5-10.

Table 5-10: Simulated dimensions of the four-port combline resonator diplexer with different Q-factors

Dimensions	Values
Cavity width (a)	50.6 mm
Cavity length (b)	48.8 mm
Cavity height (h)	24.2 mm
Tuning screw (t)	4 mm
Input transformer diameter (r1)	7.20 mm
Combline diameter (r2)	7.60 mm
Wall thickness (w)	3 mm
Iris of the wall (g)	4.4 mm
Height of the iris (k)	10.7 mm
Distance between wall and input transformer (s1)	7.20 mm
Distance between input transformer and resonator (s2)	9.55 mm
Distance between resonator and resonator (s3)	17.10 mm
Distance between input transformer and resonator (s4)	8.6 mm
Distance between resonator and resonator (s5)	17.2 mm

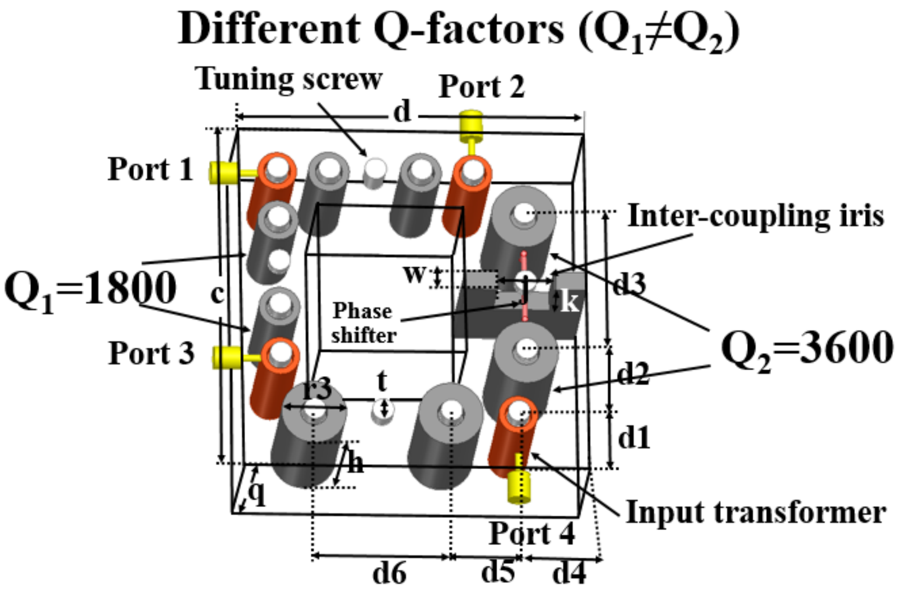

Figure 5-48: Geometrical structure of the second-order four-port diplexer with dissimilar Q-factors

The simulated S-parameters of the four-port diplexer with different Q-factors is shown in Figure 5-49. The fractional bandwidth is 2.89% and 2.35% .The passband IL in the Rx band is less than 0.47 dB and, in the Tx band, 0.55 dB, respectively. The RL in both channels is better than 20 dB in the passband. Figure 5-50 represents the comparison of measured Tx/Rx isolation of a conventional three-port diplexer and the four-port diplexer with dissimilar Q-factors (Q_1=1800, Q_2=3600). At the centre frequency of 1.73 GHz and 2.13 GHz for Rx and Tx modules, the simulated Tx/Rx isolation of the conventional three-port diplexer is 26.3 dB and it is 41.9 dB for the four-port diplexer. Figure 5-51 depicts the simulated phase response of Tx filter branches, S_{31} and S_{24}, at the centre frequency of 2.13 GHz. From the simulation results, the phases of S_{31} and S_{24} are 90.68° and -87.66°, respectively. Therefore, the phase difference between the Tx and Rx branches is 178.35°, which is only a 1.65° error compared to the analytical model. Figure 5-52 shows the wide-band simulation of the four-port diplexer with the different Q-factors. It can also be seen that the simulated wideband has a spurious response at 4.425 GHz, resulting from the resonance of the negative wire, and at 6.125 GHz, from second mode of the combline structure.

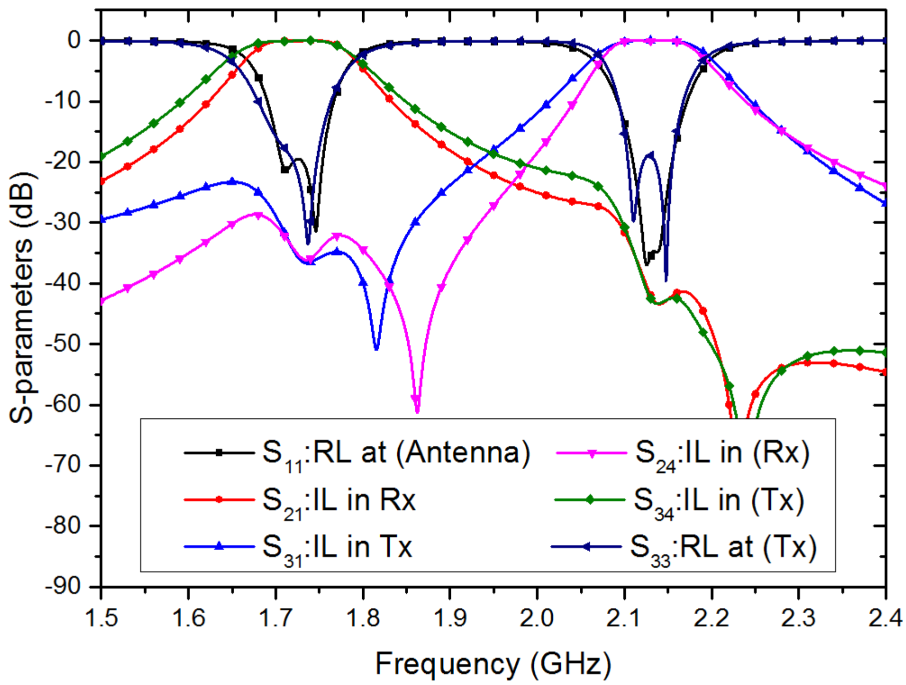

Figure 5-49: Simulation results of S-parameters of the four-port diplexer with dissimilar Q-factors at Rx=1.73 GHz, Tx= 2.13 GHz

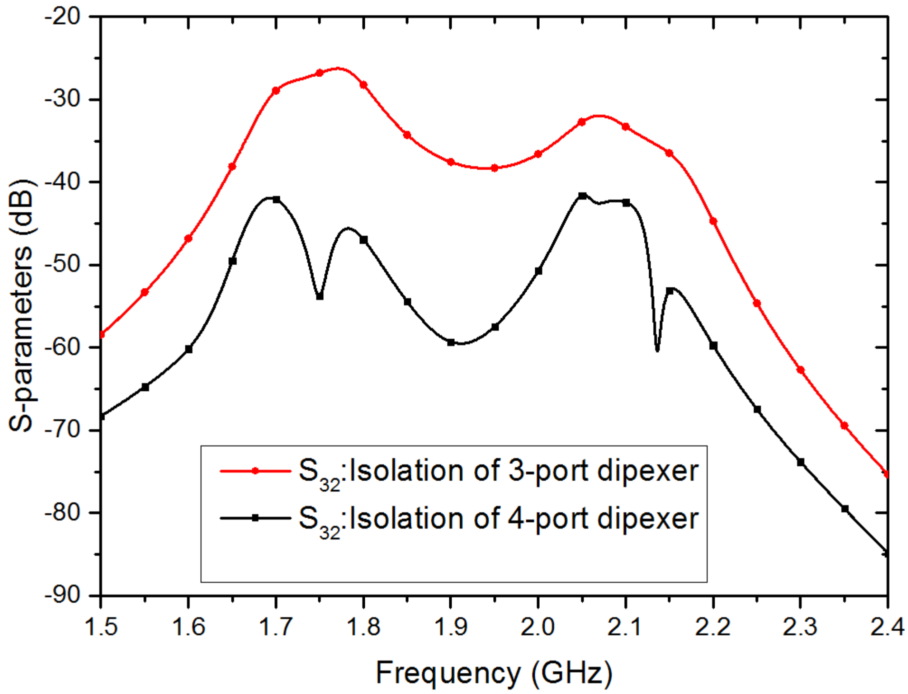

Figure 5-50: Simulation results of signal isolation, S_{32}, of the four-port diplexer with dissimilar Q-factors and three-port diplexer

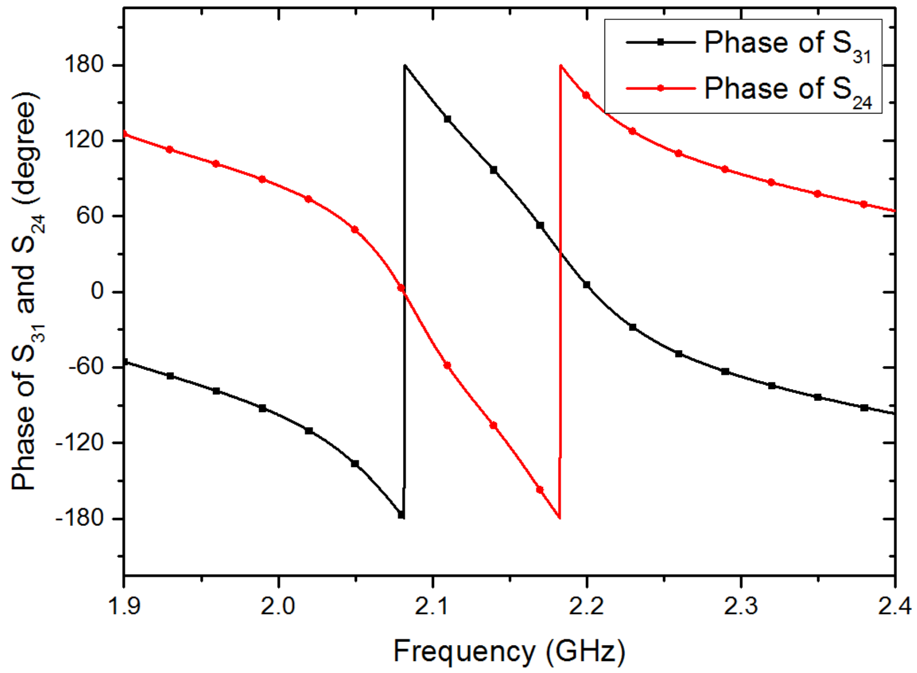

Figure 5-51: Simulation results of phase of S_{31} and S_{24} with 178.35 phase difference at 2.13 GHz

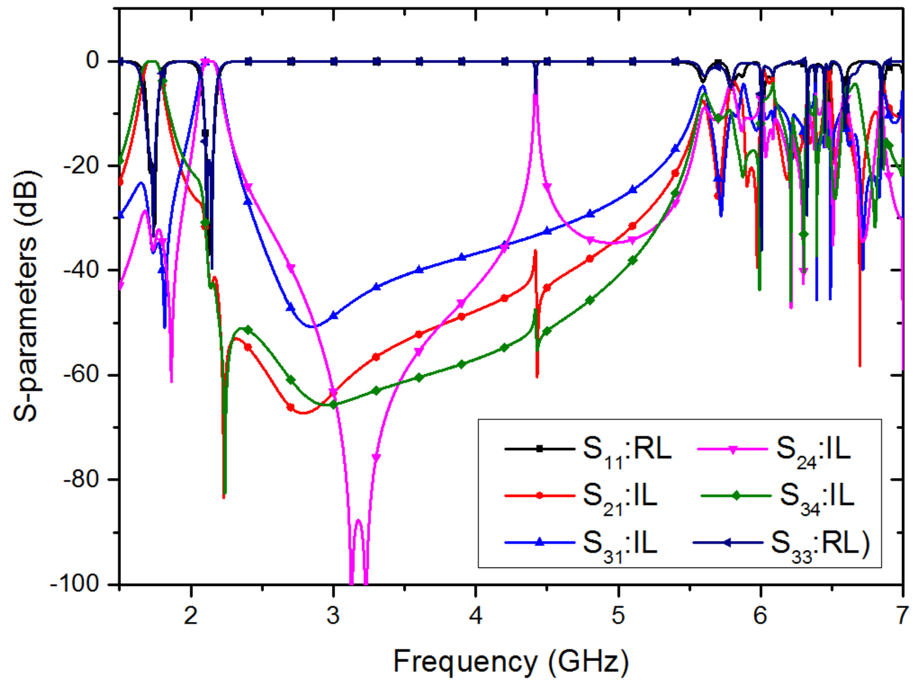

Figure 5-52: Simulations of wide-band response of the four-port diplexer with different Q-factors

5.5.6 Fabrication and measurement results

The fabricated prototype of the four-port diplexer with different Q-factors is shown in Figure 5-53. The prototype of the four-port diplexer is fabricated by using a computer numerically controlled (CNC) machine and aluminium and copper are used as structural materials. Tuning screws are implemented between each resonator to compensate for manufacturing errors as well as to optimise the resonant frequencies and inter-resonator couplings.

The measurement results of the second-order four-port diplexer with unequal Q-factors for each diplexer branch are shown in Figure 5-54. From Figure 5-54, the passband ILs of the Tx and Rx bands are less than 0.42 dB. The RLs in both channels are better than 20 dB in the passband with the 20-dB bandwidth of 50 MHz. From Figure 5-54, the measured isolation of the conventional three-port diplexer is 26.28 dB and it is 40.11dB for the four-port diplexer. The phase responses of S_{31} and S_{24} at the centre frequency of 2.13 GHz are plotted in Figure 5-56. The measured phases of S_{31} and S_{24} are 82.91° and -95.42°, respectively, resulting in a phase difference of 178.33°, which is only a 1.67° phase error compared to the mathematical model.

Theoretically, infinite signal cancellation is achievable if the signals propagating through both branches have the same amplitude and a 180° phase difference. Practically, the amplitude and phase errors result from fabrication and tuning screws as well as negative coupling. Therefore, the four-port diplexer with different Q-factors has slightly better isolation than the design with the same Q-factors.

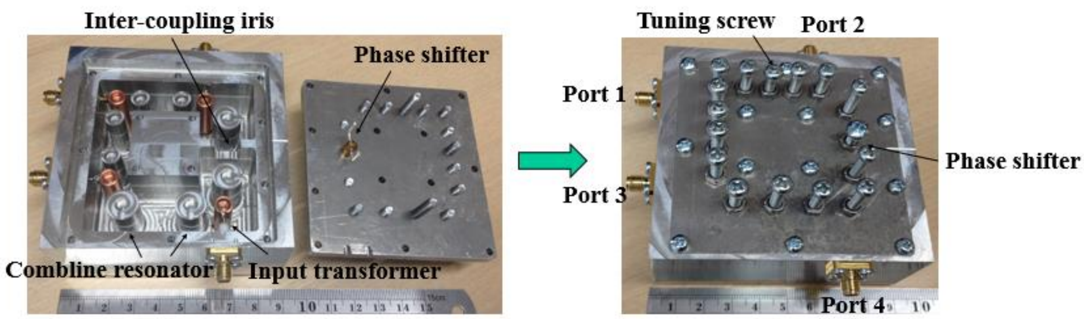

Figure 5-53: Photographs of the four-port diplexer with different Q-factors

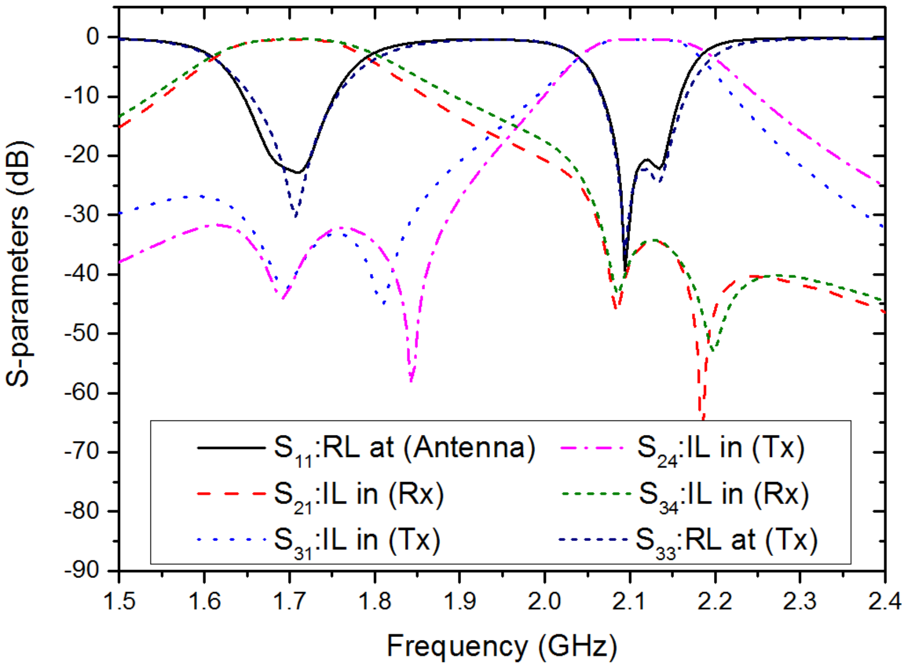

Figure 5-54: Measurement results of S-parameters of the four-port diplexer with dissimilar Q-factors where Q_1=1800, Q_2=3600 at Tx=2.13 GHz, Tx=1.73 GHz

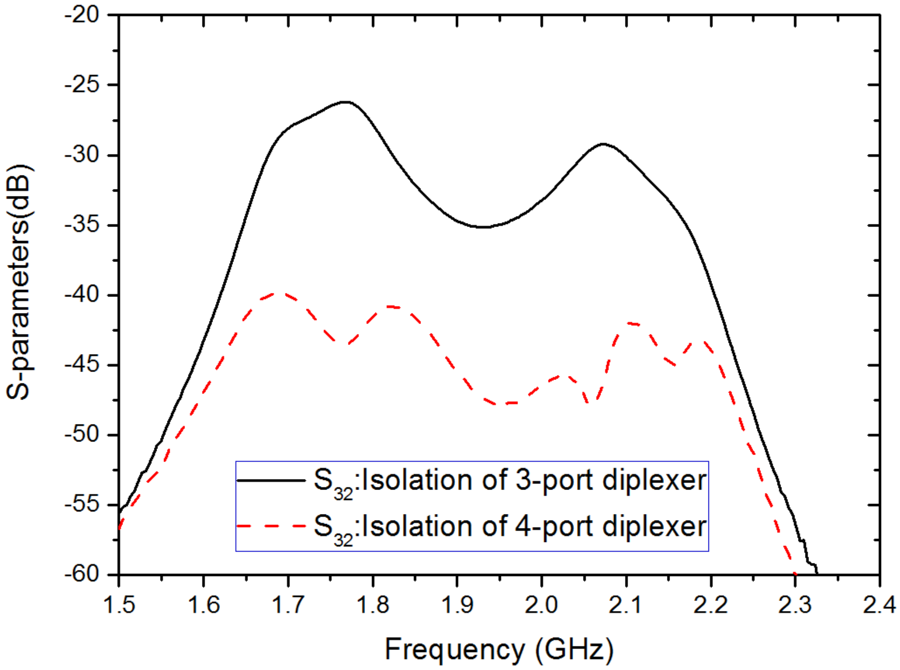

Figure 5-55: Measurement results of signal isolation, S_{32}, of the four-port diplexer with the dissimilar Q-factors (40.11 dB) and three-port diplexer (26.28 dB)

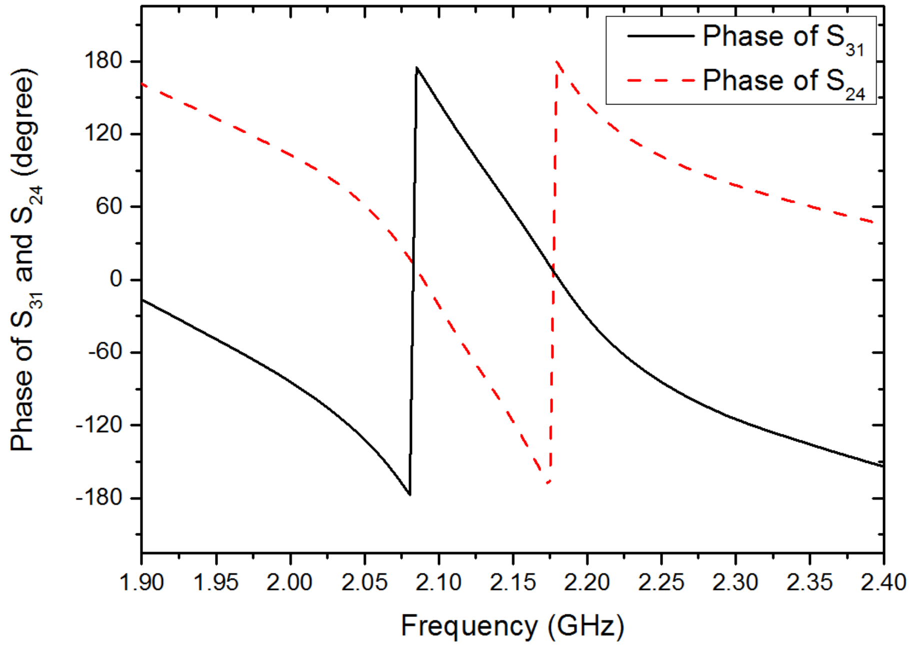

Figure 5-56: Measurement results of phases of S_{31} and S_{24} with 178.33° phase difference at 2.13 GHz

5.6 Summary

An equivalent circuit of a second-order combline filter with the introduction of input transformers has been presented in this chapter. Two different designs of four-port diplexer prototypes, based on filter designs with similar and dissimilar Q-factors, have been fabricated and measured to verify the new design technique. High signal isolation between Tx and Rx modules is achievable by only using second-order filter topology and the design technique is based on amplitude and phase cancellation between two diplexer branches of the four-port diplexer. The four-port diplexer is designed at the centre frequency of Tx at 2.13 GHz, Rx at 1.73 GHz with BW=50MHz. The new design can enhance the isolation (S_{32}) more than 14 dB compared to the conventional diplexer.

Table 5-11 presents the figure-of-merits and extensive comparisons between the novel four-port diplexer designs and the published research works with different diplexer architectures.

Table 5-11: Comparison of four-port diplexer with the state-of-the-art diplexer

Ref.	Architecture	Degree	IL, dB Tx/Rx	$1^{st}/2^{nd}$ Passband, GHz	Types	Power handling	Size	Isolation, dB
[7]	3-port	2	1.83/1.52	1.1/1.3	Dual-mode micrstrip ring resonator	low	$0.82\lambda_g \times 0.82\lambda_g (\lambda_g^2)$	>26
[56]	3-port	3	1.6/2.1	9.5/10.5	Substrate integrated surface	low	58.4×18.7 mm^2	>35
[57]	3-port	5	0.6/0.6	2.52/2.67	Coaxial rsonators	high	95×28×25 mm^2	>55
[58]	3-port	12	0.96/1.22	2.54/2.67	Triple-mode dielectric loaded resonators	high	10×10×5 mm^2	>50
This work	3-port	2	0.46/0.48	1.73/2.13	Combline resonators	high	75×73×26 mm^2	>26.28
This work	4-port with the same Qs	2	0.46/0.48	1.73/2.13	Combline resonators	high	75×73×26 mm^2	>35
This work	4-port with different Qs	2	0.42/0.42	1.73/2.13	Combline resonators	high	88×89×26 mm^2	>40

Chapter 6
Conclusion and future work

6.1 Conclusion

The motivation of this project is to reduce the size, losses and complexity of design of the microwave filter and diplexer used in the RF front end of cellular base stations. A novel method for achieving high Tx/Rx isolation using a four-port diplexer has been presented. Three- and four-port diplexers were intensively analysed and synthesised for solving S-parameter equations. The mathematical model was developed and some analytical and simulation results were obtained to verify the model. The new technique achieves high isolation with two back-to-back low degree diplexers. However, one diplexer can have significantly lower Q than the other.

A second-order capacitively coupled bandpass filter was presented as an example of the Chebyshev response. Then, the half-wavelength microstrip resonator and Q-factor were discussed to calculate the insert loss of filters. The second-order four-port diplexer using a microstrip open-loop resonator with coupled-feed was presented as a low Q-factor resonator. The delayed-line was successfully used to tune the phase between ports 2 and 4 to achieve a 180° phase shift. Another alternative solution of a microstrip open-loop resonator by using tapped-feed was designed as well, without a coupling port between the input and the microstrip open-loop resonator.

An equivalent circuit of a second-order combline filter with the introduction of input transformers was also presented. Two different designs of four-port diplexer prototypes, based on filter designs with similar and dissimilar Q-factors, were fabricated and measured to verify the new design technique. To achieve the filter design with a 180° phase shift between two diplexer branches, the 90° positive inverter and -90° negative inverter coupled filter are required. The four-port diplexer was designed at the centre frequency of Tx at 2.13 GHz, Rx at 1.73 GHz with BW=50MHz. The new technique design can enhance the isolation (S_{32}) more than 14 dB compared to the conventional diplexer.

6.2 Comparison of each different filter methodology

The methodology of design four-port diplexer by using microstrip is compared to others. First of all, two typical input/output (I/O) coupling structures for coupled microstrip resonator filters, namely the coupled line and the tapped line structures, are shown with the microstrip open-loop resonator as shown in Figure 6-1. The coupling of the coupled line structure in Figure 6-1 (a) can be found from the coupling gap (g) and the line width (w). Normally, a smaller gap and a narrower line result in a stronger I/O coupling or a smaller external quality factor of the resonator. For the tapped line coupling, usually a 50 ohm feed line is directly tapped onto the I/O resonator, and the coupling or the external quality factor is controlled by the tapping position (x), as indicated in Figure 6-1(b). For example, the smaller the (x), the closer is the tapped line to a virtual grounding of the resonator, which results in a weaker coupling or a larger external quality factor.

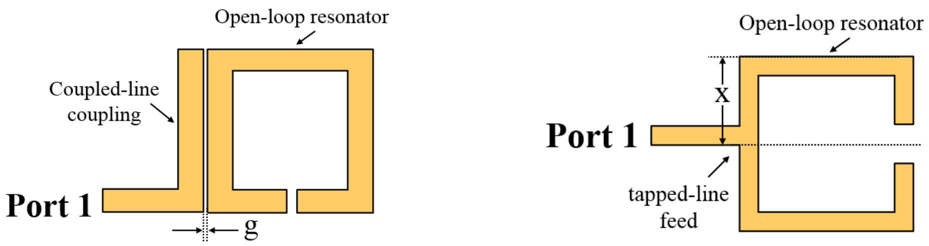

(a) (b)

Figure 6-1: Typical I/O coupling structures for open-loop resonator filters (a) Coupled-line coupling (b) Tapped-line feed

Secondly, each of the open-loop resonators is essentially a folded half-wavelength resonator. These coupled structures result from different orientations of a pair of open-loop resonators, which are separated by a spacing (s). It is obvious that any coupling in those structures is proximity coupling, which is, basically, through fringe fields. The nature and the extent of the fringe fields determine the nature and the strength of the coupling. It can be shown that at resonance of the fundamental mode, each of the open-loop resonators has the maximum electric field density at the side with an open gap, and the maximum magnetic field density at the opposite side. Because the fringe field exhibits an exponentially decaying character outside the region, the electric fringe field is stronger near the side having the maximum electric field distribution, whereas the magnetic fringe field is stronger near the side having the maximum magnetic field distribution. For the coupling structures in Figure 6-2(a), the electric and magnetic fringe fields at the coupled sides may have comparative distributions, so that both electric and the magnetic couplings occur. In this case the coupling may be referred to as mixed coupling. It follows that the electric coupling can be obtained if the open sides of two coupled resonators are proximately placed, as Figure 6-2(b).

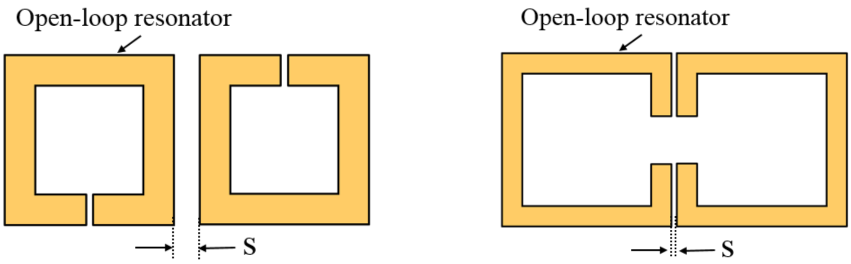

(a) (b)

Figure 6-2: Typical coupling structures for open-loop resonator filters (a) Mixed coupling (b) Electric coupling

The coupled-feeds have strong coupling value which are useful to compensate for manufacturing errors. However, the input/output coupled feeds sometimes have a small coupling gap between input and output ports, which are difficult to address in the fabricating process. Another alternative method of input/output coupling by using tapped-feed is introduced to transfer the signal from input to resonator directly. By the way, the input/output coupling by using tapped-feed is difficult to compensate for manufacturing errors because the input/output feeds have to fix at the exact position of the resonators. It can be seen that there always exists a trade-off between coupling-feed and tapped-feed. After successfully design filters and three-port diplexer, the phase shifter for four-port diplex was successfully tuned by the delayed-line.

Thirdly, as diplexer designs based on the microstrip structure can achieve low cost, small filter size and ease of integration but provide low power handling and high signal losses due to dielectric and ohmic losses. An alternative technology to reduce overall signal losses and increase power handling with the same or better isolation compared with the microstrip technology is combline coaxial resonator structures. The combline resonator by using metallic rod is shown in Figure 6-3.

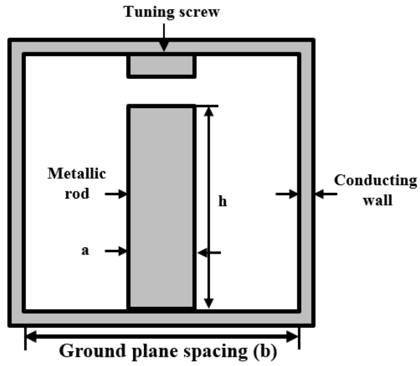

Figure 6-3: Combline resonator

The input/output coupling of combline four-port diplexer in this thesis is based on the coupling feeds (input transformer) because when thee-port diplexer structure with tapped-feeds is designed, the T-junction which used to connect two filters together suffers from the problem of not being matched at all ports. The input/output coupling technique of combline resonators is useful property of being matching network and tuning screws are implemented in each resonator to compensate for manufacturing errors as well as to optimise the resonant frequencies and inter resonators couplings.

In case of Q-factors of combline resonator, the most Q-factors are depended on the size of resonator and the ground plane spacing. Therefore, if the four-port diplexer design is still based on the same Q-factor, the size and cost will increase. The solution is that the combination of high Q-factor and low-Q factor could be used. This technique is also considered to reduced cost and size reduction as well as keep low losses.

From the physical viewpoint, the combline resonators are less than quarter wavelength long and the lines are all short circuited at the same end. Tuning screws for final electrical are loaded opposite ends of the lines which is useful to tune the resonance frequency. Normally, the combline resonator have high voltages or strong electric fields near the top of resonator and high current density or strong magnetic fields near the bottom. Based on electric and magnetic coupling, it is useful to design four-port diplexer with small size by using the principle of negative and positive coupling because both of them have the 180° phase shift. Therefore, when four-port diplexer is designed by using back-to-back three-port diplexer. A 180° phase shift in one branch can be achieved by using negative and positive coupling structure. Theoretically, infinite signal cancellation is achievable if the signals propagating through both branches of four-port diplexer have the same amplitude and 180° phase difference. Practically, the amplitude and phase errors result from fabrication and tuning screws as well as negative coupling. Therefore, the four-port diplexer with different Q-factors has slightly better isolation than the design with the same Q-factors.position of the resonators.

6.3 Future work

In order to reduce the size of the diplexer structure while keeping the same degree of filter and diplexer, a dual-mode resonator filter and diplexer should be used instead of a single-mode resonator filter. However, the structure will be complicated. Moreover, an alternative solution for size reduction by using the stepped-impedance is also interesting. This structure also has a wide spurious response. Therefore, this is another structure that could be used.

In terms of Q-factor of the four-port diplexer, the combination of different materials, such as combline and dielectric technologies would be useful to design a four-port diplexer with a high Q-factor, low loss, small size, wide spurious window and high power handling.

When analysing the four-port system, the investigating of phase and mismatched antenna were investigated. Clearly, if the antenna port impedance is not 50 Ω, then the isolation reduces. However, methods for compensating for this automatically adjusting the isolated port load impedance should be investigated.

References

[1] J.-S. Hong and M. J. Lancaster, *Microstrip filters for RF/microwave applications* vol. 167: John Wiley & Sons,New York 2004.

[2] I. C. Hunter, L. Billonet, B. Jarry, and P. Guillon, "Microwave filters-applications and technology," *Microwave Theory and Techniques, IEEE Transactions on,* vol. 50, pp. 794-805, 2002.

[3] I. Hunter, *Theory and design of microwave filters*: IET, 2001.

[4] H. S. Peng and Y. C. Chiang, "Microstrip Diplexer Constructed With New Types of Dual-Mode Ring Filters," *IEEE Microwave and Wireless Components Letters,* vol. 25, pp. 7-9, 2015.

[5] Q. Xue and J. Chen, "Compact diplexer based on double-sided parallel-strip line," *Electronics Letters,* vol. 44, pp. 123-124, 2008.

[6] Y. Zhou, H. w. Deng, and Y. Zhao, "Compact Balanced-to-Balanced Microstrip Diplexer With High Isolation and Common-Mode Suppression," *IEEE Microwave and Wireless Components Letters,* vol. 24, pp. 143-145, 2014.

[7] D. Chen, L. Zhu, H. Bu, and C. Cheng, "A Novel Planar Diplexer Using Slotline-Loaded Microstrip Ring Resonator," *IEEE Microwave and Wireless Components Letters,* vol. 25, pp. 706-708, 2015.

[8] K. Shamsaifar, T. Rodriguez, and J. Haas, "High-Power Combline Diplexer for Space," *IEEE Transactions on Microwave Theory and Techniques,* vol. 61, pp. 1850-1860, 2013.

[9] A. V. G. Subramanyam, D. Sivareddy, V. V. Srinivasan, and V. K. Hariharan, "Multipaction-free combline diplexer for deep space applications," in *2014 IEEE International Microwave and RF Conference (IMaRC)*, 2014, pp. 217-220.

[10] R. Ludwig, *RF Circuit Design: Theory & Applications, 2/e*: Pearson Education India, 2000.

[11] R. J. Cameron, C. M. Kudsia, and R. R. Mansour, *Microwave filters for communication systems*: Wiley-Interscience, 2007.

[12] R. Levy, R. V. Snyder, and G. Matthaei, "Design of microwave filters," *Microwave Theory and Techniques, IEEE Transactions on,* vol. 50, pp. 783-793, 2002.

[13] J. Hong and M. Lancaster, "Microstrip slow-wave open-loop resonator filters," in *Microwave Symposium Digest, 1997., IEEE MTT-S International*, 1997, pp. 713-716.

[14] T. Yang, P. L. Chi, and T. Itoh, "High Isolation and Compact Diplexer Using the Hybrid Resonators," *IEEE Microwave and Wireless Components Letters,* vol. 20, pp. 551-553, 2010.

[15] C. Collado, J. Pozo, J. Mateu, and J. M. O. Callaghan, "Compact duplexer with miniaturized dual loop resonator," in *2005 European Microwave Conference*, 2005.

[16] E. E. Djoumessi and K. Wu, "Compact Packaged Diplexer Based on Highly Selective Dual-Mode Bandpass Filter," *IEEE Microwave Magazine,* vol. 12, pp. 89-93, 2011.

[17] M. H. Weng, C. Y. Hung, and Y. K. Su, "A Hairpin Line Diplexer for Direct Sequence Ultra-Wideband Wireless Communications," *IEEE Microwave and Wireless Components Letters,* vol. 17, pp. 519-521, 2007.

[18] M. L. Chuang and M. T. Wu, "Microstrip Diplexer Design Using Common T-Shaped Resonator," *IEEE Microwave and Wireless Components Letters,* vol. 21, pp. 583-585, 2011.

[19] R. R. Mansour, "Filter technologies for wireless base stations," *Microwave Magazine, IEEE,* vol. 5, pp. 68-74, 2004.

[20] J. Zhou, M. J. Lancaster, F. Huang, N. Roddis, and D. Glynn, "HTS narrow band filters at UHF band for radio astronomy applications," *IEEE transactions on applied superconductivity,* vol. 15, pp. 1004-1007, 2005.

[21] Q. Zhang, Y. Bian, J. Guo, B. Cui, J. Wang, T. Yu*, et al.*, "A Compact HTS Duplexer for Communication Application," *IEEE Transactions on Applied Superconductivity,* vol. 20, pp. 2-7, 2010.

[22] C. Feng, X. Guo, B. Cao, B. Wei, X. Zhang, Y. Heng*, et al.*, "Design and Optimization of a Compact Superconducting Quadruplexer at VHF-Band With an Accurate Equivalent Circuit Model," *IEEE Transactions on Applied Superconductivity,* vol. 23, pp. 1502206-1502206, 2013.

[23] Y. Heng, X. Guo, B. Cao, B. Wei, X. Zhang, G. Zhang*, et al.*, "Design and Optimization of a Superconducting Contiguous Diplexer Comprising Doubly Terminated Filters," *IEEE Transactions on Applied Superconductivity,* vol. 23, pp. 1501706-1501706, 2013.

[24] X. Guan, F. Yang, H. Liu, Z. Ma, B. Ren, W. Huang*, et al.*, "Compact, Low Insertion-Loss, and Wide Stopband HTS Diplexer Using Novel Coupling Diagram and Dissimilar Spiral Resonators," *IEEE Transactions on Microwave Theory and Techniques,* vol. 64, pp. 2581-2589, 2016.

[25] X. Guan, W. Huang, B. Ren, P. Wen, H. Liu, Z. Ma*, et al.*, "Miniaturized High-Temperature Superconducting Diplexer Using Common Resonator and Cross Coupling Structure," *IEEE Transactions on Applied Superconductivity,* vol. 27, pp. 1-4, 2017.

[26] G. L. Matthaei, "Comb-line band-pass filters of narrow or moderate bandwidth," *Microwave J,* vol. 6, pp. 82-96, 1963.

[27] M. Höft and S. Burger, "Q-factor improvement of combline resonators," in *German Microwave Conf., Ulm, Germany*, 2005, pp. 53-56.

[28] G. Shen and D. Budimir, "Novel resonator structures for combline filter applications," in *2002 32nd European Microwave Conference*, 2002, pp. 1-3.

[29] D. Sh-Asanjan and R. R. Mansour, "A novel coaxial resonator for high power applications," in *2014 44th European Microwave Conference*, 2014, pp. 295-298.

[30] N. E. A. Rashid, M. T. Ali, and N. Hamzah, "Properties of dielectric combline resonator for base station filters," in *RF and Microwave Conference, 2004. RFM 2004. Proceedings*, 2004, pp. 76-79.

[31] X.-F. Liang and W. Blair, "High Q TE01 mode DR cavity filters for wireless base stations," in *Microwave Symposium Digest, 1998 IEEE MTT-S International*, 1998, pp. 825-828.

[32] R. Snyder, "Dielectric resonator filters with wide stopbands," *Microwave Theory and Techniques, IEEE Transactions on,* vol. 40, pp. 2100-2103, 1992.

[33] X.-g. Sun, W.-z. Li, and L. Ge, "Dielectric loaded cavity filter with wide spurious free region and better out-of-band rejection," in *Microwave Conference, 2006. APMC 2006. Asia-Pacific*, 2006, pp. 1200-1203.

[34] C. Wang, K. Zaki, A. E. Atia, and T. G. Dolan, "Dielectric combline resonators and filters," *Microwave Theory and Techniques, IEEE Transactions on,* vol. 46, pp. 2501-2506, 1998.
[35] X. Wang, Q. Y. Wang, Y. H. Zhao, and H. Li, "Design of a Compact Diplexer," in *2008 IEEE MTT-S International Microwave Workshop Series on Art of Miniaturizing RF and Microwave Passive Components*, 2008, pp. 170-172.
[36] D. M. Pozar, *Microwave Engineering*: Wiley, 2004.
[37] S. Bastioli, L. Marcaccioli, and R. Sorrentino, "An original resonant Y-junction for compact waveguide diplexers," in *2009 IEEE MTT-S International Microwave Symposium Digest*, 2009, pp. 1233-1236.
[38] S. B. Cohn, "Microwave bandpass filters containing high-Q dielectric resonators," *Microwave Theory and Techniques, IEEE Transactions on,* vol. 16, pp. 218-227, 1968.
[39] S. J. Fiedziuszko, I. C. Hunter, T. Itoh, Y. Kobayashi, T. Nishikawa, S. N. Stitzer*, et al.*, "Dielectric materials, devices, and circuits," *Microwave Theory and Techniques, IEEE Transactions on,* vol. 50, pp. 706-720, 2002.
[40] Q.-X. Chu, X. Ouyang, H. Wang, and F.-C. Chen, "-Mode Dielectric-Resonator Filters With Controllable Transmission Zeros," *Microwave Theory and Techniques, IEEE Transactions on,* vol. 61, pp. 1086-1094, 2013.
[41] S. Fiedziuszko, "Dual-mode dielectric resonator loaded cavity filters," *Microwave Theory and Techniques, IEEE Transactions on,* vol. 30, pp. 1311-1316, 1982.
[42] S. W. Wong, Z. C. Zhang, S. F. Feng, F. C. Chen, L. Zhu, and Q. X. Chu, "Triple-Mode Dielectric Resonator Diplexer for Base-Station Applications," *IEEE Transactions on Microwave Theory and Techniques,* vol. 63, pp. 3947-3953, 2015.
[43] P. M. Iglesias and I. C. Hunter, "Non-uniform Q-factor distribution in microwave filters," in *Microwave Conference (EuMC), 2012 42nd European*, 2012, pp. 1182-1185.
[44] H. Salehi, R. K. Reddy, T. Lukkarila, and S. Amir, "Spurious suppression of dielectric filters in practical wireless systems," in *Microwave Symposium Digest, 2008 IEEE MTT-S International*, 2008, pp. 1087-1090.
[45] M. Meng, I. C. Hunter, and J. D. Rhodes, "The Design of Parallel Connected Filter Networks With Nonuniform Q Resonators," *Microwave Theory and Techniques, IEEE Transactions on,* vol. 61, pp. 372-381, 2013.
[46] J. Konpang, M. Sandhu, N. Somjit, and I. Hunter, "Novel RF interference rejection technique using a four-port diplexer," in *2016 46th European Microwave Conference (EuMC)*, 2016, pp. 524-527.
[47] P. Martin and J. Ness, "Coupling bandwidth and reflected group delay characterization of microwave bandpass filters," *Applied Microwave and wireless,* vol. 11, pp. 86-96, 1999.
[48] G. Mahttei, L. Young, and E. Jones, "microwave filters, Impedance matching networks and coupling Structure," *Norwood, MA, Artech House,* 1980.

[49] S. B. Cohn, "Dissipation Loss in Multiple-Coupled-Resonator Filters," *Proceedings of the IRE,* vol. 47, pp. 1342-1348, 1959.
[50] J. Konpang, M. Sandhu, N. Somjit and I. Hunter, "Novel Synthesizing Technique for Interference Rejection in Future Integrated Base Station," in *Proceedings of TJMW2016*, 2016.
[51] I. J. Bahl, "A designer's guide to microstrip line," *Microwaves,* pp. 1-380, 1977.
[52] Jia-Sheng H. and M. J. Lancaster, "Theory and experiment of novel microstrip slow-wave open-loop resonator filters," *Microwave Theory and Techniques, IEEE Transactions on,* vol. 45, pp. 2358-2365, 1997.
[53] J. Konpang, M. Sandhu, N. Somjit, and I. Hunter, "Four-port microstrip diplexer for RF interference rejection," in *2016 13th International Conference on Electrical Engineering/Electronics, Computer, Telecommunications and Information Technology (ECTI-CON)*, 2016, pp. 1-4.
[54] H. U. Manual, "Ansoft Corp," *Pittsburgh, PA, USA,* 2005.
[55] M. Hagensen, "Narrowband Microwave Bandpass Filter Design by Coupling Matrix Synthesis-Demonstration of practical filter design using coupling matrix synthesis and three-dimensional electromagnetic simulation techniques," *Microwave Journal; International ed,* vol. 53, p. 218, 2010.
[56] S. Sirci, J. D. Martínez, J. Vague, and V. E. Boria, "Substrate integrated waveguide diplexer based on circular triplet combline filters," *IEEE Microwave and Wireless Components Letters,* vol. 25, pp. 430-432, 2015.
[57] P. Zhao and K.-L. Wu, "An iterative and analytical approach to optimal synthesis of a multiplexer with a star-junction," *IEEE Transactions on Microwave Theory and Techniques,* vol. 62, pp. 3362-3369, 2014.
[58] Z.-C. Zhang, Q.-X. Chu, S.-W. Wong, S.-F. Feng, L. Zhu, Q.-T. Huang*, et al.*, "Triple-mode dielectric-loaded cylindrical cavity diplexer using novel packaging technique for LTE base-station applications," *IEEE Transactions on Components, Packaging and Manufacturing Technology,* vol. 6, pp. 383-389, 2016.